Investigation on Reaction Mechanisms of Nano-energetic Materials and Application in Joining

by

Hongtao Sui

A thesis

presented to the University of Waterloo

in fulfilment of the

thesis requirement for the degree of

Doctor of Philosophy

in

Mechanical and Mechatronics Engineering

Waterloo, Ontario, Canada, 2019

Examining Committee Membership

External Examiner

NAME	Catalin Florin Petre
Title	Defense Scientist

Supervisor(s)

NAME	John Z. Wen
Title	Associate professor

Internal Member

NAME	Zhongchao Tan
Title	Professor

Internal Member

NAME	Adrian Gerlich
Title	Associate Professor

Internal-external Member

NAME	Luis Ricardez Sandoval
Title	Associate Professor

Author's Declaration

I hereby declare that I am the sole author of this thesis. This is a true copy of the thesis, including any required final revisions, as accepted by my examiners.

I understand that my thesis may be made electronically available to the public.

Abstract

Nano-energetic materials, also known as metastable intermetallic composites (MICs), have shown promise in applications such as propellants, pyrotechnics, and explosives. The work in this thesis pursues a deep understanding of the reaction mechanisms of typical nano-thermite composites and the functions of CNTs in nano-thermite reactions. The thesis begins with the development of nano-thermite composites with layered structure using Al and Fe_2O_3 nanoparticles via the Electrophoretic Deposition (EPD) process. The nano-thermite composites show a consistency in onset temperature even with different ratios of Al and Fe_2O_3, which suggests uniform interfacial formation, where the nano-thermite reactions are initiated. This work investigates the reaction mechanisms of typical nano-thermite composites: Al/CuO and Al/NiO. The results show that the Al/CuO nano-thermite system exhibits a gas-solid reaction mechanism, whereas the Al/NiO system exhibits a condensed-phase reaction mechanism. Furthermore, the functions of CNTs in nano-thermite reactions are investigated. The mass transfer mechanisms and thermal conductivities affect the energy release and reaction rate. Improvements in thermal conductivity and mass transfer are able to enhance the reactivity of nano-thermite composites. Measurements indicate that CNTs possess extremely high thermal conductivity compared with Al and metal oxidizers. Meanwhile, the NiO nanoparticles and CNTs react to release CO or CO_2 at the initial stage of the thermite reaction. The CO or CO_2 carry the oxygen atoms to the Al layers, followed by the reaction between Al and CO_2. Overall, the function of CNTs in nano-thermite reactions using the Al/NiO nano-thermite composite is to change the reaction from a solid-solid

mechanism to a condensed-phase mechanism. Finally, silicon wafers are welded using nano-thermite composites in order to achieve the application attempt. It has been shown that increasing energy release and decreasing apparent activation energy can provide an enhanced amount of energy to the interfacial area, which produces better mechanical strength in the welded zone.

Acknowledgements

I would first like to thank my advisor, Dr. John Z. Wen. He has taught me much more than how to conduct experiments. He has taught me how to obtain deep understanding from initial experimental data, and has supported me in every step along the way. I would like to appreciate my committee members, Dr. Catalin Florin Petre, Dr. Zhongchao Tan, Dr. Adrian Gerlich, and Dr. Luis Ricardez Sandoval, who evaluate the thesis and attend the thesis defense in their extremely busy schedule. I would like to acknowledge my colleagues, Mr. Florin Saceleanu, Ms. Lauren Lesergent, Ms. Boyu Li, and Ms. Yiqi Zhang, who discuss the experiments with me to help obtain more understandings on the results. My thanks are also extended to my wife, parents, and friends, who encourage me during the four years. I also acknowledge support from the Natural Sciences and Engineering Research Council of Canada (NSERC) through the Discovery and Discovery Accelerator Supplements grants.

Table of Content

List of Figures

List of Tables

Chapter 1: Introduction

Energetic materials have shown their promise in applications such as propellants, pyrotechnics, and explosives. Metal-based energetic materials, also known as thermite composites, have been attracting more attention in recent decades due to their higher energy density compared with other types of energetic materials. Micro-sized powders have been used in traditional thermite systems, which have been utilized in many industrial areas. However, the drawbacks of these conventional thermite composites restrict the universality of their use. To improve the performance of thermite composites, nano-sized powders known as metastable intermetallic composites (MICs) or nano-thermite composites, with lower onset temperatures and higher burning rates than those of bulk metal, are developed. Nano-thermite composites show a significant improvement by providing energy with fast reaction rates in microscale applications. Although the research on nano-thermite composites has been conducted for several decades, the existing investigation technologies limit the progress of fundamental research on nano-thermite reactions. The work in this thesis introduces methods to solve the problems pertaining to the investigation of nano-thermite composite reaction mechanisms. A welding attempt using nano-thermite is also conducted.

1.1 Energetic materials

Energetic materials include a wide range of materials that can store vast amounts of energy. In the monomolecular compound category, the common energetic materials are TNT, RDX, HMX, and CL-20 [1]. The monomolecular energetic materials can perform exothermic

reactions with high-speed reaction rates. However, energy densities of monomolecular compounds are relatively low compared to metal-based fuels. Metal-based fuels can contain Zr, Ti, Mg, Al, and B among other elements. The comparison of energy densities amongst these elements can be seen in Figure 1.1.

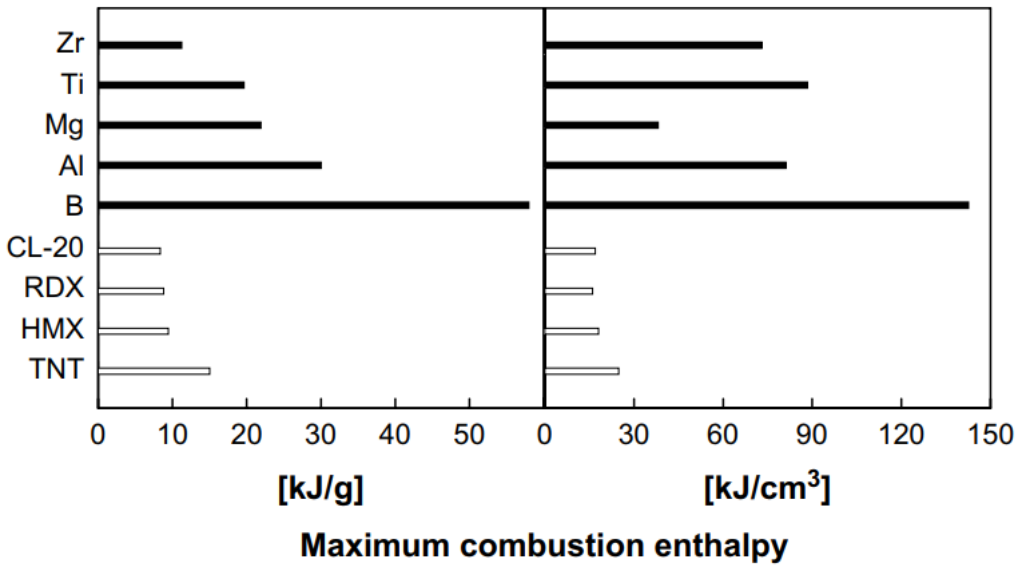

Figure 1.1 Reaction enthalpy of monomolecular energetic materials and metal fuels [1]

Metal fuels selected for energetic applications show higher energy release, both by mass and by volume, compared to monomolecular energetic materials. The metal fuels used for energetic purposes are formed with powder morphology, leading to slower and more controllable reaction rates compared with monomolecular energetic materials. For two decades, metal-based energetic materials have drawn a growing interest in the scientific domain and civil industry, thanks to their attractive capacity of producing localized gas, heat, and power [2].

1.2 Thermite composites and applications

Goldschmidt first defined thermite in 1908 [3] when he was trying to produce pure metals. Thermite refers to the combination of two or more components that store great amounts of chemical energy that can be released rapidly. Thermite reactions describe the reaction between oxidizer and fuel, which involves reduction of the metallic oxidizer and oxidation of the fuel. The fuels can be aluminum, magnesium, titanium, zinc, silicon, or boron. Because of its high volumetric energy density and affinity for oxygen, aluminum is used widely as the fuel component [4]. Aluminum is abundant in the earth's crust and possesses the features of high reactivity as well as benign products. Meanwhile, the aluminum oxide shell serving as a passivation shell is able to prevent reactive Al from further oxidation and achieve safer storage. The oxidizers of thermite composites include such elements as copper oxide (CuO) [5-16], iron oxide (Fe_2O_3) [17-19], molybdenum oxide (MoO_3) [9, 20, 21], tungsten oxide (WO_3) [9], and nickel oxide (NiO) [2, 22].

Thermite reactions produce a large amount of energy as shown in Table 1.1. The adiabatic reaction temperature can reach above 3000K with phase change and more than 5000K without phase change.

Eq. 1.1 shows the typical thermite reaction:

$$M+AO \rightarrow MO+A+\Delta H \quad , \qquad \text{(Eq. 1.1)}$$

where *M* and *AO* are the metal (fuel) and oxidizer, respectively, *MO* and *A* refer to the newly produced oxidizer and metal, respectively, and ΔH is the enthalpy of the reaction.

Table 1.1 Thermochemical properties of thermite systems [23]

Reactants		Adiabatic reaction temperature (K)		State of products		Gas production		Heat of reaction	
Constituents	g/cm^3	No phase changes	with phase changes	State of oxide	State of metal	moles gas per 100g	g of gas per g	-Q, cal/g	-Q, cal/cm^3
2Al+3CuO	5.109	5718	2843	liquid	1-g	0.5400	0.3431	974.1	4976
$2Al+Fe_2O_3$	4.175	4382	3135	liquid	l-g	0.1404	0.0784	945.4	3947
2Al+3NiO	5.214	3968	3187	liquid	l-g	0.0108	0.0063	822.3	4288
$2Al+MoO_3$	3.808	5574	3253	l-g	liquid	0.2425	0.2473	1124	4279
$2Al+WO_3$	5.458	5544	3253	l-g	liquid	0.1434	0.1463	696.4	3801
$4Al+3WO_2$	8.085	4176	3253	l-g	solid	0.0662	0.0675	500.6	4047
$4Al+3MnO_2$	4.014	4829	2918	liquid	gas	0.8136	0.4470	1159	4651

Thermite reactions can expose a minimal area to an extremely high temperature. This heat generated on a small spot can be used to cut metal or weld metal components by melting joining components, and by injecting molten metal from the thermite reaction products [24]. For example, thermite may be used for repairing locomotive axle-frames by welding thick steel sections without removing the parts from their installed locations [24]. The traditional applications in railway welding use micro-sized powders of aluminum and iron oxide. The mixture is ignited with a stick of magnesium. Due to the significant amount of heat production, the thermite reaction is a type of self-sustained reaction. During joining, the

railway parts are connected in an enclosed sand mold with a defined gap. The melting iron liquid, produced by the thermite reaction, flows down to the bottom of the reaction crucible and injects into the gap between two railway sections [24].

Due to the high energy density of metal and metal-oxide composites and simple apparatus, thermite composites have shown attractive properties related to micro-thrust [25-27], micro-initiation [28, 29], gas for actuation [30, 31], gas for chemical reaction [32], heating and welding [33], and switching [2, 34]. In the past century, they have been extensively used in the military, mining, and demolition sectors.

1.3 Drawbacks of traditional thermite composites

One of the drawbacks of using metal fuels is the relatively low reaction rates upon ignition. Due to the longer distance of mass and heat diffusion paths, micro-sized powders have a long ignition delay compared to the onset of monomolecular energetic compounds. This leads to longer self-sustaining combustion time between metal powders and oxygen [1]. In addition, the micro-sized metal fuels are not fully consumed during the reaction to provide energetic benefits for applications such as explosives, propellants, and pyrotechnics. The reaction rates between metal powders and oxygen are limited by the oxygen transport time required to reach the surface of powders and the diffusion rate through the Al_2O_3 shell [35].

Mixtures of Al micro-powders and metal oxides in thermite composites increase the interfacial contact between reactants to make the thermite reaction tunable. However, the contact between Al micro-powders and metal oxides does not reduce ignition delay, and does

not result in a significant increase in reaction rates. Ignition delay is associated with the diffusion of oxygen through a natural Al passivation shell. Even with different reaction mechanisms between Al and oxides, the oxygen provided by the oxide leads to an increasing amount of contact area. The oxygen concentration outside of Al powders can provide only a negligible effect on the diffusion processes of oxygen. Meanwhile, the passivation shell of Al_2O_3 increases as the thermite reaction proceeds, leading to a thicker oxide shell and a longer diffusion path for oxygen. The ignition delay of metal powder combustion causes reduced efficiency, which also leads to high activation energy and a slow reaction rate. The delayed reaction rate is associated with a heat loss of longer duration, which may cause a quenching effect in some applications. The heat loss affects the consistency significantly when using thermite in MEMS applications. Although a significant improvement in enhancing the performance of thermite welding has been made by combining chemical compounds [36], traditional composites exhibit relatively slow reaction rates that make it difficult to meet the requirements of micro-scale applications [37]. Meanwhile, initiation of composites composed of metal and metal oxide is very difficult, such as the ignition between Al-Fe_2O_3 thermite [24]. A magnesium stick must be ignited in advance of the initiation of the thermite system to provide a pre-heating source for the purpose of joining railway bars. Because of the high thermal conductivity of metal and metal oxide, the self-sustained thermite reaction needs to be granted a heat source to compensate for the heat loss to the surrounding environment. Due to the ignition delay and slow reaction rate of conventional Al-Fe_2O_3 thermite, a large amount of preheating energy is required until the heat loss can be

compensated for by the thermite reaction. On the other hand, nano-thermite composites are good candidate in the applications, such as initiators for micro-chips or ignition of solid propellant [38-40]. The fast reaction rates and high energy release of nano-thermite composites are able to compensate the heat loss effect on micro-applications and ignition of other type of propellant.

Furthermore, the combustion of Al powders also has the problems of long ignition delay and slow reaction rate. Coupled with the agglomeration effect of metal powders, the ignition delay of Al micro-sized powders leads to insufficient combustion [41, 42]. Al powders are combined with ammonium perchlorate (AP) along with a binder, which must melt and undergo agglomeration before ignition. The agglomerated Al micro-powders cannot react completely during the thermite reaction, which may undergo a long ignition delay. Due to the ignition delay, the Al micro-sized powder cannot even burn until it is ejected from the propulsion chamber, which reduces the combustion efficiency. The problems of conventional thermite result in minimal useful applications.

1.4 Nano-thermite composites

Even with significant efforts to improve traditional thermite composites, the performance of low reaction rates and long ignition delays cannot meet the demands of microscale applications. To improve the performance of thermite systems, researchers must develop new systems using particles of different dimensions.

Thermite composites are composed of metal and metal oxide powders. The schematic view of a thermite composite can be seen in Figure 1.2.

The thermite reactions of Al and metal oxide powders are initiated at the interface of the reactants. It can be expected that the diffusion length of reactive chemical components is based on the diameters of the particles involved in thermite reactions. The reduction of particle size can significantly improve the performance of thermite composites. To achieve this goal, researchers introduced nanoscale particles to thermite composites.

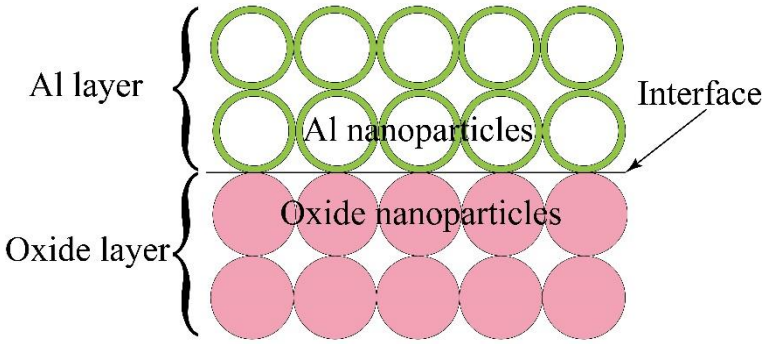

Figure 1.2 Schematic view of thermite composite with the interface between reactants

The reaction rate is controlled by the mass diffusion path through an oxide layer. The growth of the oxide layer with the thermite reaction can prevent thermite reactions, which reduces reaction rates. With decreasing particle size, the surface area to volume ratio can be increased significantly, which leads to increased reactivity by several orders of magnitude. The phenomenon was first described by Aumann et al., who used a Al/MoO_3 nano-thermite composite with the dimensions of ~0.02 µm to 0.05 µm to obtain a reaction 1000 times faster than conventional thermites due to the increased surface contact and shortened diffusion path

[43]. This nano-thermite reaction exhibits different reaction mechanisms compared with conventional thermite systems. After achieving the nano-thermite reaction, researchers made efforts into the investigation of nano-thermite systems to identify the thermal properties and combustion performance. Nano-thermite composites are also known as metastable intermolecular composites (MIC) due to their performance similar to mono-molecular energetic materials.

Metal fuels have several component options, such as aluminum, boron, zinc, and silicon. However, as with aluminum micro-powders, aluminum nanoparticles have been widely used due to their high energy density, abundance in the earth's crust, and low cost. Most importantly, Al nano-particles can form a natural oxide shell that prevents further oxidation, and can build interfacial contact with metal oxide without undergoing a pre-reaction.

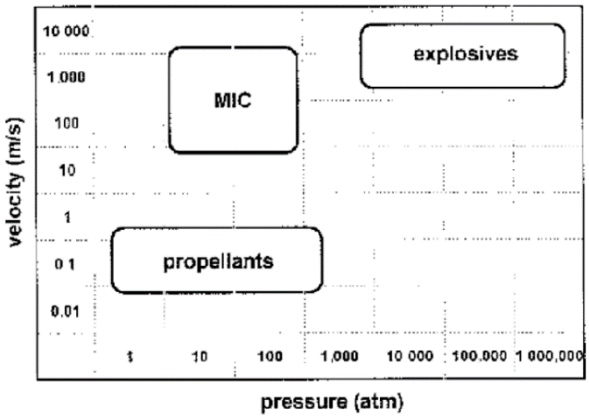

Figure 1.3 The different performance regarding pressure and flame propagation velocity using different types of energetic systems [4]

Comparisons between nano-thermite composites, propellants, and explosives have been

made in previous research regarding reaction pressure, velocity, and reaction enthalpy [4]. The results are shown in Figure 1.3.

Nano-thermite composites (MICs) exhibit different performance compared with propellants and explosives. Nano-thermite composites generate pressures similar to propellants, and possess comparable velocities to explosives. Conventional propellants have a relatively longer diffusion path, whereas MICs can react with a diffusion path on the nano-scale, which leads to the faster reaction rate of MICs. On the other hand, explosives possess a similar or even smaller diffusion distance between reactants. This can lead to comparable reaction rates between MICs and explosives. However, although the velocity of MICs is similar to explosives, the low amount of gas production results in low pressure. The energy densities of MICs are considerably higher than monomolecular energetic materials, which leads to potential applications either using it alone or by adding it to other types of energetic materials.

Nano-thermites have attracted considerable interest for a wide range of applications involving energetic formulations, such as pyrotechnic devices, propellants, and initiators. In the civil sectors, the localized energy release favours nano-thermites for joining purposes, as it can melt joint components and prevent the whole device from being exposed to high temperatures. In recent years, the nano-thermite reaction has been extended to describe a broader class of reactions; for example, the reaction between metallic components composed of the bimetallic energetic nanostructures of Ni/Ti, Co/Al, Ni/Al, and Pt/Al. These bimetallic nano-thermites, often composed of core-shell structures or nano-scale multilayers, provide a

direct interface between two reactive metals and then promote a thermite reaction without gas generation.

Overall, nano-thermite composites possess distinct and superior thermochemical and combustion properties over traditional energetic materials. Meanwhile, nano-thermite composites show different reaction mechanisms compared with micro-sized energetic fuels.

1.5 Motivation

Nano-thermites, composed of nanoparticle components, have drawn much attention and show great potential in a wide range of applications including gas generators, micro-initiators, micro-thrusters, and micro-joining, etc. [2]. Depending on a particular application, tunable and controllable nano-thermite compositions and products are usually required. For example, gas generators need a thermite reaction that produces more gas and heat, with a fast reaction rate, that reaches higher temperatures and pressures. On the other hand, gas phases produced in thermite reactions would jeopardize the quality of joining in welding applications. In welding, less gas production and a relatively benign reaction rate are usually required. Generally speaking, it is better to be able to control the phases of products, energy release, and reaction rate for specific applications. Investigations into the reaction mechanisms of nano-thermite are therefore becoming significant to understand the reaction process. For example, Sullivan and Zachariah characterized the reaction mechanisms and reaction kinetics of a variety of nano-thermites [44, 45]. They found that most oxidizers such as CuO and SnO_2 generate pressure, which suggests the decomposition of oxidizers before the thermite reaction

occurs, indicating that the reaction rate is controlled by the chemical reaction of aluminum. The nano-thermite reaction rate between Al and Fe_2O_3 is limited by the decomposition of Fe_2O_3. However, a deep understanding of the reaction mechanisms is still required.

The utilization of nanoparticles causes many challenges in handling and mixing. The increased surface area to volume ratio produces a higher surface energy, causing an agglomeration effect. Therefore, various preparation technologies have been developed to form thermite composites with a more uniform distribution to maximize the interfacial contact of components. However, pre-mixed nanoparticles are not suitable for the direct investigation of nano-thermite reaction mechanisms. The observation of reaction mechanisms can only be achieved by indirect approaches, such as optical emission, pressurization change, and mass spectrum technology [45]. Meanwhile, indirect investigation may lead to a misunderstanding of the reaction mechanisms. For example, a pressurization increase in the chamber upon the ignition of nano-thermite composites is possibly caused by heating the surrounding atmosphere rather than the decomposition of oxidizers [45]. The O_2 gas detected by the mass spectroscopy device is perhaps produced from the decomposition of oxidizer after the nano-thermite reaction is completed [46].

For the reasons stated above, nano-thermite composites with multi-layered structures are proposed in this work to form uniform interfaces, which are more suitable for the investigation of reaction mechanisms. The thermite reactions are initiated in principle on the interfacial area between reactants. The interfaces formed in multi-layered structures can provide a homogeneous contact between two reactive layers.

The developed technologies that form multi-layered structures include physical vapor deposition such as electron beam evaporation, magnetron sputtering and atomic layer deposition [47, 48]. In these methods, the electron beam or plasma is used on metal targets to produce ions of elements which are ejected from the targets. The elements are coated on a substrate to form thin layers. For example, Petrantoni et al. [49] fabricated multilayered Al/CuO with magnetron sputtering. The aluminum and copper oxide were deposited on a silicon oxide substrate, separately. The aluminum and copper targets that received argon plasma were altered for depositing different types of layers. In magnetron sputtering, the precursor materials are usually metal targets ejected by plasma. The products on the substrate are not formed with nanoparticles, and show different reaction mechanisms [49]. Meanwhile, the layered structures formed with sputtering have several problems. The aluminum layers formed without a passivation shell can react with the copper oxide layer spontaneously in the nano-thermite composites with multilayers. The reaction mechanisms are still unclear with these structures, especially with the investigation of nanoparticles. Consequently, sample preparation methods that form layered structures using nanoparticles are required to investigate the reaction mechanisms of nano-thermite composites. Overall, the reaction mechanisms of nano-thermite composites with various nanoparticle components and the practical preparation technologies to form proper structures are exigencies for the applications of nano-thermite composites.

1.6 Objectives

The first objective is the investigation of reaction mechanisms using different combinations of nano-components is conducted. First of all, fabrication techniques that form multi-layered structures without impurities are developed. Then, nano-thermite composites with multi-layered structures are heated up to initiate the nano-thermite reaction. First of all, Al/Fe_2O_3 nano-thermite composite is selected, which is formed via electrophoretic deposition (EPD). Then, the microstructure and thermochemical properties of the Al/Fe_2O_3 thermite system are investigated to confirm the formation of a uniform interface between reactive layers and the thermite reaction that can be initiated. The aluminum and iron oxide nanoparticles are deposited on a stainless steel electrode to form detailed multi-layered structures. The solid-solid interfacial contact of two depositing layers is observed using SEM images. Thermal gravimetric analysis (TGA) is performed to study the onset temperature and degree of the thermite reaction. Differential scanning calorimetry (DSC) is used to measure the energy release and the ignition temperature of the corresponding thermite composites. Furthermore, the typical nano-thermite composites, Al/CuO and Al/NiO, are selected, and a method is employed to directly observe the distinct reaction mechanisms. The nano-thermite composites are then formed via vacuum filtration technology. The experiments on the reaction mechanism will show the various reaction routes. Finally, to enhance the heat conductivity and interfacial contact, carbon nanotubes (CNTs) are added to the nano-thermite composites. Meanwhile, the improvement of the reaction mechanism from condensed-phase

to gas-solid reaction increases the interface formation between reactants. The functions of CNTs in the nano-thermite reaction are then investigated in this work.

The second objective of this thesis is to conduct the joining of silicon wafers in the application attempt. In the experiments, the thermite composites containing nanomaterials are used to achieve the joining of silicon wafers. In this work, the energetic properties and reaction kinetics of nano-thermite composites with thin film structure formed via a vacuum filtration method are investigated. The diversity of energy release and reaction rate produces the different microstructures and chemical compositions in the welding zone, which determines joint qualities. The apparent activation energy is one of the parameters to determine the reaction rate, and is evaluated in this work. Furthermore, the energy release and apparent activation energy of nano-thermite composites are then related to the joining quality.

1.7 Thesis organization

Chapter 2 is a review of the relevant literature to examine the synthesis, characterization, and application of nano-thermite composites. The background of developing thermite composites and the design principles of nano-thermites are included in this chapter. Furthermore, the characterization method is reviewed with respect to measuring nanoparticle size, microstructure, thermochemical properties, and reaction kinetics. Also, the methodology of fabrication and characterization, the determination of reaction kinetics in previous research are demonstrated in this chapter. In chapter 3, the multi-layered structure

of Al/Fe_2O_3 nano-thermite composites is developed through the EPD process. The energetic properties of the microstructures of layered composites are then measured in this chapter. Chapter 4 is an investigation of the diversity of reaction mechanisms with Al/CuO and Al/NiO nano-thermite composites using multi-layered structures. The systems show gas-solid and condensed-phase reaction mechanisms corresponding to Al/CuO and Al/NiO nano-composites. The use of different types of oxides results in nano-thermite composites possessing distinct reaction routes when the nano-thermite reaction is initiated. In Chapter 5, the reaction route of Al/NiO nano-thermite composite with the condensed-phase reaction mechanism is tuned by adding CNTs into the nano-thermite, which is then improved with respect to the reactivity of the nano-thermite system. The functions of CNTs in the thermite reaction are investigated by adding different layers of either Al or NiO. Chapter 6 covers an application attempt using nano-thermite composite to weld silicon wafers. The energy release and reaction kinetics can affect the joining quality of the interfacial area of silicon wafers. Therefore, the measurements of the energy release and apparent activation energy are conducted. The properties of different nano-thermite composites in relation to both thermodynamics and kinetics produce the distinct welding zone in relation to the microstructure, chemical composition, and microhardness of the interface, which further determines the joining quality of the silicon wafers. In Chapter 7, the major contributions of this thesis, along with recommendations for future work, are presented.

Chapter 2: Literature review

2.1 Background

In this chapter, the relevant literature is reviewed to provide sufficient knowledge and information for completing the thesis. As stated in Chapter 1, the conventional thermite composites using micro-sized powders cannot satisfy the requirements of micro-scaled systems. The nano-thermite composites are then developed. First, conventional thermites using micro-sized particles, prepared using a mixture of thermite compositions, are introduced. The concept of reducing micro-sized particles in conventional thermites to nano-scaled particles is described. Nano-thermites show improved properties compared with conventional thermites. The comparison between micro- and nano-sized thermites emphasizes the improvement of nano-thermite reactivity.

Although the nano-thermites prepared with nanoparticles have advantages, such as high energy release rate, high heat production, and low ignition temperature, etc., new difficulties in storing, handling, and mixing arise, which require the development of new preparation technologies. Physical mixing, sol-gel, and self-assembly are among the most popular methods to prepare nano-thermites. In addition, the ball milling procedure can produce nano-thermite composites with various structures. However, it is a dangerous process that may cause an explosion during the preparation procedure. Meanwhile, ball milling may reduce the active content of fuels. Vapor deposition, including electron beam evaporation, magnetron sputtering, and atomic layer method, forms thermites with nano-sized layered

structures. The disadvantages involving the in-situ reaction during fabrication are also discussed in this chapter.

Degrees of interfacial contact between components impact the reaction zone by controlling the diffusion path, which further affect the energetic properties, including the ignition temperature and reaction kinetics. For characterization, scanning electron microscopy (SEM) is employed to observe the microstructure of nanocomposites. The energetic properties can be measured using TGA/DSC, which shows the initiation temperature, phase change, and energy release produced by thermite reaction.

Due to the advantages of high energy density, high burning rate and low ignition temperature, as mentioned above, nano-thermites have been used in numerous applications, such as micro thrusters, microinitiators, and micro joining, etc. [28, 29, 38-40, 50-53]. The applications of nano-thermites will be reviewed here in this chapter in more detail.

2.2 Comparison of micro- and nano-thermite composites

2.2.1 Energetic properties

Monomolecular compounds including TNT (trinitrotoluene), Nitrocellulose and nitroglycerine exhibit higher burning rates due to the mixing of reactants at monomolecular levels. The maximum heat generation of the compounds is limited by the reaction enthalpy and the degree of reaction completion. The composite mixtures in the monomolecular level exhibit a very rapid exothermic reaction controlled primarily by the chemical kinetics

processes of the molecular decomposition. In contrast, the energy density of those monomolecular energetic materials is relatively low compared with thermites.

Higher energy density and controllable burning rates are required in some applications. In comparison with monomolecular energetic materials, thermites demonstrate relatively controllable energetic properties via tuning of the interfacial contact between components. As mentioned in the literature mentioned [2], conventional thermites using micro-sized particles can not meet the demands of applications in small areas such as MEMS systems. The heat loss is one of the most challenging issues that can suspend flame propagation. Thermites using micro-sized particles have drawbacks caused by longer reactant diffusion paths that significantly reduce the burning rate. Rossi et al. [2] reviewed the literature and showed that examples containing nano-sized particles have superior energetic properties over conventional thermites using micro-sized particles. The higher requirement in reaction rate indicates the exigency of improving the performance of thermites.

Regarding ignition temperature, micro-sized thermites experience an ignition event at well above the melting point of aluminum in aluminum-based series [54]. The higher ignition temperature means that more activation energy is required to ignite the thermite composites. One DTA/DSC result demonstrates the phase change of the Al/Fe_2O_3 series using micro-sized particles as shown in Figure 2.1.

Figure 2.1 shows that the exothermic peak belonging to the thermite reaction is substantially higher than the melting point of aluminum. The DSC result for the 8Al+3Fe2O3

sample exhibits an exothermic peak with a wide range in temperature, indicating a longer diffusion path, which results in an extended reaction time.

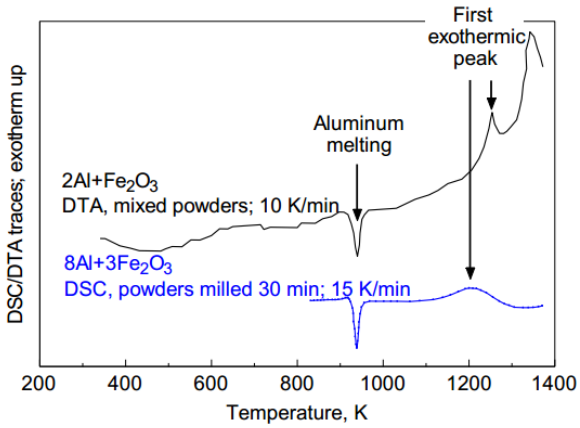

Figure 2.1 DTA and DSC traces for Al-Fe_2O_3 mixtures [54]

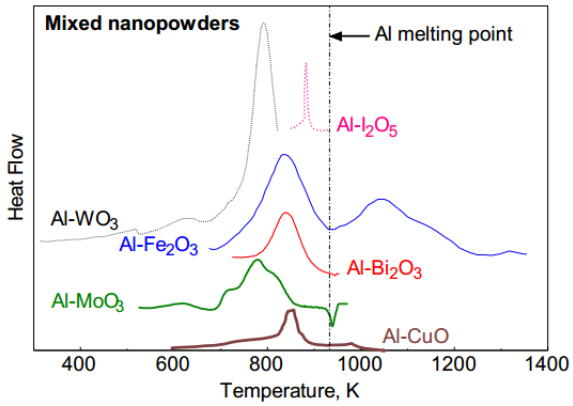

Figure 2.2 DSC traces for thermites prepared using nano-powders of aluminum mixed with different oxidizers [54]

On the other hand, thermite reactions with nano-sized particles are traced with DSC, demonstrating the onset temperature as shown in Figure 2.2 [54]. Each result comes from different literature sources using different conditions, such as mixing methods, heating rates, and proportion of components. All of the results show the ignition temperature below the aluminum melting point.

2.2.2 Reaction kinetics

The lower ignition temperatures of nano-thermites are associated with improved ignition mechanisms, enabling rapid flame propagation as shown in Figure 2.3, where decreasing Al nanoparticle sizes exhibit higher burning rates [55].

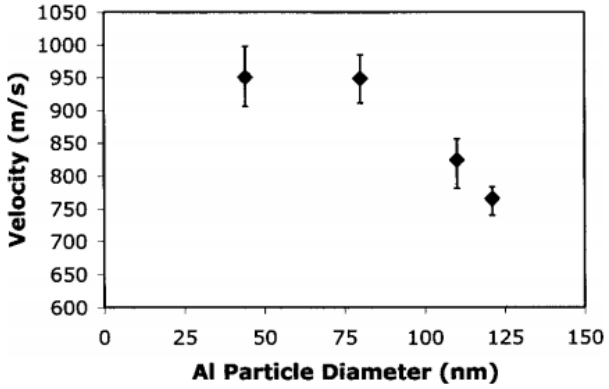

Figure 2.3 Combustion velocity as a function of particle diameter for high-density samples. Error bars represent maximum and minimum velocities for at least four repeatability tests [55]

The Al nanoparticles demonstrate faster burning rates and lower activation energy compared with bulk Al samples, as shown in the literature [43]. The average particles with sizes between 24 to 65 nm were measured with 0.5 eV of activation energy for oxidation, which is smaller than the value of 1.7 eV for bulk aluminum. Meanwhile, Al/MoO_3

nanocomposites with the average size of 0.02 and 0.05 μm show a combustion rate that is 1000 times that of conventional powders [43].

2.3 Definition of nano-thermite composites

Nano-thermite, also called metastable intermolecular composites (MICs), refers to composites using nanoparticles that are less than 100 nm in diameter. Meanwhile, mixtures that exhibit interactions between reactants with a diffusion path less than 100 nm, such as nano-laminates, are also deemed nano-thermite composites. MICs are a new type of energetic material (EM) that stores a significant amount of chemical energy, which can be defined as inorganic nano-scaled energetic materials (nEMs) [2]. As mentioned in the last chapter, aluminum-based composites are among the most popular series of nano-thermites due to the high reaction enthalpy of aluminum, low cost, and a massive amount of storage in the earth's crust. Metal-oxidizer systems, such as Al/CuO, Al/Fe_2O_3, and Al/NiO, etc., exhibit the most attractive features in applications. Besides metal-oxidizer systems, metal-metal and metal-metalloid components have also been developed, with the common feature that the starting components are always capable of producing a highly exothermic reaction. The products of this initial reaction, intermetallic alloys or metal-metalloid compounds, often continue oxidizing if the reaction is initiated in an oxidizing gaseous environment [1]. In this thesis, all of the work is performed using metal-oxide systems.

2.4 Design principle of nano-thermite composites

Al nanoparticles are most widely used as the fuel composition, which benefits from all of the advantages of Al nanoparticles as stated previously. Although researchers have an interest in boron-based nano-thermites [56], the low energy density (B/CuO~3.09 kJ/g vs. Al/CuO~4.08 kJ/g) is one of the limitations in using boron-based nano-thermites [23]. Therefore, we only discuss Al-based nano-thermite systems in this section. A significant number of oxidizers shown in the literature [23] provide many choices in the selection of oxidizers, while only a few of them have been systematically investigated. It is evident that not every series is suitable for applications as energetic materials. The thermochemical properties are one of the most important considerations, but others have to be taken into account to achieve specific purposes. First of all, the reaction rate should be enhanced to minimize the heat loss to achieve the self-sustained reaction and faster burning rate. Depending on different ignition mechanisms and chemical compositions of products, the reaction kinetics are tunable. To simplify the discussion, we only take into account the thermal diffusivity. Secondly, the particle sizes, purity of the mixture and preparation technologies affect the degree of interfacial contact between nanoparticles, which determines the degree of completion and reaction rate. Here, the particle sizes of nanoparticles are assumed to be uniform based on the purpose of the discussion about how to choose the proper oxidizers. Meanwhile, this point is involved with the surface morphology, which is very difficult evaluate theoretically. Thirdly, the mass diffusion can limit the combustion rate and must be considered.

The thermal diffusivity, heat generation rate, and the adiabatic reaction temperature are hence the critical factors considered in the strategy of designing nano-thermites with respect to choosing the proper oxidizers.

2.4.1 Thermal conductivity and adiabatic temperature

Tables 2.1 and 2.2 [2] show the calculated diffusivity at 300 K for each case including the popular organic energetic materials and using Fe_2O_3, MoO_2, CuO, NiO, SnO_2, SiO_2, and TiO_2 oxidizers. These tables show high reaction enthalpy values with Al as guidance for choosing the proper oxidizer.

Table 2.1 Diffusivity, heat of reaction, and adiabatic temperature [2]

Organic EMs	Diffusivity at 300 K α (cm^2/s)	Heat of reaction ΔH (cal/g)	Adiabatic reaction Temperature T_{ad}(K)
PETN	1.29×10^{-3}	1435	4140
HMX	0.77×10^{-3}	1350	3255
NC	10^{-3}	960	3000

Meanwhile, the adiabatic temperature can be found in the literature [2, 23] as shown in Table 1.1. The stoichiometric ratios of Al and oxidizer are assumed, and the reactions of thermites continue until completion; no chemical compounds are left in an unreacted state.

Based on the thermal diffusivity, Figure 2.4 demonstrates the MO to Al diameter ratio as a function of diffusivity, which indicates the decreasing tendency of diffusivity when the MO to Al diameter ratio increases. Consequently, d_A is set equal to d_{MO}.

Table 2.2 Diffusivity of nano-thermites with different diameter ratios of fuel and oxidizer [2]

MIC	Diffusivity at 300K α (cm²/s) $d_{Al}=d_{MO}$	Diffusivity at 300K α (cm²/s) $d_{Al}=0.1\times d_{MO}$	Diffusivity at 300K α (cm2/s) $d_{Al}=10^{-3}\times d_{MO}$
Al/MnO_2	31.64×10^{-3}	17×10^{-3}	16.1×10^{-3}
Al/CuO	60×10^{-3}	33×10^{-3}	30×10^{-3}
Al/Fe_2O_3	85×10^{-3}	49×10^{-3}	45×10^{-3}
Al/NiO	61×10^{-3}	35×10^{-3}	32×10^{-3}
Al/SnO_2	190×10^{-3}	116×10^{-3}	107×10^{-3}
Al/SiO_2	16.5×10^{-3}	9×10^{-3}	8.3×10^{-3}
Al/TiO_2	48.5×10^{-3}	27.3×10^{-3}	25×10^{-3}

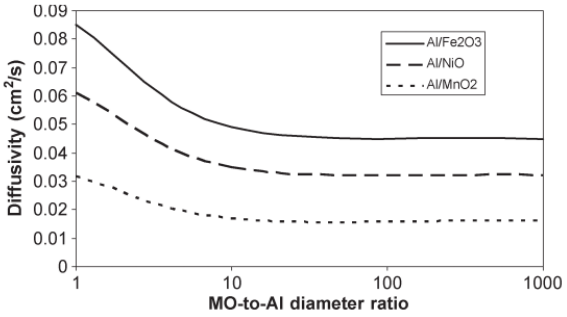

Figure 2.4 Example of diffusivity evolution as a function of the MO-to-Al diameter ratio for three MICs: Al/Fe_2O_3, Al/NiO, and Al/MnO_2 [2]

2.4.2 Heat of reaction for different nEMs

The organic nEMs and nano-thermites listed above are plotted in a diagram showing the diffusivity and heat of reaction for each composition. As discussed above, the desired systems are expected to possess the specified features, including high heat generation, and high thermal diffusivity. Figure 2.5 demonstrates the two characteristics of different systems and indicates the potential of each system.

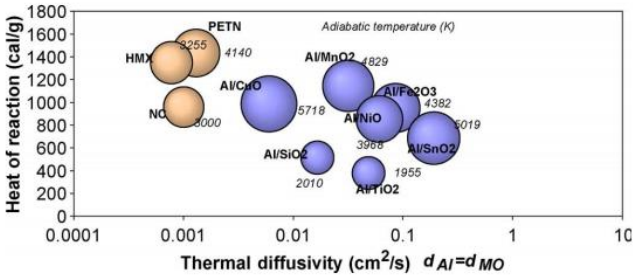

Figure 2.5 Thermal diffusivities and heat of reaction for different nEMs systems [2]

Following the principle of high heat generation and high thermal diffusivity, the systems placed in the upper right corner are considered to have the best potential as nEMs due to high heat generation and high thermal diffusivity. On the other hand, the bottom left systems are not good candidates. Figure 2.5 exhibits the promising candidates: Al/CuO, Al/MnO_2, Al/Fe_2O_3, and Al/NiO systems.

The discussion about choosing potential oxidizers for nano-thermites gives direction for designing nanocomposites. However, the thermochemical properties of nanocomposites do not completely follow the principles listed in Figure 2.5, which is related to the data of heat of reaction and thermal diffusivity collected under certain assumptions; assumptions such as the stoichiometric ratio, the heat diffusion mechanism not being the only mechanism to affect

reaction kinetics, spherical and equal-sized nanoparticles, and no effect from the preparation methods. For example, flame propagation is not only based on the heat diffusion mechanism. A different nano-thermite system with specific ignition mechanism can produce gas phase, such as oxygen, which can be evaporated forward to ignite the next available nanocomposite, demonstrating effective convection ignition. In this case, the thermal diffusivity is not the critical factor for the burning rate. Even for a single system, different equivalence ratios exhibit different reaction kinetics under distinct ignition mechanisms.

2.5 Methodology of preparation of nano-thermite composites

Nanoparticles exhibit improved energetic properties compared with micro-scaled particles, such as higher burning rate, higher energy release rate, and lower ignition temperature. The reaction rate and energy release of solid reactants are generally controlled by mass & heat transfer accompanying the reaction and the degree of intimate contact of reactant components. The increased specific surface area and interfacial contact in nanocomposites, on the other hand, enhance the rate of energy release by facilitating diffusion during the thermite reaction [57-59]. Despite this, challenges in dealing with nanoparticles arise, leading to the development of preparation technologies to fabricate nano-thermite composites using nanoparticles or nano-laminates. The focus is on aspects of handling, mixing, and fabrication. First of all, the nanoparticles have small sizes that can float in the atmosphere for a long time and jeopardize the research environment. Sullivan [4] discussed the flow of relaxation for different particle sizes as shown in Table 2.3.

Table 2.3 Gravitational settling time and the stopping distance of different sizes of aluminum particles thrown with an initial velocity of 1000 m/s in the air [4, 60]

Particle Diameter (nm)	Slip Correction Factor	Time to fall 1 m by gravity	Stopping Distance if Initial velocity = 1000 m/s
10,000	1.016	117 seconds	87.6 cm
1,000	1.164	169 minutes	1.00 cm
100	2.85	115 hours	0.246 mm
10	22.2	61.7 days	19.1 μm
5	43.6	18.0 weeks	9.40 μm
2	108	45.3 weeks	3.72 μm
1	216	1.75 years	1.86 μm

Secondly, the increased specific surface area of nanoparticles leads to higher surface energy that tends to result in the agglomeration of individual nanoparticles. Thirdly, the highly reactive nanoparticles can cause a reaction with oxygen and fire in the atmosphere if improper storage methods are applied. To use nanoparticles safely and efficiently, researchers have developed several techniques to solve the problems in handling. In the review, the preparation methods and corresponding structures are divided into two parts depending on the final structure of nanocomposites. The first part shows nanocomposites with porous or condensed structures using nanoparticle components, including physical mixing, sol-gel, self-assembly, and arrested reactive milling. The second part shows nanocomposites with a layered structure, such as those produced by vapor deposition and electrophoretic deposition (EPD).

2.5.1 Types of nEM structures

The energetic properties and reaction kinetics are significantly affected by the types of nEM structures that determine the degree of interfacial contact and diffusion path in the thermite reaction. Different preparation technologies form distinct microstructures of nanocomposites. The microstructures include powder, pellet, monolithic bulk, fully condensed, core-shell, thin film, and multilayers. Powders of nanocomposites can be formed by using nanoparticle components with physical mixing technologies [8, 61, 62]. Reactive components are dispersed in solution and undergoes sonication. The solution is then dried until the nanocomposites remain in a beaker. The powders of nanocomposites can be compressed in pressing dies to change the structure from powder to pellet form [13].

Sol-gel and self-assembly form nanocomposites with monolithic structure after gelation and drying [59, 63-67]. Nanocomposites with monolithic structure contain approximately 10% impurities, produced by the remaining polymer residue [2]. Fully condensed nanocomposites can be formed using arrested reactive milling by embedding one component into the matrix [12, 68-76]. The components reach each other at the nanometric scale, while the structure of powder is at the micro level. Furthermore, core-shell structures can be fabricated with vapor deposition. Ohkura et al. [7] reported a core-shell structure using the Al/CuO thermite system. CuO nanowires grow up via the simple thermal annealing method from a copper thin film formed by deposition. Then, Al film is deposited on the CuO nanowire via magnetron sputtering to form a core-shell structure.

The nanocomposites with multi-layer structures are fabricated using magnetron sputtering method [39, 47-49, 77-81]. Multi-layer structures have well-defined structure and direct

contact between reactive components, which are applied to a wide range of micro-level uses, such as initiators, micro joining, and propellants.

2.5.2 Physical mixing

Physical mixing is the simplest method to prepare nanocomposites. Nanoparticles of Al and oxidizer are mixed and dispersed in a solvent, and then ultrasonicated in a bath until thoroughly dispersed. In most cases, organic solvents are employed due to the poor reactivity between Al and organic solvents. As the literature [8, 61, 62, 82] reported, Al/MoO_3, Al/Bi_2O_3, Al/$KMnO_4$, and Al/CuO, etc. have been dispersed in either isopropanol or hexane, followed by complete evaporation of the solvent at a temperature of ~50 °C.

Physical mixing is widely used for the preparation of MICs because it has apparent advantages, such as its simple apparatus requirement, it is easy to mix and disperse the nanoparticles, and it avoids direct contact of Al nanoparticles with oxygen. On the other hand, the small-scale operation limits the use of this method in the industrial sector. In addition, the degree of dispersion of nanoparticles is not controlled very well. Meanwhile, Al nanoparticles that have contact with the solvent and stay a relatively long time in solution until the complete evaporation of liquid, can be oxidized due to the reactivity of Al nanoparticles with an organic solvent, such as isopropanol. The exposure between Al nanoparticles and the atmosphere increases the oxidation degree of Al nanoparticles when the quantity of solvent is reduced due to evaporation. Furthermore, Al and oxidizers nanoparticles that have different velocities when precipitating to the bottom of the bath are predicted to lead to the separation of Al and

oxidizers, which has an adverse effect on nanoparticle dispersion. Finally, the nanoparticles left on the bottom of the bath after complete evaporation have a loose structure, and the reactants have no intimate interfacial contact, which can reduce the energy release rate and burning velocity. Therefore, compression of the nanoparticle mixture must be conducted to form pellets. The friction between nanoparticles produces heat that may cause further oxidation or ignition of nanocomposites.

2.5.3 Sol-gel

The sol-gel method has been used widely to produce nanocomposites with more intimate and homogeneous contact between components as an alternative to physical mixing technologies. Several types of nanocomposites have been formed successfully with sol-gel approaches, such as Al/Fe_2O_3, Al/Cr_2O_3, and Al/NiO, etc. [63-66, 83]. The sol-gel process involves several steps to achieve a mixture of nanoparticles. First of all, the hydrated salts of metals, such as $Fe(NO_3)_3 \cdot 9H_2O$ and $Cr(NO_3)_3 \cdot 9H_2O$, for example, are dissolved in ethanol to form a solution which can remain unchanged for even several months, which is called sol. Secondly, the so-called gel can be formed by adding propylene oxide into sol to condense the solution to form a three dimensional structure with pore sizes between 5 and 50 nm. The Al nanoparticles are added and mixed with the solution just before the formation of the gel. Then, the fluid in the pores is removed by evaporation under various conditions to form xerogel (dried without supercritical fluid) or aerogel (dried supercritical). The difference between aerogel and xerogel mainly depends on the structure; aerogel has a collapsed

structure, whereas xerogel has a non-collapsed structure, and this depends on whether the fluid CO_2 is applied for the evaporation of fluid in the pores.

In comparison with the physical mixing method, sol-gel offers superior control of the distribution of nanoparticles to generate shorter diffusion paths in the ignition to improve the energy release rate. However, the impurities introduced into the chemical composition of composites reduces the active content, which may represent 10% in total mass of samples [2]. The high porosity introduces an interval between components, which interrupts the diffusion of reactants and further reduces the reaction rate of thermite. Meanwhile, the sol-gel approach is restricted by the types of hydrated salt that can be gelled. Finally, the introduction of Al nanoparticles must occur at a particular stage, and it may take a long time and many experiments for a new researcher to grasp the skills.

2.5.4 Self-assembly

Several research groups reported the fabrication method called self-assembly to obtain nanocomposites with an ordered structure. Either the nano-oxidizer rod or hydrated metal salt is applied as the precursor. The oxidizers are functionalized by polymers, such as poly (4-vinyl pyridine) [5], P4VP (polyvinyl pyridine) [18], and Brij S10 ($C_{18}H_{37}(OCH_2CH_2)_nOH$, n~10, average Mn ~711) [66] as reported in the literature. After the functionalization of oxidizer, Al nanoparticles can surround nano-oxidizers on the surface to form solid-solid contact with homogeneous distribution. In the case of using hydrated metal salts, polymers

serving as a gelation agent are mixed with the solution for gelled oxidizer as in the corresponding step in the sol-gel process.

Self-assembly requires similar steps as sol-gel techniques such as adding propylene oxide for gelling the sol to achieve condensation. The difference between the two technologies is due to the functionalization process that makes Al nanoparticles absorb to the surface of the oxidizer, which can produce the more ordered structure of nanocomposites, resulting in a more intimate interfacial contact to improve solid-solid chemical reaction. Zhang et al. [66] prepared two samples in which one was formed with sol-gel while another was fabricated with a self-assembly method. The two samples used the same particles, and very similar process, except that Brij S10 was added as a functionalization agent to the sample undergoing self-assembly.

In the self-assembly process, Al nanoparticles do not need to be added into the salt solution at a specific stage just before the formation of a gel, because Al nanoparticles can be absorbed to the surface of the oxidizer without precipitation, causing the separation of reactants as in the sol-gel process. Furthermore, the polymers introduced to the mixture serving as surfactants are impurities that reduce energy density. Therefore, a new method has been developed by charging Al and Fe_2O_3 nanoparticles via diffusion charging of gas ions without adding a surfactant.

The self-assembly method solves several problems of the sol-gel process and improves the energetic properties; the Al nanoparticles do not need to be added into the solution at a specific stage, which makes it easier to control; the distribution of Al and oxidizer

nanoparticles is not under the random condition whereas Al nanoparticles are absorbed by oxidizers of either nanorod or foam; while it has similar disadvantages to the sol-gel process, including high porosity which reduces the energy density, the presence of polymers that restrict the direct contact between components; and the high cost of custom-made oxidizers.

2.5.5 Arrested reactive milling

The design principle of nano-energetic materials suggests that the components should have an intimate contact to shorten the diffusion path. The preparation methods, especially for sol-gel and self-assembly shown in the above sections have drawbacks involving the porous structures that result in indirect contact, as well as the restriction of oxidizer types. Nanocomposites with fully dense structures formed via arrested reactive milling have been developed to increase the contact of components. As the literature has reported, several composites of Al/MoO_3 [68, 73, 75, 76], Al/CuO [12, 72, 74], Al/Fe_2O_3 [71, 84], and $Al_{0.5}Mg_{0.5}$/$NaNO_3$ [69] have been formed using ball milling method. Arrested reactive milling employs particles or mesh and mixes components using a steel ball and shaker mill to achieve inclusion into the matrix. The precursor materials used in arrested reactive milling are usually in micro-scale; it is not necessary to use nano-scale materials. The control agent of the organic solvent is added and mixed with powders to inhibit cold welding and partial reaction during milling. Due to the introduction of energy into the mixed system caused by mechanical shaking, the thermite reaction can be initiated and self-sustained. Therefore, the milling process is interrupted just before the self-sustained reaction occurrs to avoid the

ignition of the nanocomposite. Depending on the particle sizes, the ratio of components, the shake frequency, the size of the balls, the ball to powder mass ratio (BPR), etc., and the specific stage at which the milling process is interrupted fluctuates. The temperature was monitored with a thermistor attached to one side of the milling vial. The ignition signal can be seen from digital data marked by a sharp rise in vial temperature.

The method solves the problems of introducing impurities. However, arrested reactive milling has some limitations. One crucial issue is the presence of a fraction in composites, which is caused by the local reaction initiated by mechanical friction. The local reaction accounts for a small percentage of the entire amount, which cannot sustain further reaction. In addition, the safety issue must be considered in the process. The mixed particles are milled until the moment just before self-sustained ignition occurs, which may cause an explosion, damaging the processing equipment and facility. Furthermore, the particles are ground in an organic solution that can react with fuel components to reduce its active content.

2.5.6 Thermite nanocomposites with layered structures

Nanocomposites with layered structures have attracted much more attention in recent decades. Layered structures can be fabricated with specific thicknesses and multi-layered design and thus serve as useful tools in research. Thermite foils have been employed to study ignition characteristics, propagation behavior, and reaction mechanisms of nano-thermites [47, 48]. Meanwhile, nanocomposites with layered structures are suitable for many applications. For example, propellant configurations require a layered propellant with a

tailored burn rate [85]. Some literature [28, 29, 40] shows that initiators with layered structures are more easily combined with micro-chambers, which are used to ignite propellant as source of thrust. According to the literature, two primary methods used for the formation of nano-thermite compositions with layered structures are vapor deposition [47, 48, 79-81, 86-88] and electrophoretic deposition (EPD) [11, 89-91]. The vapor deposition process has been widely used in a variety of types of oxidizer or metal layers that have direct contact with either Al nano-layers or Al nanoparticles. The fabrication of nano-thermite thin film structures via EPD is only reported by a few groups that demonstrate the potential applications of energetic materials through mild fabrication conditions.

Vapor deposition can be divided into two categories, physical vapor deposition (PVD) and chemical vapor deposition (CVD), based on whether or not sequential particles are applied to start chemical reactions on the surface of substrates (in the case of CVD). Vapor deposition has broad applications in industrial sectors, for example in the semiconductor industry. In the deposition of energetic materials, the PVD category is further classified as electron beam evaporation [48, 80] and magnetron sputtering [47, 79, 86-88], whereas atomic layer deposition is in the CVD category [81].

The atomic layer deposition method has been utilized in the deposition of oxidizers as reported in previous research, including Co_3O_4 [92], WO_3 [93], and NiO [94]. Atomic layer deposition does not aim to accomplish the formation of nano-thermite composites, and there are no reports of successful deposition of Al nano-layers via atomic layer deposition.

However, it is an ideal process that is able to deposit oxidizer thin films with excellent uniformity and controllability of thickness, etc.

Ferguson et al. [81] reported the formation of a thin layer of SnO_2 on Al nanoparticles via atomic layer deposition. $SnCl_4$ and H_2O_2 are used as the particles, which are exposed to Al nanoparticles with a particular sequence within the temperature range of 250 °C and 350 °C following the reaction Eq. 2.1.

$$SnCl_4+2H_2O_2 \rightarrow SnO_2+4HCl+O_2 \qquad \text{(Eq. 2.1)}$$

Strictly speaking, the composite of Al/SnO_2 is not a layered structure at the microscopic scale; it features a core-shell structure. However, the structure can ensure intimate contact between reactants, resulting in violent thermite reactions. The drawbacks of the technology include the requirement for high temperature (250 to 350°C) that initiates the reaction, as well as the formation of HCl that can react with a passivized shell of Al_2O_3 that will prevent the thermite reaction.

In the PVD process, electron beam evaporation was used in the early stage for the deposition of multi-layered Rh/Si [48] and Al/Ni [80] as the energetic materials. The self-propagation explosive reaction of Al/Ni composites with a flame propagation rate of 4m/s was observed. Later on, the magnetron sputtering process was employed to deposit multi-layers. To gain a more efficient momentum transfer, the atomic weight of sputtering gas or electrons should be close to the atomic weight of the target. The sputtering, which uses an inert gas (mostly argon), replaces the process of electron beam evaporation to achieve a more efficient deposition.

Al/Ni [47, 79, 87] and Al/CuO_x [86, 88] multi-layers were formed via the magnetron sputtering process by alternating targets to fabricate different layers and repeat the deposition several times. The formation of CuO_x layers utilizes the reaction between Cu and oxygen in the chamber by infusing oxygen into the chamber and mixing it with argon. The thickness of individual bilayers varies from 25nm to 80nm for Al/Ni composites, which can reach 1μm for bilayer of Al/CuO_x. The total foil thickness can be 14μm.

Magnetron sputtering forms nanocomposites with multi-layered structures having immediate contact between reactive components. The Al nano-layers without passivation shell may lead to spontaneous thermite reaction if the thickness is less than 100nm [49]. The bare layers may cause unstable properties. Meanwhile, the costly device required limits the applications, and storage of composites is of particular concern.

Furthermore Sullivan et al. [11, 89] reported the formation of thin films on a conductive electrode via the EPD process. The Al and CuO nanoparticles were dispersed in ethanol to test the stability of the suspension. As reported by Sullivan, the suspension could not remain stable, and the mixture of water and ethanol was used to disperse CuO and Al for the deposition of the thin film. The nanoparticles were deposited on a platinum electrode sputtered onto a silicon wafer for the flame propagation measurement. The comparison between the samples formed with drop cast and EPD was conducted and showed a more homogeneous distribution in the sample that underwent the EPD process. Figure 2.6 shows the SEM image and elemental mapping of composites created via the EPD process.

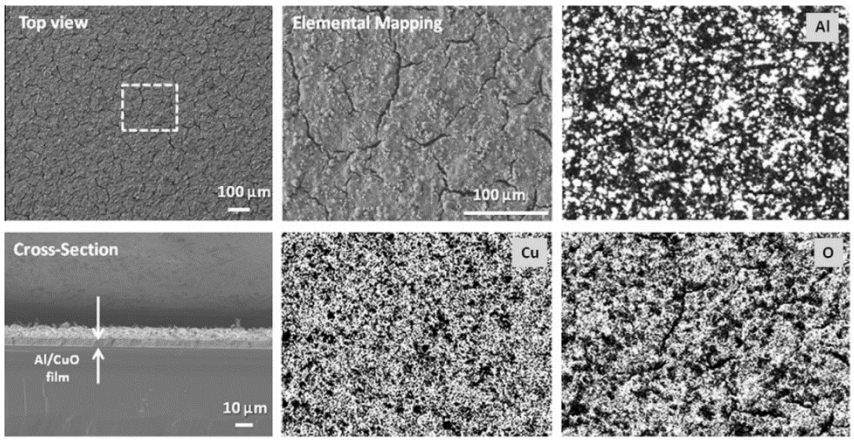

Figure 2.6 Scanning electron microscopy top and cross-sectional images of an Al/CuO thermite film prepared by EPD [89]

Meanwhile, Zhang et al. [91] reported the co-deposition of Al and Fe_2O_3 on nickel sheet. The sample with an equivalence ratio of 1.8 showed the optimum combustion properties, which were consistent with most of the results. However, the EPD process for co-depositing nanoparticles has apparent drawbacks. In practical applications, a free-standing structure is required to match the morphology of the equipment. The deposition on the conductive electrode can not be peeled off from the electrode without damage. Meanwhile, the increasing amount being deposited results in cracks on the sample due to the evaporation of the solvent. Furthermore, the ratio of deposited nanocomposites is not equal to the ratio in solution, which makes the process difficult to control.

2.5.7 Fabrication methods

Nano-composites can be fabricated via physical mixing, self-assembly, sol-gel, etc. Briefly speaking, physical mixing is the most straightforward fabrication technique, but suffers from

its small-scale operation and poor controllability. Self-assembly produces a controllable structure in the derived products; however, products are highly porous and have a low energy density. The sol-gel method is widely applied for the preparation of Al/Fe_2O_3 nanocomposites although impurities may be introduced and reduce the rate and level of energy release. In addition, it reduces the elemental diffusivity. Most importantly, these methods are not appropriate to form nano-thermite composites with multi-layered structure.

2.5.7.1 Electrophoretic deposition (EPD)

Electrophoretic deposition refers to processes of electrocoating, cathodic electrodeposition, anodic electrodeposition, and electrophoretic coating (electrophoretic painting). The colloidal particles, which are dispersed and suspended in a liquid solvent, can form double charged layers caused by the polar medium. The particles are able to migrate towards the corresponding electrode when an electric field is applied, and are deposited on the surface of the electrode. Meanwhile, the surface electric charge of particles provides a repulsive force that makes the solution stable without the precipitation of particles. The EPD process is a complex process involving many parameters that determine the deposition on electrodes, which provides versatility in the industrial sectors. Basically, the negatively charged particles can be deposited on positive electrodes, whereas positively charged particles deposit on the opposite electrodes. The schematic view illustrating the EPD process is shown in Figure 2.7.

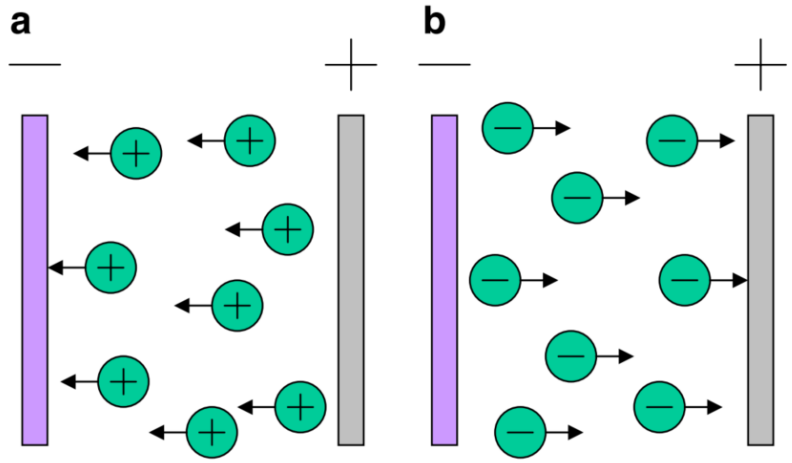

Figure 2.7 Schematic view of the EPD process showing (a) Cathodic deposition; and (b) Anodic deposition [95]

2.5.7.2 Vacuum filtration (VF)

The EPD process provides several advantages for the formation of thin layers and the investigation after the thermite reaction has occurred. These advantages include the tunable thickness of the layer, simple apparatus requirements, and electrodes serving as the supports for the thin film to avoid cracking. However, the types of oxidizers that can be deposited on conductive electrodes restrict the EPD process. For example, the experimental results show that CuO (40nm) cannot be deposited via the EPD process without a surfactant and additive, which introduces impurities that reduce the degree of contact between reactive components. Therefore, an alternative method to form different types of oxidizer layers is selected. Unlike the EPD process in which the particles must be charged with the proper surface morphology, pH value, and type of solvent, etc., vacuum filtration does not require stable solutions. It is the extension of physical mixing in which the solvents are evaporated to leave the nanoparticles. However, the vacuum filtration method can deposit any oxide nanoparticles

and Al nanoparticles, and can be used to form nano-thermite composites with layer-by-layer structure. The thin film for the application attempt formed with vacuum filtration allows for a controllable amount of nanocomposites, and a safer preparation. Meanwhile, the shortened duration of exposure to the air atmosphere decreases the spread of nanoparticles into the air, which provides a safer experimental environment.

2.5.8 Summary

The previous techniques used for the fabrication of nano-thermite composites have been summarized. The synthesis methods, formed structure, and disadvantages are shown in Table 2.4. The structures are essential to investigate the reaction mechanisms due to the indirect contacts between reactants. However, the previous fabrication methods have disadvantages that limit further investigation.

Table 2.4 Summary of previous preparation methods

Synthesis	**Formed structure**	**Disadvantages**
Physical mixing	Powders	Non-uniform distribution; exposure for a long time in the air causes severe oxidation
Sol-gel	Monolithic bulk	Porous structure; long preparation cycle; difficult control in preparation; impurities; restricted in the type of hydrated salt
Self-assembly	Monolithic bulk	Porous structure, long preparation cycle, impurities; restricted in the type of hydrated salt
Arrested reactive milling	Powders	Dangerous; high temperature during milling may cause oxidation
Magnetron sputtering	Multi-layers	High cost for devices; storage difficulties; no passivation shell leading to in-situ reaction
Electrophoretic deposition	Thin film	Not a free-standing structure, difficult to control

2.6 Characterization of nanocomposites

The relevant literature on the characterization of nano-thermite composites is reviewed in this section.

2.6.1 Aluminum nanoparticles

2.6.1.1 Particle size and active content of Al nanoparticles

First of all, the Al nanoparticles have a natural aluminum oxide shell serving as the passivation agent, which prevents further oxidation of the aluminum active core. The particle size and active content of Al nanoparticles have dramatic effects on the energetic properties of nano-thermite. Furthermore, the particle size distribution, surface morphology, and the aluminum oxide state (amorphous, γ, or α-Al_2O_3) also influence the interfacial contact and the penetration of elements through aluminum oxide, which are taken into account in the characterization of aluminum nanoparticles. On the other hand, these factors such as size distribution and morphology cause difficulties in evaluating the effects of energetic properties. The average particle size and spherical morphology are considered in practical applications to estimate the average amount of energy release, burning rate, and ignition temperature. The ignition temperatures of thermite composites with nano-scaled structures are lower than the phase transfer of Al_2O_3. For the reasons above, this thesis does not consider the effect of particle size distribution, surface morphology, or phase change of Al_2O_3, which are only reviewed in the section to provide knowledge into the characterization of aluminum nanoparticles. The particle size is regarded as the average size specified by the suppliers.

The particle size and active content are the key factors that determine the energetic properties of nano-thermite. Generally speaking, increasing the particle size reduces the reaction rate due to the reduction of surface area to volume, which decreases the surface contact between reactants. The development of electron microscopy provides a straightforward technology in the characterization of particle size, although it is labor intensive to observe different locations for a large number of particles. The most common

characterization of particle size is via specific surface measurements [1]. Usually, a Brunauer–Emmett–Teller (BET) measurement is applied through surface gas adsorption to obtain the particular area information. Finally, the active surface area can be translated to the average particle size [96].

The aluminum oxide shell reduces the active content, which decreases the fuel supply component in a thermite reaction. Information covering aluminum oxide thickness, crystallization, microstructure, and homogeneity of the oxide layer is critically important for understanding the mechanisms of metal nanoparticle oxidation. In turn, the mechanisms of oxidation affect both ignition and inetics of nanocomposites [97]. The thickness and microstructure can be investigated with high-resolution TEM as shown in Figures 2.8 and 2.9.

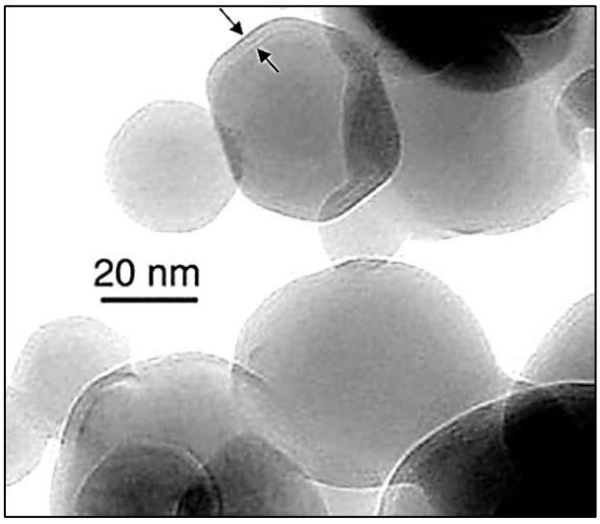

Figure 2.8 High-resolution TEM image showing Al nanoparticles with aluminum oxide shell [98]

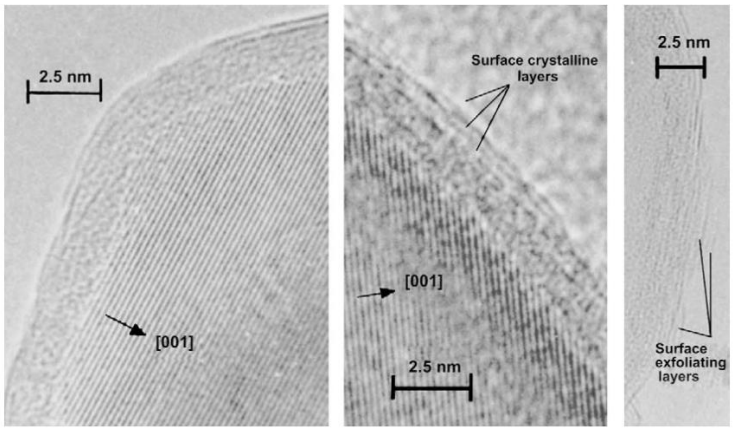

Figure 2.9 High-resolution TEM (HF TEM) images giving information on the microstructure of the Aluminum oxide shell with different crystallization status [97]

The conventional thinking is that the Al oxide shells are crystalline in structure. However, recent research shows that the amorphous aluminum oxide film, up to a certain critical oxide-film thickness, and even for high oxidation temperatures, can be thermodynamically rather than kinetically more stable than the corresponding crystalline γ- Al_2O_3 film [99]. The amorphous phase of aluminum oxide presents in stable status at the outside of aluminum core. The thickness of the shell is usually 2 nm to 3 nm [100], but can be extended to 0.5 nm [101] to 4 nm [99].

Although high-resolution TEM imaging can provide the specific thickness information of Al nanoparticles in one spot, the thicknesses of Al_2O_3 passivation shells are different from each other, and even by combining the particle size distribution data, the error rate in estimating active content is considerably large. The distinct shapes of particles and the density difference between different phases of Al_2O_3 are also difficult to ascertain. The

thermodynamics research into oxide film thickness exhibits the thermodynamically stable phase of amorphous Al_2O_3.

The active content of Al nanoparticles can be determined via thermogravimetric analysis (TGA) heating of nanoparticles in air atmosphere until there is no further increase of mass. The active content can be calculated from the mass change caused by oxidation of Al. The accuracy of TGA is considerably better than high-resolution TEM, although it still has drawbacks that affect accuracy, such as the absorption of gas on the surface of nanoparticles and incomplete oxidation due to a fast heating rate.

2.6.1.2 Ignition of Al nanoparticles

This section describes the ignition of Al nanoparticles with oxygen. A wide range of heating rates are applied to ignite Al nanoparticles, including the order of 50 °C/min for the low heating rate and 10^6 °C/s for the high heating rate. The ignition temperature of Al nanoparticles is measured using TGA/DSC for the low heating rate. The ignition temperature depends on particle size, near the melting point of Al_2O_3 (2327 K) for more massive particles and much closer to the melting point of Al (933 K) for smaller particles [4]. TGA/DSC is used for the thermal analysis of ignition temperature and phase transformation of Al_2O_3 as shown in Figure 2.10. The Al_2O_3 shell undergoes a phase change from amorphous oxide, passing through γ, δ, and θ- Al_2O_3, to α-Al_2O_3.

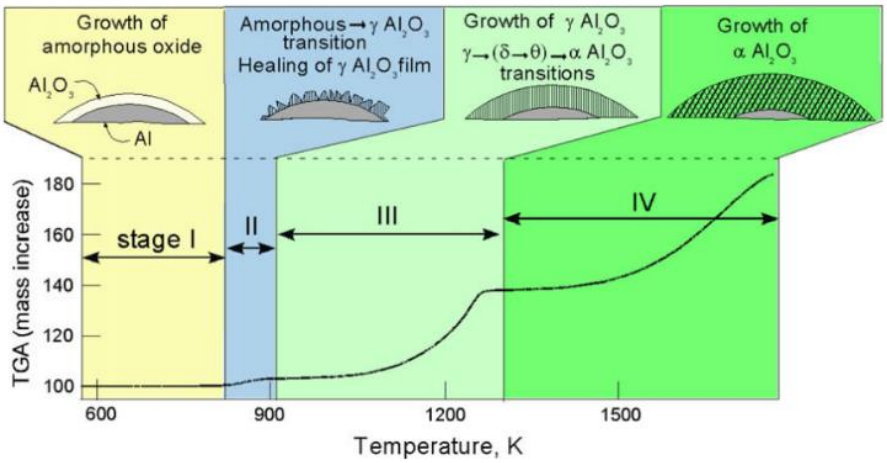

Figure 2.10 Phase change of the Al_2O_3 passivation shell as a function of temperature [97]

When using nanoparticles, two main regimes can describe the thermite reaction [102]. The slow oxidation regime at a temperature lower than the melting point of aluminum is the primary reaction mechanism whereby oxidation is the diffusion of oxygen through the oxide shell. On the other hand, the fast oxidation regime features the diffusion of both aluminum and oxygen at temperatures above the melting point of aluminum. The rupture of an oxide shell may cause reaction rate enhancement. The dynamic reaction surface can be seen in Figure 2.11.

In the slow reaction regime, oxygen diffuses through the oxide shell to reach the aluminum core, which leads to the growth of the oxide shell from the surface of the aluminum core. In the fast reaction regime, both melting aluminum and oxygen diffuse through the oxide shell, which form a dynamic reaction surface to result in the growth of aluminum oxide.

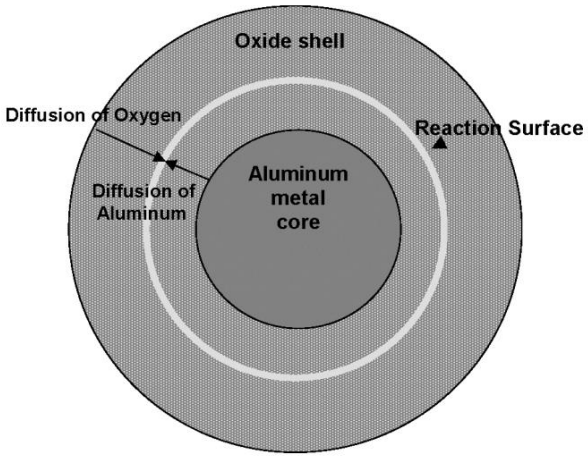

Figure 2.11 Schematic view of aluminum core and shell, dynamic reaction surface [102]

The ignition event, which occurs at a high heating rate, can be studied by recording the signs of ignition, using methods such as optical emission [84]. The details of igniting particles at high heating rates will be discussed in later sections covering the ignition of nanocomposites. There are two ignition mechanisms of Al nanoparticles with high heating rates, which still are being studied and have not been elucidated clearly. The two ignition mechanisms are: diffusion and melt dispersion, and each is supported by different research groups.

The diffusion mechanism [102-105] suggests that the high heating rate makes aluminum melt and expand to cause mechanical stress on the Al_2O_3 shell, and the melted Al diffuses outwards through the Al_2O_3 shell. In contrast, the melt dispersion mechanism [106, 107] claims that the volumetric expansion of melted Al produces significant stress that can cause rupturing of the Al_2O_3 shell. Then, the Al molten cluster ruptures from the core at high velocity. No agreement on the Al oxidation mechanism under high heating rate is achieved due to the technical limitations that are not capable of investigating rapid change.

2.6.2 Nano-thermite composites

2.6.2.1 Reaction of nanocomposites

During the reaction of Al and oxygen, oxygen diffuses through the Al oxide shell and reaches the Al active core below the melting point of Al (~933K). Another mechanism for oxidation occurs after reaching the melting point is the diffusion of molten Al outward from the Al particles. The mechanism of Al and O_2 describes the solid-gas reaction. The solid-solid reaction occurs with more intimate contact between reactants and also implies more complex reaction mechanisms depending on the type of oxidizers used. As mentioned in the previous section, particle sizes of less than 100nm can undergo the thermite reaction before reaching the melting point of Al, which indicates a solid-solid chemical reaction as being the reaction mechanism, without involving molten Al. The oxidizers (so far, it is not clear whether the oxidizers remain inert until the moment of ignition or whether they decompose before the ignition of nanoparticles) diffuse through Al oxide and reach the aluminum core. The reaction mechanism determines the initiation process of nanocomposites and controls combustion propagation, pressurization, and gas generation.

Research into traditional thermite using micro-sized particles based on different types of oxidizers has been conducted [108]. The oxidizers were divided into two main classes based on chemical stability, characterized by differential thermal analysis (DTA) measurements: 1) chemically stable and 2) chemically unstable. Class 1 was further divided into two subclasses based on physical stability: 1-1) physically stable and 1-2) physically unstable. Class 2 can

be divided into two subclasses: 2-1) oxidizers that decompose with the liberation of oxygen upon heating and 2-2) oxidizers that are oxidized further into higher oxides upon heating in an air atmosphere. Class 1-1 includes NiO, TiO_2, Cr_2O_3, Al_2O_3, Ta_2O_5, and Nb_2O_5, showing neither exothermal nor endothermic processes in the DTA results. Class 1-2 involves evaporation or sublimation of oxidizers, including B_2O_3, MoO_3, and WO_3, and shows an endothermic process belonging to the evaporation of oxidizers. The oxidizers V_2O_3, CrO_3, Li_2O_2, and BaO_2, which are included in class 2-1, undergo decomposition and release oxygen. FeO and CuO in class 2-2 are oxidized in air atmosphere upon heating, which produces heat that may help in the ignition of thermite composites. The author of the above discussed the properties of different oxidizers that affect the ignition mechanism of thermite composites. However, the thermites with nanoparticle components have anincreased surface area to volume ratio, and thus exhibit different thermochemical properties compared with micro-sized particles, and these thermites are poorly understood. The difficulties in understanding the reaction mechanism of nano-thermite composites are due to the network structure of nanocomposites, which shows no direct observation to demonstrate the decomposition and diffusion through the aluminum shell. Several research projects [44, 45] have been conducted to investigate the reaction mechanism by measuring the pressure and optical signal in a combustion cell with Ni coil ignition and two ports (one is a high-speed Si photodetector, and another is a piezoelectric pressure sensor) located on the sides of the cell.

The reaction mechanism of nanocomposites is challenging to understand, and is the subject of considerable debate due to the complex reaction mechanisms under different heating rates.

After ignition has occurred by introducing sufficient energy, called activation energy, the nanocomposite undergoes self-sustained flame propagation, where the heat produced by the thermite reaction ignites the next local area of the nanocomposite. A rough estimate of this heating rate is system-dependent and has been speculated to be anywhere from 10^4-10^8 K/s [4]. The ignition condition can be reproduced under the heating rate, and it is a critical challenge to obtain uniform heating under the high heating rate. Meanwhile, the triggering moment of ignition is difficult to observe directly, and reproducing the ignition temperature does not match the specific system. The efforts to produce a high heating rate were made to investigate the ignition of nanocomposites.

Laser ignition was applied by researchers to provide a high and adjustable heating rate on the order of 10^6-10^7 K/s by several groups [109-112]. The heating rates can exceed 10^9K/s in some of the works [113-116]. The reaction of samples can be collected using a high-speed camera and thermocouples by recording the optical signals. As an example of using laser ignition, Al/MoO_3 nanocomposites were physically mixed and compressed into a pellet, and then ignited with a 50-W CO_2 laser, coupled with a high-speed camera and thermal pyrometer [117]. However, some issues make the interpretation of laser ignition experiments difficult. The consistency of prepared samples and the difference in efficiency of absorption of the laser by different material components cause them to heat at very different rates.

An alternative to heating nanocomposites with high heating rates on the order of 10^5~10^6 K/s is to use a shock tube [84, 118, 119]. The nanocomposites of Al/Fe_2O_3 and Al/MoO_3 prepared using arrested reactive milling are located near the end of the tube, where an

incoming shock wave lifts and disperses it. The shock wave then is reflected by the wall and heats the particles quickly to cause combustion of the nanocomposites. The ignition temperatures of Al/Fe_2O_3 and Al/MoO_3 composites are 1400 K and 1800 K, respectively, which are significantly higher than the melting point of Al [84].

Another technology that can provide high heating rates of nanocomposites involves coating nano-thermite onto thin platinum or nichrome filament or wire, which can be heated electrically [12, 71, 73]. The heating rate, on the order of 10^2-10^5 K/s, is recorded with a pyrometer focusing on an uncoated filament surface adjacent to the powder coating. The optical emission is the onset of ignition measured with a high-speed camera. This heated filament method offers the advantage of heating samples uniformly.

2.6.2.2 Combustion properties of nanocomposites

The most common method to investigate the reaction kinetics of nano-thermites is to collect data on flame propagation rates. The burning rate reflects the combustion properties combining the energetic properties, reaction mechanism, and propagation mechanism, including the onset temperature, energy release amount, energy release rate, ignition delay, and energy propagation. The design principle of using nanoparticles requires a high burning rate to compensate for heat loss when the method is applied to a small area. The flame propagation velocity has been measured by electric conductivity [120] and high-speed cameras. The nanocomposites are ignited and combusted in various sample configurations, such as open channels [19, 62, 121-123], cylindrical tubes [8, 124], and microchannels [20].

As discussed above, nanocomposites undergo self-sustained reactions upon ignition. The energy released by the thermite reaction is transferred to the subsequent local area and ignites it. Four possible propagation mechanisms have been described: thermal conduction, convection, radiation, and acoustic/compaction. Acoustic/compaction is considered to be the mechanism for detonations, and is not essential for nanocomposites [4]. Energy transfer conducted by radiation transfer is possible, but is a relatively small contribution compared to convection [4, 125]. Al/MoO_3, Al/WO_3, Al/CuO, and Al/Bi_2O_3 were tested under loose powder and packed conditions, and showed reduced propagation rates under the packed condition [8, 55]. The author concluded that convection flame propagation mechanism was dominant in the transfer of energy in low density samples.

In comparison with loose powders, packed samples have less gas between particles, which leads to small amounts of gas being heated up rapidly and expanding to transfer energy at a high rate. The thermal properties of the loosely packed or even pressed nanocomposites are poorly quantified. The intervals produced with loose or loosely packed samples lead to no direct contacts between local areas, and this hinders the heat transfer when the flame front moves forward. On the other hand, the expanded gas may damage the quality of results in some of the applications, such as those requiring gasless products in joining purposes. The fully condensed composites [47, 86] with nano-layered structures, generally formed with magnetron sputtering as mentioned above, were achieved to reduce the convection flame propagation mechanism, and this is compatible with the MEMS system [2]. Research exploring Al/CuOx multi-layer composites with combustion rates of 1.5m/s and 1m/s,

substantially slower than that of using powder ignition, has been conducted [86, 126]. As observed in previous research [55], the convection mechanism dominated the flame propagation in nanocomposites having relatively loose structures. The nanocomposites with layered structure have no interval between layers; therefore no heated gas is available to help transfer energy via convection to dramatically increase the flame propagation rate. However, nanocomposites with layered structures of Al/CuO and Al/Ni multi-layers have been reported, and no other research has reported other composites deposited with a sputtering process. As mentioned above, based on different types of oxidizers, the reaction mechanisms determine whether there is oxygen release, and Al/CuO and Al/Ni are the types of composites that release small amounts of gas. Whether the convection flame propagation mechanism is caused by the gas that exists in the interval of samples or whether the oxygen is released by the decomposition of oxidizers is poorly understood.

2.6.2.3 Thermal analysis

Thermal analysis can provide the onset temperature, energy release, and multi-step reaction. In most cases, the combination of differential scanning calorimetry (DSC) and thermogravimetric analysis (TGA) is used to record the endothermic and exothermic reaction coupled with mass change caused by oxidation or decomposition, etc. The samples under thermal analysis can receive uniform heating. XRD analysis can be used at the same time to provide information about phase change under different temperatures. The nanocomposites Al/CuO and Al/MoO_3 are prepared and analyzed with DSC and XRD to investigate the multi

reactions [12, 73]. It is worthwhile to mention that thermal analysis can test the degree of interfacial contact by measuring the ignition temperature and energy release, and it can also give a low heating rate. Thermal analysis can help researchers interpret the reactivity of nanocomposites and the initiation of nanothermite composites under low heating rates. The results from the thermal analysis, however, can not explain the ignition mechanism under high heating rates.

2.6.3 Characterization methods

2.6.3.1 X-Ray Diffraction (XRD)

X-Ray Diffraction (XRD) is the common technique to investigate the crystalline phases of samples; it uses diffracted X-rays to collect information for both reactants and products. In brief, the crystalline phases in the samples can be detected when they possess periodicity in their atomic structure. The constructive interference of diffracted X-rays can identify the atomic arrangement of samples, also known as the crystal lattice. The works are based on the Bragg's law as shown in Eq. 2.2:

$$n\lambda = 2dsin(\theta) \qquad \text{(Eq. 2.2)}$$

Where λ is the incident X-ray wavelength. d and θ are the planar spacing of the crystalline phases and incident angle, respectively. Therefore, Bragg's law measures the relationship between incident radiation and planar distance, which is able to identify the specific crystal phase. An incident of X-rays irradiate the sample, and the rays are reflected by the atoms. The path difference of X-rays reflected by the several lattice planes changes

when the X-rays sweep with various angles of θ. With the satisfaction of Bragg's law in which the path difference of two X-rays is equal to the integral multiple of the wavelength, the detector can receive a strengthened intensity of X-rays, which shows the peak in the result. Typically, the X-rays sweep along the surface at various incident angles. A detector collects the diffracted X-rays and measures the intensity. With the known λ and θ, the planar distance *d* can be determined, which corresponds to the specific type of samples.

The nanoparticles used in this thesis are formed as crystalline structures, which can be detected using X-ray diffraction. XRD can provide information on the crystal phases of both reactants and products, which confirms that the thermite reaction has been conducted. Meanwhile, it is able to test whether the thermite reaction is a multi-step reaction and if the intermediate phases have formed.

2.6.3.2 Thermogravimetric Analysis (TGA)

TGA is a device that uses a sensitive scale that can detect the mass change of samples undergoing reaction. The programmable heating furnace to heat samples in the crucible is installed with a TGA device. The TGA device can test the increase of mass caused by the absorption of surrounding gas, such as the oxidation behavior. The sensitive scale can also detect the mass decrease of the sample caused by the decomposition to release the gas phase to the surrounding environment. In this thesis, the TGA instrument used is coupled with a DSC device that will be introduced in the next section. Due to the presence of the Al_2O_3 shell, the active content of Al nanoparticles must be measured. Meanwhile, the procedure of

preparing nano-thermite composites exposes the Al nanoparticles to the air, or forms contact between Al nanoparticles and an organic solvent. It is necessary to measure the active content before and after the preparation procedure. The reaction between Al and O_2 can increase the entire mass of the samples, which provides the information used to calculate the active content of Al nanoparticles. The details of the calculations will be shown in later chapters.

2.6.3.3 Differential Scanning Calorimetry (DSC)

DSC is a useful tool to measure the heat flow through samples. When a reaction occurs in a sample, it usually releases or absorbs energy, which corresponds to an exothermic or endothermic reaction. The samples need to release or receive energy from the surrounding environment, which causes heat flow that can be detected by the DSC device. The DSC device compares the reference sample and the unknown sample to provide quantitative information on the energy absorption or release of the unknown sample. The TGA/DSC device used in this thesis is shown in Figure 2.12.

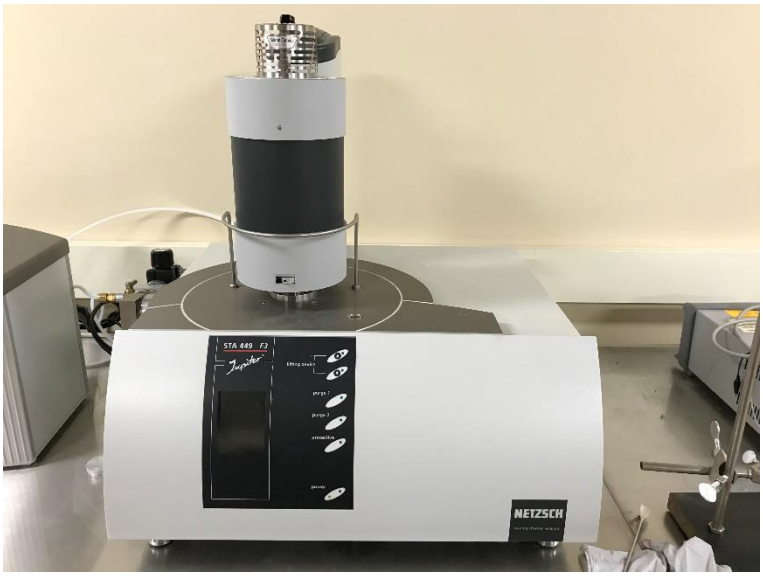

Figure 2.12 TGA/DSC device in our lab

Furthermore, the DSC device can provide information about the onset temperature and the peak temperature of a reaction. It is important to measure the onset temperature to providing information on the ignition mechanism, and the peak temperature for calculating the activation energy in reaction kinetics. The details of the DSC data will be presented in later chapters.

2.6.3.4 Scanning Electron Microscopy (SEM)

SEM is a valuable tool to investigate the surface morphology and elemental contrast of samples. It provides excellent resolution to see the nanoparticles in detail. The electron beam generated in the SEM device interacts with the surface of samples using different types of electron beams. The two main types of electron beams produced by the samples are secondary electron beam (SE) and back-scattered electron beam (BSE). Generally, the SE

detector is mounted on the side of the chamber, whereas the BSE detector is mounted on the top of the chamber. The SE possesses less energy and is affected by the electric field that restricts the SE flight to the top area. However, the BSE has a higher energy that can fly to the head area and be received by the BSE detector.

The former beam reflects the surface morphology of the sample, whereas the latter electron beam carries the information on atomic weight. The samples must be conductive to eliminate charging on the sample surface. If they are not conductive, they must be treated with conductive coating, such as gold or carbon.

In this thesis, the SEM apparatus is used to measure the layered structure of samples composed of Al and oxide nanoparticles. The SE beam shows the cross-section morphology, whereas the BSE beam reflects the elemental contrast. In the BSE signals, the heavier elements show as brighter images on the screen. Therefore, the latter beam clearly shows the different layers in the cross-section of the samples. Due to the non-conductive nature of Al and oxide nanoparticles, gold was coated onto the cross-section of the samples. Furthermore, the magnification of images can reach up to 100,000 times in this thesis, which shows the morphology of nanoparticles and products after the thermite reaction. Overall, the SEM instrument provides information on the morphology of the cross-section and the detailed morphology of nanoparticles and products.

2.6.3.5 Energy Dispersive X-Ray Spectroscopy (EDS)

EDX is a powerful characterization technique coupled with SEM analysis. The X-rays are generated as part of the primary electron interaction with the sample surface. The primary electrons irradiate the surface of the sample, which forms electrons with a lower level of energy. When the formed electrons eject the higher energy electrons, the electrons with lower energy level fill the holes of ejected electrons at the same time that the X-rays form as part of this transition from higher energy level to lower energy level. The wavelength of the X-rays corresponds to the specific energy unique to particular elements, which provides both the identity and relative abundance of each element in the composition..

EDX can provide qualitative information on the types of elements. However, it can estimate the relative abundance with low accuracy in the quantitative analysis due to various factors. First of all, the X-rays generated are emitted in all directions. In addition, they may not all escape from the samples. It can be said that the accuracy of the quantitative analysis depends on the energy of the X-rays, the composition, amount, and density of materials. For these reasons, the EDX method used in this thesis aims to provide qualitative information on the elements' distribution, and only a semi-quantitative analysis. This means that the quantitative information serves as a reference.

In this thesis, EDX provides information coupled with SEM images to show the multi-layered structure and the distribution of elements throughout the layers. The distribution of elements is detected in the samples before and after the thermite reaction, which shows the positional change of the elements. Coupled with TGA/DSC and SEM images, the migration of elements measured using EDX shows the thermite reaction process, which reflects the

reaction mechanism during the thermite reaction. The details of the application of EDX will be shown in later chapters.

2.6.3.6 Microhardness

Indentation hardness refers to determining the hardness of materials with respect to deformation. Microhardness is one type of indentation hardness that has been widely used in the literature to describe hardness testing with low applied loads. In the measurement, a certain force through a diamond indenter of a specific geometry is applied to the surface of a sample. The hardness on the microscopic scale can be observed using microhardness testing.

Microhardness testing measures the hardness of the welding zone of silicon wafers. One application of nano-thermite composites is to weld small and brittle parts by providing a local heat source. Actually, the best way to investigate the joint quality is to test the tensile strength. However, due to the brittle and small nature of silicon wafers, the tensile strength test cannot be conducted. The clips holding the silicon wafers damage the parts before loading is applied. To investigate the joining quality, we conducted microhardness testing for the welding zones welded with various nano-thermite composites. Due to the narrow welding zone (~ 30 μm) microhardness testing is employed to measure hardness on the microscopic scale.

2.6.4 Reaction kinetics

In this thesis, the application of using nano-thermite composites to weld two silicon wafers is conducted. Thermodynamics and reaction kinetics affect the joining quality and

microstructure of the welding zone. The energy release and reaction rate determine the energy that can be received by the welding zone to form an interfacial connection between the two silicon wafers. The welding experiments were conducted at room temperature without a pre-heating process. The reaction rate becomes essential due to the heat loss effect on the surrounding environment. The energy release can be measured directly using a DSC device as mentioned in the last section. However, the evaluation of the reaction rate cannot be tested directly by using instruments. The reaction rate can be expressed with the equation described by Borchardt and Daniels [127, 128].

$$\frac{da}{dt} = k(T)[1-a]^n \qquad \text{(Eq. 2.3)}$$

Where $k(T)$ and n are specific rate constants at temperature T and reaction order, respectively. Furthermore, $k(T)$ can be expressed with the following equation [128].

$$k(T) = Ze^{-\frac{Ea}{RT}} \qquad \text{(Eq. 2.4)}$$

Where Z and Ea are the pre-exponential factor and activation energy. R is the gas constant (8.314 J/mol K). Eq. 2.5 can be deduced by substituting Eq. 2.3 into Eq. 2.4.

$$\frac{da}{dt} = Ze^{-\frac{Ea}{RT}}[1-a]^n \qquad \text{(Eq. 2.5)}$$

The reaction rate is one of the composite properties, which is related to the apparent activation energy. Estimating the apparent activation energy is essential in evaluating the reaction kinetics of thermite composites. It should be noted that the apparent activation energy is calculated in this work. The activation energy means the barrier at which the reaction can be initiated. However, the thermite reaction includes a mass and heat diffusion process, which is not the reaction between chemical compositions. Therefore, the apparent

activation energy is appropriate to determine the reaction kinetics in the thermite reaction. The Kissinger method is applied in the evaluation of the apparent activation energy [128]. Then, Eq. 2.6 can be deduced by differentiation of Eq. 2.5.

$$\frac{d}{dt}\left(\frac{da}{dt}\right) = \frac{da}{dt}\left[\frac{E\frac{dT}{dt}}{RT^2} - Zn(1-a)^{n-1}e^{-\frac{Ea}{RT}}\right] \qquad \text{(Eq. 2.6)}$$

At the peak temperature, the maximum reaction rate is achieved. Therefore, $\frac{d}{dt}(\frac{da}{dt})$ is equal to zero. The following equation can be obtained.

$$\frac{E\frac{dT}{dt}}{RT^2} = Zn(1-a)^{n-1}e^{-\frac{Ea}{RT}} \qquad \text{(Eq. 2.7)}$$

The Kissinger approach assumes that $n(1-a)^{n-1}$ is irrelevant to a heating rate and approximately equal to one. Eq. 2.8 can be expressed in Eq. 2.7.

$$\frac{E\frac{dT}{dt}}{RT^2} = Ze^{-\frac{Ea}{RT}} \qquad \text{(Eq. 2.8)}$$

Then, the following equation can be yielded from Eq. 2.8 by taking the logarithm of both sides [128].

$$\ln\left(\frac{\beta_i}{T_{Pi}^2}\right) = \ln\left(\frac{ZR}{E_a}\right) - \frac{E_a}{RT_{Pi}} \qquad \text{(Eq. 2.9)}$$

Where, β is the heating rate, equal to $\frac{dT}{dt}$. According to Eq. 2.9, the apparent activation energy *Ea* can be calculated with the slope of $\ln\left(\frac{\beta_i}{T_{Pi}^2}\right)$ *vs* $\frac{1}{T_{Pi}}$.

Using the peaks in the DSC results and the calculation, the apparent activation energy for each nano-thermite composite can be obtained. Based on the specific energy release and reaction rate of nano-thermite composites, this provides the welding zone with different qualities, which helps in the preparation of the proper nano-thermite composites for future applications.

2.7 Applications of nano-energetic materials

Metastable intermolecular composites (MICs) have been used in a wide range of applications, such as propellants [53, 85, 129-132], pyrotechnics [133], microinitiators [28, 29, 40], gas for actuation [30, 134-136], gas for chemical reactions [32, 137], and micro-joining [138-140]. Nanocomposites are used for different purposes based on their energetic properties. One of the typical nanocomposites used for propellants and micro-thrusters is the combination of Al, ammonium perchlorate (AP), and hydroxyl-terminated polybutadiene (HTPB), where AP serves as the oxidizer and HTPB works as the binder. The nano-sized Al nanoparticles were mixed with an oxidizer and improved the burning rate and stability as reported [129]. The particle sizes of AP in the reported literature remain at a micro-size level that reduces the entire combustion rate.

Typically, solid propellants have been used for rocket boosters, and in conjunction with MEMS technology to fabricate micron or millimeter-scale devices that provide thrust. These devices are composed of three main parts: combustion chamber, igniter, and propellant. In general, polysilicon resistors are doped to create the igniter. An easier fabrication method is required to produce the fuel ignition components for the devices. The solid-phase and conductive fuels are prepared and then combined with micro-electrodes in the chamber that can allow the current passing through the fuel foil to ignite the fuel uniformly. Graphite additive makes the propellant conductive, and 20% of the additive by volume enabled conventional composite-type propellants to become conductive [29]. The drawback of the initiator is apparent as the conventional propellant produces gas phase can damage the

propellant before ignition occurs due to the presence of an ignition delay for most of the solid energetic materials, which leads to unreliable and uncontrollable reactions. Another research work studied the formation of Au/Ti nanocomposite as an initiator for the replacement of a wire igniter in micro spacecraft, and showed improvement in the total impulse [40]. The Au/Ti double-layered structure was formed with electron beam evaporation that required a high device cost.

2.8 Summary

The review of the fabrication, characterization, and application of MICs is included in this chapter. The fabrication technology describes the preparation methods used to mix fuel and oxidizer to form homogeneous composites. Physical mixing and arrested reactive milling fabricate the combination with powdered materials, in which the former uses nanoparticle components and the latter employs the microparticles. Sol-gel and self-assembly are similar to each other when the salt components are applied. The only difference between the two technologies is that the surfaces of the nanoparticles are functionalized for absorption to obtain a more uniform structure in self-assembly. An alternative to using oxidizer nanorods in self-assembly is to functionalize the surface of oxidizers, which can absorb Al nanoparticles. The monolithic gel with porous structure can be formed using these two methods. Sputtering and EPD process enable the formation of nanocomposites with layered structures that are suitable for the applications of ignition and micro-joining. The summary of the fabrication, characterization, and application is shown in Table 2.5.

Table 2.5 Summary of fabrication, characterization, and application

	Methods	Specification
Fabrication	Physical mixing	Powder structure
	Sol-gel	Porous structure
	Self-assembly	Porous structure
Fabrication	Arrested reactive milling	Condensed structure
	Sputtering	Multi-layers structure
	EPD	Thin-film structure
Characterization	TGA/DSC	Thermal analysis
	SEM	Microstructure
	EDAX	Elemental mapping
	XRD	Phase analysis
	High-speed camera	Reaction kinetics
Application	Propellant	Propulsion resource
	Pyrotechnics	Propulsion resource
	Initiator	Ignition
	Micro-joining	Heat resource

Chapter 3: Layered nano-thermite composites with EPD process[1]

3.1 Overview

Thermochemical properties and microstructures of layered aluminium (Al) and iron oxide (Fe_2O_3) nano-thermite were investigated via thermogravimetric analysis (TGA), differential scanning calorimetry (DSC) and scanning electron microscopy (SEM) for developing a new type of metastable intermolecular composites (MIC). The nanoparticles of Al and Fe_2O_3 were dispersed in solution and deposited separately on stainless steel electrodes by means of the electrophoretic deposition (EPD) process. These nanoparticles were dispersed and deposited without any surfactant and additive, which eliminates potential contaminates in products. In order to produce layered structures, nanoparticles were deposited in a sequence which promotes effective bonding between two different types of nanoparticles. SEM images demonstrate a layered structure with the intimate contact between Al and Fe_2O_3. DSC data was collected to characterize the onset temperature and energy release per unit mass from the layered composites with different molar ratios of Al/Fe_2O_3. It is revealed, based on the consistent onset temperatures from different composites, that the ignition of Al and Fe_2O_3 layers is closely associated with oxygen which is produced from thermal decomposition of Fe_2O_3. In addition, the thickness of the reaction zone is restricted by the diffusion length of oxygen across the layer-to-layer interface, which results in a varying degree of reaction

[1] Chapter 3 has been published in the journal. The publisher provide the right to include it in a thesis or dissertation [149].

completion within the composite and subsequently the distinct energy release values per unit mass. The decomposition of Fe_2O_3 nanoparticles, diffusion path of oxygen and interfacial contact between Al and Fe_2O_3 layers are found to determine the energetic properties of layered thermite composites.

3.2 Introduction

This study focuses on the microstructure and thermochemical properties of Al/Fe_2O_3 thermite system. Among a variety of thermite systems, Al/Fe_2O_3 composite has been widely researched for developing propellants [141], explosives [142], free standing heat source [143], airbag ignition material [144], and welding torches [145], etc. In comparison with other thermite systems such as Al/NiO with the reaction enthalpy of 3.44 kJ/g and Al/WO_3 with the reaction enthalpy of 2.91 kJ/g, Al/Fe_2O_3 composite exhibits a greater reaction enthalpy (3.95 kJ/g) and has been considered as a very attractive source for localized heating [23]. Meanwhile, the adiabatic temperature of the Al/Fe_2O_3 thermite reaction is only 113 °C above the boiling point of iron, which possibly facilitates the gasless energy production [23].

The objectives of this study are, 1) to fabricate and characterize the microstructure of layered composites of Al/Fe_2O_3 nano-thermite; and 2) to investigate their ignition mechanism and energetic properties. To achieve these goals, Al and Fe_2O_3 nanoparticles are deposited on a stainless steel electrode to form multi-layer structures. The solid-solid interfacial contact of two depositing layers is examined using scanning electron microscopy (SEM) images. The thermal gravimetric analysis (TGA) is performed to study the active content and mass change

during reaction. Differential scanning calorimetry (DSC) is used to measure the energy release and the ignition temperature of corresponding thermite composites.

3.3 Methodology

3.3.1 Materials and experimental setup

Al nanoparticles with an average diameter of 18 nm and 99.8% purity (which accounts for the mass fraction of Al nanoparticles over other impurities in the sample) were provided by *Microbonds Inc.* The purity of Al nanoparticles was specified by the supplier. In order to examine the potential oxidation of these nanoparticles during fabrication, transportation and handling, the mass fraction of their Al_2O_3 shells was measured via TGA using representative samples and compared with the reference values. The Fe_2O_3 nanoparticles were purchased from *Sigma*, which have a specified diameter of 20 nm. In order to describe energetic properties as the functions of molar ratio of Al/Fe_2O_3, the mass of deposited samples was adjusted accordingly.

The stoichiometric ratio (27/80 in mass) was obtained through evaluating the following reaction

$$2Al + Fe_2O_3 \rightarrow Al_2O_3 + 2Fe \qquad \text{(Eq. 3.1)}$$

The deposited mass on the stainless steel was adjusted by changing the EPD parameters including the depositing time and electric field potential. The Hamaker's equation shows the dependence of deposited mass on these EPD parameters [146]

$$w = \int_{t1}^{t2} \mu EAC dt \qquad \text{(Eq. 3.2)}$$

where w and μ are the weight of materials deposited and the electrophoretic mobility constant, respectively. E, A, and C are the electric field strength, the surface area of electrode and the mass concentration in suspension, respectively. t is the depositing time when the electric field is applied. In this study, the mass concentration of nanoparticles was controlled by measuring the mass of nanoparticles added into the solution and the volume of the solution.

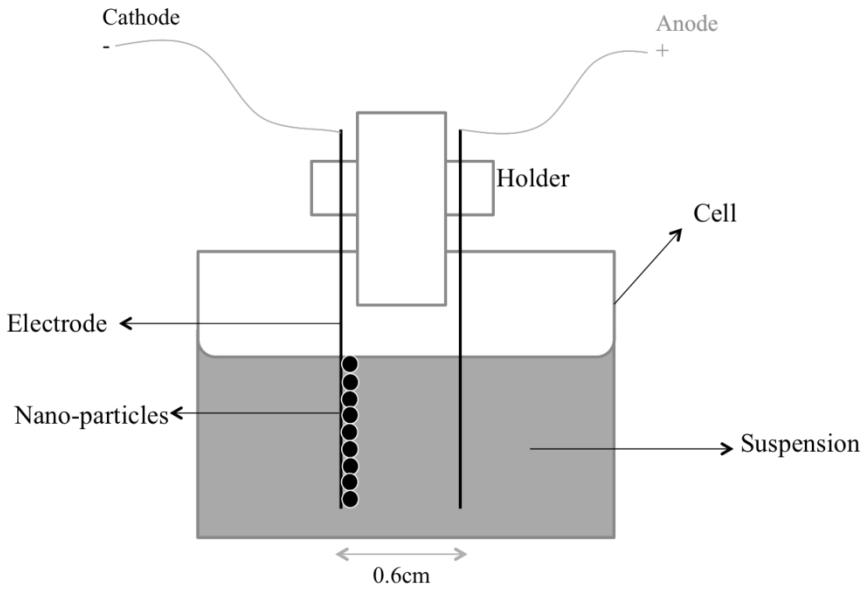

Figure 3.1 Schematic diagram of experimental setup of EPD device

The schematic diagram of EPD process is shown in Figure 3.1. The distance between these two electrodes was set to 6 mm. The deposits of Al and Fe_2O_3 were found on the cathode, which indicates that Al and Fe_2O_3 nanoparticles were charged positively in ethanol and isopropanol, respectively. Al and Fe_2O_3 were coated separately. The Al nanoparticles were deposited with the electric fields of 10 V/cm, 20 V/cm and 30 V/cm, which correspond to 6 V, 12 V and 18 V of the electrical potential, respectively. The depositing times were set to

30 s, 1 min, and 1.5 min, respectively. The deposition rate of Fe_2O_3 nanoparticles was found being slower than that of Al nanoparticles. The electric field strengths for Fe_2O_3 suspensions were 30 V/cm, 40 V/cm and 50 V/cm and with the depositing durations of 1 min, 1.5 min and 3 min, respectively. The deposition mass was determined by measuring the weight of electrodes before and after each deposition step.

The uniform interface can be formed by depositing Fe_2O_3 and Al nanoparticles separately in a sequence that can improve the effective bonding and contact of reactive components.

The layered structure has well-defined geometric structure and the thermite reaction occurs in the interfacial zone when the temperature rises to the ignition temperature. The ignition temperature is assumed to be independent of the molar ratio of fuel and oxidizer due to the reaction characteristics that only occur at the interface. The first step to achieving layer-by-layer structures is to use the EPD process to deposit nanoparticles. The electrodes serving as the substrate for deposition can also be the supports that eliminate the breakage of thin layers and makes handling easier. The available solvents for dispersing and depositing the particles are ethanol, distilled water, and isopropanol. Distilled water reacts with Al nanoparticles and evaporates at a slow rate in the atmosphere compared with other organic solvents. Ethanol is an ideal candidate for dispersion, but the Fe_2O_3 solution using ethanol solvent cannot remain in a stable condition, and precipitation occurs within a short time. Therefore, isopropanol is chosen to disperse the Fe_2O_3 nanoparticles and deposit them on the electrodes. After the deposition of the first layer, the electrode is extracted out of solution and dried for several minutes in the oven until there is no mass change. The deposited electrode is then inserted

into the Al solution for another deposition and treated in the same way as above. To retain the layered structure without damage, we cut the electrode with nanocomposite together using scissors to fit the size of the crucible for TGA/DSC measurement.

3.3.2 Selection of solvents for aluminum and iron oxide nanoparticles

During EPD the stability of nanoparticle suspension in its solution plays an important role in producing a good quality of deposits. In some solvents nanoparticles are naturally charged, which is able to suspend nanoparticles in solution and produces a satisfying electrophoretic mobility under the electric field. A double layer structure is formed surrounding the nanoparticle, as shown in Figure 3.2(a), when it is dispersed in a solvent. Meanwhile near the electrode, the electrical double layer is also formed [146], as shown in Figure 3.2(b). The different types of nanoparticles exhibit distinct electronic properties in the solution. Thus it is necessary to choose the proper solvent for effectively dispersing Al and Fe_2O_3. Besra and Liu discussed about the selection principle of solvents for EPD process [95]. It was suggested that the particle size, dielectric constant, conductivity of suspension, viscosity of suspension, and zeta potential are major parameters which affect the stability of suspension and the quality of deposition. In this study, the organic solvents are expected to have little reactivity towards these particles. The selection of solvents was therefore mainly based on the dielectric constant and viscosity of suspension.

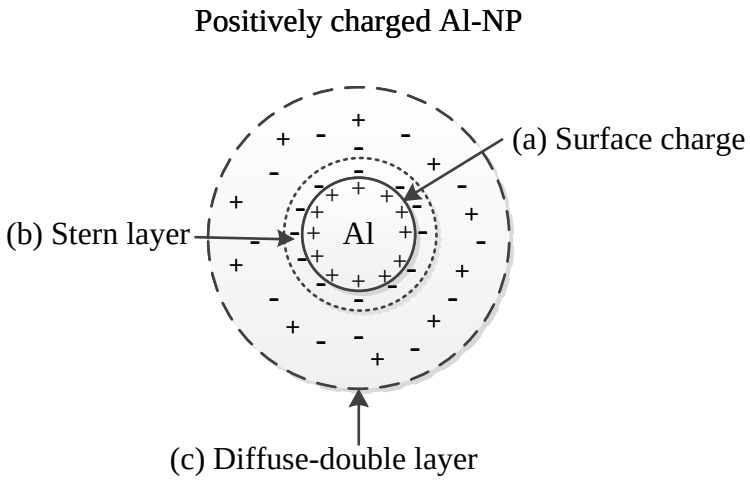

Figure 3.2 Schematic view of aluminum nano-particles with the double layers structure: (a) surface charge, (b) stern layer, (c) diffuse layers of counter-ions [146]

Table 3.1 shows the physical properties of a number of solvents under consideration [95]. Note that a very small dielectric constant would result in unsuccessful deposition due to insufficient dissociation, whilst a very high dielectric constant could lead to a high ionic concentration in the liquid which reduces the length of the double layer region and consequently restricts the electrophoretic mobility. An EPD process usually prefers the dielectric constant in the range of 12 to 25 [95]. Several solvents (ethanol, n-propanol, iso-propanol, n-butanol and acetone) shown in Table 3.1 meet that requirement. In order to assess their solution viscosity, the Henry equation [95] was used to illustrate the dependence of the electrophoretic mobility of nanoparticles on the physical properties of solvents

$$\mu = \frac{2}{3}\frac{\varepsilon_0 \varepsilon_r \xi}{\eta} f(\kappa r) \qquad \text{(Eq. 3.3)}$$

where μ is the electrophoretic mobility, ε_0 is the permittivity of vacuum, ε_r is the relative permittivity of the solvent, η is the solvent viscosity, and $f(\kappa r)$ is the Henry

coefficient which depends on the thickness of the double layer ($1/\kappa$) and the core radius (r) of the particle. Henry equation suggests an increase of the permittivity leads to a greater mobility of nanoparticles. On the other hand, increasing the viscosity can result in a decreased mobility. Three kinds of solvents, i.e., ethanol, iso-propanol and distilled water, were chosen and tested for their reactions with Al nanoparticles. The samples were sonicated and then settled for three hours before nanoparticles were filtered out and examined. If the reaction between a solvent and the Al nanoparticles happens, the color of nanoparticles would become whiter. The color change of nanoparticles indicates the phase change from Al to Al_2O_3. Based on these tests, ethanol (HPLC grade with 90% purity) was chosen to disperse and deposit Al nanoparticles.

Table 3.1 Physical property of solvents

Solvents	Viscosity (cP)=10^{-3} Nsm^{-2}	Relative dielectric constant
Methanol	0.557	32.63
Ethanol	1.0885	24.55
n-Propanol	1.9365	20.33
Iso-propanol	2.0439	19.92
n-Butanol	2.5875	17.51
Ethylene glycol	16.265	37.7
Acetone	0.3087	20.7
Acetylacetone	1.09	25.7

Iron oxide nanoparticles were also dispersed and tested in distilled water, ethanol, and

isopropanol, respectively. These solutions were settled for ten minutes after sonication. Then the degree of dispersion of nanoparticles was examined. Based on the comparison isopropanol was selected to prepare the Fe_2O_3 suspension. It was found the suspensions of Al and Fe_2O_3 nanoparticles in ethanol and isopropanol, respectively, possess a good stability after sonicated for 20-30 minutes at 40 KHz.

The Al nanoparticle loading of 1% by weight was added into a 20 mL disposable scintillation vial. After adding ethanol into Al powder, the vial was put into a 2510 Branson ultrasonicator and ultrasonicated for 20 minutes at 40 KHz. The ethanol dispersed Al nanoparticles were kept in a turbid liquid and settled for hours, to produce homogeneous Al thin films via EPD. The higher density and varying charging states Fe_2O_3 nanoparticles were found to affect EPD process. Through several trails, the powder loading was set to 3% by weight. Fe_2O_3 nanoparticles were first added into a vial, followed by adding isopropanol. The suspension was ultrasonicated for 30 minutes at 40 KHz.

3.3.3 Characterization

The active contents of Al nanoparticles before and after deposition were first examined via TGA in air, to access whether oxidation occurred during EPD process. The NETZSCH STA model 449F3A-0918-M Jupiter was used. The cross-section microstructures of deposited films were investigated with SEM (LEO 1550 Zeiss) under up to 100,000 times in magnification. All these samples were coated with a thin gold layer via a UHV sputter system with the current of 20 mA for 139 seconds to provide a sufficient conductivity. The ignition

temperature and energy release of the layered nano-composite on the electrode were characterized with TGA/DSC with the heating rate of 10°C/min in the range of 25°C to 800°C. TGA/DSC measurements were conducted for Al/Fe_2O_3 composites under argon atmosphere.

To investigate the dependence of the deposited mass on EPD parameters, Al and Fe_2O_3 films were produced on electrodes separately when the deposition mass (mg/cm^2) was investigated as the function of deposition time. The yield of EPD process was calculated by measuring the weight of the electrode before and after deposition. The Al nanoparticles were deposited on the electrode for 30 seconds, 45 seconds, 1 minute, and 1.5 minute under 30V/cm of applied electric field. The Fe_2O_3 nanoparticles underwent the electric field strength of 40V/cm for 1, 1.5, 2, and 3 minutes.

To characterize the energetic properties of the layered Al and Fe_2O_3 nano-composite structure, TGA/DSC curves were obtained when the composite was heated to 800°C with a heating rate of 10 °C/min and in argon. The layered composite sample was kept on the electrode and then placed into the crucible, in order to avoid any damage on the structure. In the TGA/DSC reaction chamber, an uncoated stainless steel electrode was placed in the reference crucible to retain the balance. Three tests were run under the same conditions in order to produce the error bar. In order to investigate these effects of different fuel/oxidizer molar ratios on the performance of layered composites, the amount of Al and Fe_2O_3 deposits were controlled by changing the deposition time and the applied electric potential. Then the fuel/oxidizer ratio was estimated by measuring the weight change corresponding to the individual EPD process.

3.4 Results and Discussion

3.4.1 Characterization of as-delivered and deposited Al nanoparticles

An aluminum oxide shell usually forms on the active core of the Al nanoparticle during fabrication and storage. For nanoparticles, this oxide shell could represent a large fraction of the total mass. A 50 nm nanoparticle with a 5 nm alumina shell was found to contain 58% of aluminum oxide, leaving a much smaller amount of the active content [147]. It is important therefore to check whether the EPD process would significantly change the active content of fuel component. TGA/DSC was performed in dry air on the as-delivered and deposited Al nanoparticles for this purpose.

Figures 3.3(a) and 3.3(b) demonstrate the TGA/DSC results of the 18 nm Al nanoparticles before and after deposited on the electrode. The solid line in each figure is referred to the DSC result which possesses a sharp exothermic peak accompanying the oxidation reaction of Al nanoparticles with oxygen. In both cases the DSC curve shows the onset temperature of approximately 507-508 °C. Moreover, the energy release from the as-delivered Al nanoparticles (3289 J/g) is greater than that of the deposited nanoparticles on the electrode (2688 J/g). This difference of energy release can be explained by the following considerations. First, part of reaction enthalpy is absorbed by the electrode during TGA of the deposited nanoparticles, which reduces the DSC peak recorded from the measurement. Secondly, as will be illustrated later, the diffusion path of oxygen is shorter than the thickness of the deposited thin film, which limits the completion of oxidation and leaves un-reacted Al

nanoparticles from TGA/DSC. The dotted line in each figure shows the TGA result demonstrating the increase of mass due to oxidation. It is important to note that the TGA curves start to increase at approximately 500 °C which is slightly lower than the onset temperature of the DSC curves. This agrees with observation from diffusion-controlled oxidation prior to the thermite reaction [104]. The percentage of mass gain of the as-delivered nanoparticles (35.1%) is about 10% higher than that of the deposited nanoparticles (25.5%), which most likely indicates the incompletion of the oxidation of nanoparticles on the electrode due to the restricted diffusion path of oxygen in the EPD deposited films.

Separate tests were performed in order to characterize the potential oxidation of as-produced thin films in air. After deposition, the samples were exposed in air for 1, 1.5 and 2 hours before TGA/DSC measurements were performed. It was expected, the mass gain of these samples during TGA would be significantly different if some Al nanoparticles in the thin film were oxidized in air. Table 3.2 shows the mass changes measured from TGA tests with these samples. Clearly the mass changes resulted from different samples are nearly constant (with about 1% deviation), indicating that the oxidization of the thin film in air is less important. This finding further suggests that the decreased mass change of deposited nanoparticles, shown in Figure 3.3, is unlikely due to oxidation of Al nanoparticles during the sample preparation stage. The uncompleted oxidation process during TGA/DSC should play a more important role in decreasing the mass change and reducing the energy release.

The mass change for as-delivered nanoparticles after TGA is 35.1%. The active content was then calculated using Eq. 3.4

$$4Al + 3O_2 = 2Al_2O_3 \qquad \text{(Eq. 3.4)}$$

The active content is the function of percentage of mass change measured by TGA, which can be expressed in Eq. 3. 5.

$$F_a = \frac{108p}{96} \qquad \text{(Eq. 3.5)}$$

where F_a is the active content of Al nanoparticles and p is the percentage of mass change in TGA result. Therefore, the active content for the as-delivered nanoparticles is 39.5%.

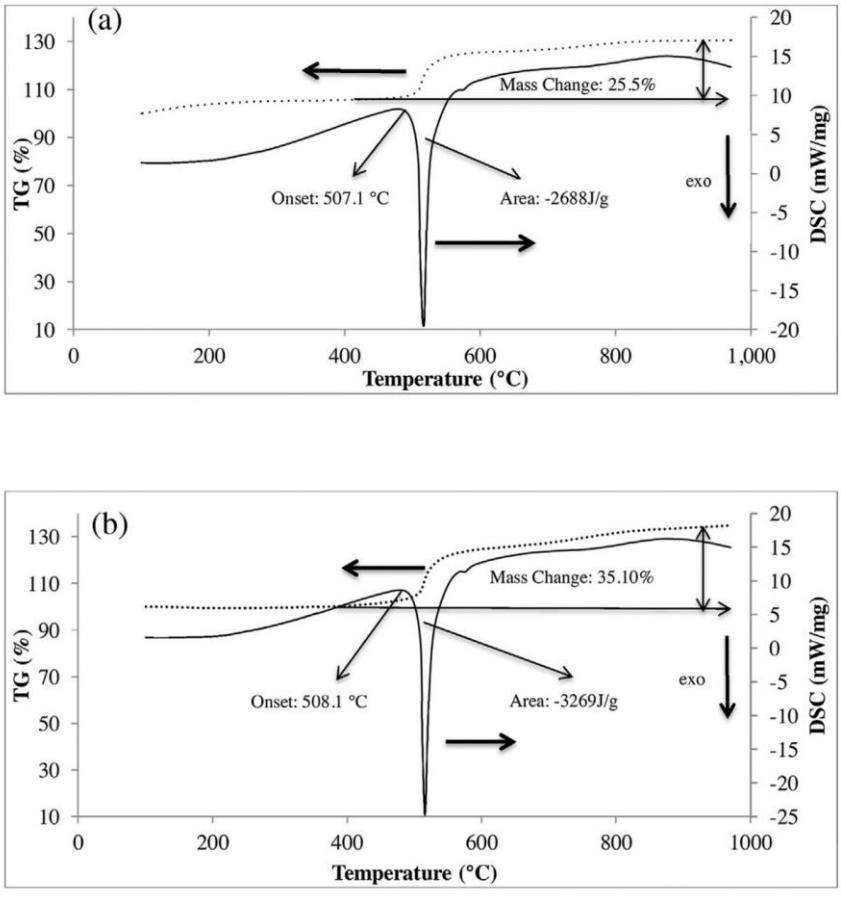

Figure 3.3 TGA and DSC results of (a) deposited and (b) as-delivered 18nm Al nanoparticles with 10 °C/min and in the temperature range of 100 °C to 1000 °C. The solid lines: DSC results. The dotted lines: TGA results

These analyses based on Figure 3.3 confirm that the EPD process, together with the power dispersion method in the solution, leads to a restrained impact on the energetic properties of Al nanoparticles on the electrode. While the EPD process did not cause increasing the onset temperature which is believed to closely relate to the growth of the alumina shell, the presence of the electrode affects the energy release from the active nanoparticles.

Table 3.2 Mass change in TGA of deposited nanoparticles

Exposure time (h)	**1**	**1.5**	**2**	**Average mass change (%)**
Mass change in TGA (%)	25.5	27.33	26.72	26.52
Deviation (%)	-1.02	0.81	-0.2	

3.4.2 Deposition mass of Al and Fe_2O_3 nanoparticles

Figure 3.4 (a) and (b) demonstrate the increase of deposition mass with deposition time. The error bars were determined by repeating the same process for three times under same conditions.

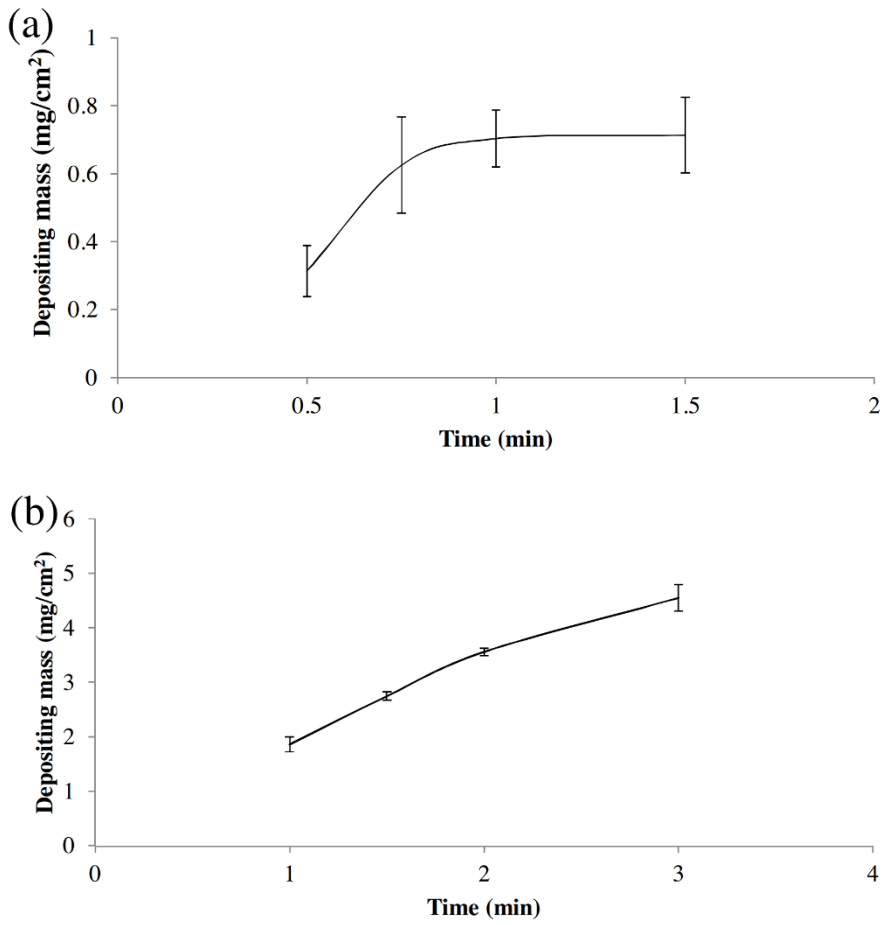

Figure 3.4 Yield of nanoparticle coating from EPD process (a) the yield of Al nanoparticles and (b) the yield of Fe_2O_3 nanoparticles

Comparing Figure 3.4 (a) and (b), the deposition rate of Fe_2O_3 nanoparticles is about three times of that of Al nanoparticles due to the greater density of Fe_2O_3, a higher concentration of Fe_2O_3 solution, and relatively higher electric field applied to the Fe_2O_3 solution. This deposition rate however decreases with increasing the thickness of deposited layer. After the deposition time of 1 minute, there is less mass change for the Al deposition on the electrode. This is due to the significantly reduced electrical conductivity of the electrode, which is caused by the relatively lower conductivity of the Al film and the weak bonding strength

between Al nanoparticles and the stainless electrode. In contrast, the mass of the Fe_2O_3 nanoparticle layer keeps increasing with the deposition time, as shown in Figure 3.4(b). Fe_2O_3 nanoparticle deposits seem to bring less influence on the conductivity of the electrode. Fig. 4 suggests the poorer electricity conductivity of the deposited Al nanoparticles than that of the deposited Fe_2O_3 nanoparticles. The deposition rate of Al nanoparticles was found to be slower with increasing electric field, while the same phenomenon was not observed with the deposition rate of Fe_2O_3 nanoparticles. It is believed that, since Al nanoparticles possess a lower electrical conductivity, the overall conductivity of the deposited Al nanoparticle film becomes smaller with increasing electric field, which reduces the deposition rate. The electrical conductivity of Fe_2O_3 nanoparticles is much higher than that of the Al nanoparticles. Based on this observation, the layered Al/Fe_2O_3 nano-composites were fabricated by depositing the Fe_2O_3 nanoparticles first. Then the Al nanoparticles were deposited on the Fe_2O_3 film. The stronger bonding between the Fe_2O_3 films with the electrode was found effectively to prevent the peel-off of the layered composites from the electrodes.

3.4.3 Microstructures of deposited films

SEM images were taken and analyzed to investigate the morphology and microstructures of the deposited films. The homogeneity of deposited layer surfaces was considered as a major factor which affects the interfacial contact between two reactive layers and subsequently influences the species diffusion length and thermite reaction rate. Figure 3.5 illustrates the SEM images of the deposited Fe_2O_3 surface with magnifications of 10,000 and

100,000 times, respectively, and the cross-section view of the Fe_2O_3 layer. The 40 V/cm electric field strength and 1.5 min deposition time were applied to produce the Fe_2O_3 layer shown in Figure 3.5.

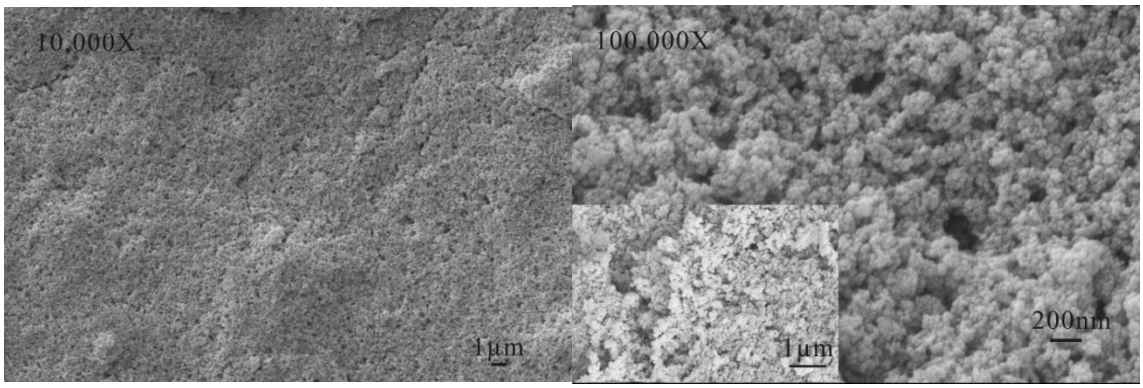

Figure 3.5 SEM images of the surface of deposited Fe_2O_3 (a) 10,000X and (b) 100,000X. Insert: the cross-section view

A relatively uniform but porous surface was produced after Fe_2O_3 nanoparticles were deposited from EPD process. The largest pores were found to have sizes of about 200 nm, which were formed mainly from evaporation of the solvent. Meanwhile, when the charged Fe_2O_3 nanoparticles moved towards the electrode, a repulsed force could enhance the porosity of the depositing surface. The cross-section view of the Fe_2O_3 layer confirms lacking of major cracks across the layer and the quality of EPD process is reasonably satisfying.

The cross-section view of the layered Al/Fe_2O_3 composites under the deposition conditions of 40V/cm electric field applied for 1.5min forming Fe_2O_3 layer and 30V/cm applied for 1min forming Al layer on the stainless steel electrode was demonstrated in Figure 3.6. This image shows, first, bonding of Fe_2O_3 nanoparticles on the stainless steel electrode

is stronger and no voids or cracks were observed. Secondly, the Fe_2O_3 film can be deposited with a larger thickness (125 μm), thanks to the selection of the solvent and the good conductivity of the as-produced film. Thirdly, it is feasible to deposit Al nanoparticles on the Fe_2O_3 film, although the thickness of the Al film is restricted by the conductivity of the composite structure and the bonding strength between Al nanoparticles and the Fe_2O_3 film. The thickness of the Al layer was measured as approximately 30 μm. Lastly, the deposited Al nanoparticle film demonstrates a more porous structure than the Fe_2O_3 nanoparticle film. Nevertheless, the layered Al/Fe_2O_3 nano-composite was successfully fabricated via EPD on the stainless steel electrode. Also the direct contact between two types of reactive nanoparticles is visible.

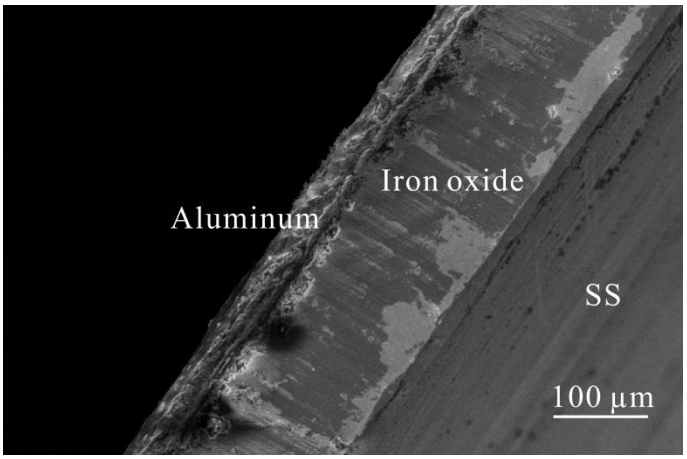

Figure 3.6 SEM image of the cross-section view of Al/Fe_2O_3 composite. Deposition condition: 40V/min and 1.5 min for Fe_2O_3, 30V/cm and 1min for Al

3.4.4 Energetic properties

TGA/DSC experiments were performed with the layered Al/Fe_2O_3 nano-composites to investigate their thermochemical stabilities and energetic properties. The onset temperature

and energy release were characterized and the results of one representative sample were shown in Figure 3.7. The EPD conditions of this sample were the same as the sample shown in Figure 3.6. The TGA/DSC curves were obtained when the composite was heated to 800°C with a heating rate of 10 °C/min and in argon. The TGA curve shows an insignificant mass change within a few percentages that was considered as an equipment effect. Since the tests were arranged in argon, the total mass should be constant. The DSC curve demonstrates a single exothermic event with the onset temperature of 494.3°C, which belongs to the thermite reaction of Al and Fe_2O_3 nanoparticles presented in the composite. The total energy release from the sample was calculated as 1659.4 J/g based on the mass of Al. The reaction stops when the system temperature reached 581.3°C. The maximum reaction rate was found at 524.1°C.

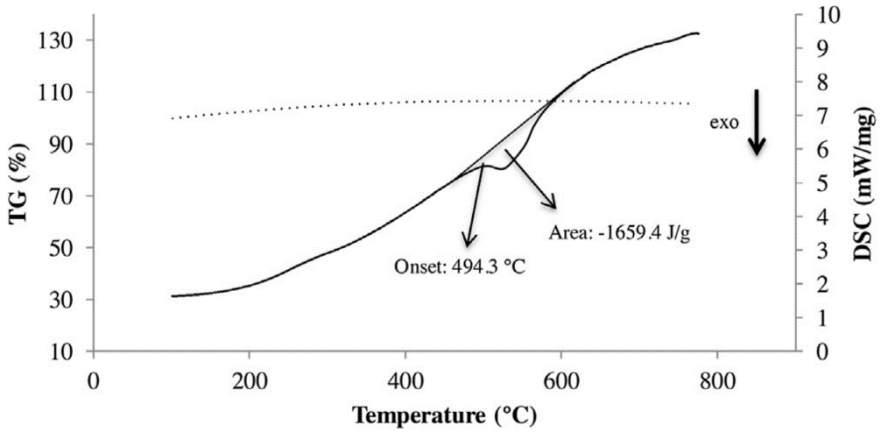

Figure 3.7 TGA/DSC results of a layered composite heated to 800°C with a heating rate of 10 °C/min using 18nm of Al NPs. The solid lines: DSC results. The dotted lines: TGA results

Figure 3.7 provides about important information on the energetic properties of the layered Al/Fe_2O_3 composite. First of all, the thermite reaction occurs before the melting point of Al (since no melting peak was observed on the DSC curve), indicating the solid-state oxidation. Therefore, the Al/Fe_2O_3 nano-thermite composite with layered structure follows the nano-thermite reaction mechanisms. It can be described that oxygen diffuses through the aluminum oxide shell of Al nanoparticles and reacts with the active Al core. Secondly, the onset temperature of the layered composite (494.3°C) was found to be lower than that of the deposited Al nanoparticles in air (505°C). This suggests the improved ignition performance of the layered nano-thermite composite due to in-situ production of oxygen from Fe_2O_3 and its much shorter diffusion length to reach the Al core. Thirdly, the energy release from the layered composite (~1.7kJ/g) was found much lower than the theoretical enthalpy of the Al/Fe_2O_3 system (3.9kJ/g) [23]. This observation can be explained by a few factors. The active content of Al is smaller in nanoparticles due to existence of the aluminum oxide shell, which reduces the energy release per unit mass of Al. The active content of 18 nm nanoparticles was estimated using Figure 3.3(b) and its value was found as approximately 40% of the total mass calculated with Eq. 3.6. Another major factor which affects the energy release is believed to be the incomplete thermite reaction within the layered composite which contains originally separated fuel and oxidizer components. Upon ignition at the interface between two layers, the temperature of the composite increases and the diffusion rates of active components (Al, oxygen and Fe) are accelerated. Driven by the temperature enhanced diffusion, these reactants, especially oxygen released from Fe_2O_3, moves towards the Al layer

and hence the reaction zone is extended in the vertical direction of the layered structure. It is therefore reasonable assuming that the thickness of the reaction zone is determined by the diffusion length of oxygen at local conditions. The diffusion path of oxygen however is restricted by the newly formed products. Meanwhile, since combustion enthalpy is partially absorbed by the stainless steel substrate, temperature is reduced and subsequently the diffusion length of oxygen is reduced.

3.4.4.1 Molar ratio effects on energy release

The effects of the molar ratio of Al/Fe_2O_3 on the onset temperature and energy release per unit mass were investigated by changing the deposition amounts of reactive components. Eight representative samples were fabricated and characterized for this purpose. The EPD deposition conditions and derived sample data are shown in Table 3.3.

Caused by the deposition characteristics of EPD process, the thickness of each layer changes with the molar ratio of Al/Fe_2O_3 nanoparticles added to the corresponding solutions. Since the reaction zone is mainly located around the interface between two layers, adding more fuel or oxidizer would not necessarily alter the energetic properties of layered composites.

The energy release from each sample is shown in Figure 3.8. The energy release per unit mass of Al is increased from 1228 J/g to 1659 J/g when the molar ratio changes from 1.14 to 1.4, due to the increase of the active Al content which provides more fuel to the thermite reaction zone. Further increasing the molar ratio of Al/Fe_2O_3 however does not result in

greater energy release values. Instead, when the molar ratio is increased from 1.4 to 3.96, the energy release per unit mass keeps decreasing.

Table 3.3 Deposition condition and amount of each layer

Sample	Fe_2O_3 3% of solid loading			Al 1% of solid loading			Molar ratio of Al/Fe_2O_3
	Time (min)	Electric field (V/cm)	Amount (mg)	Time (min)	Electric field (V/cm)	Amount (mg)	
1	1.5	40	11.5	1	30	2.2	1.14
2	1.5	40	8.9	1	30	2.1	1.40
3	1.5	40	7.2	1.5	30	2.4	2.00
4	1.5	40	9.9	1.5	30	4.0	2.40
5	1	40	5.8	1.5	30	2.5	2.54
6	1	40	7.8	1.5	30	4.1	3.10
7	1	40	2.9	1.5	30	1.7	3.46
8	1	40	4.5	1.5	30	3.0	3.96

Since there is a limited reaction zone around the interface of the layered structure, as discussed before, Al nanoparticles away from the reaction zone will not be able to ignite and hence the degree of complete combustion decreases with increasing Al mass. Meanwhile, there is relatively lower amount of Fe_2O_3 nanoparticles available in the composites with greater molar ratios. Less oxygen is produced from the thermal decomposition of Fe_2O_3, which further leads to incomplete combustion of nano-thermite. Thanks to these two factors,

energy release per unit mass is significantly reduced with larger molar ratios of Al/Fe_2O_3 in the composite.

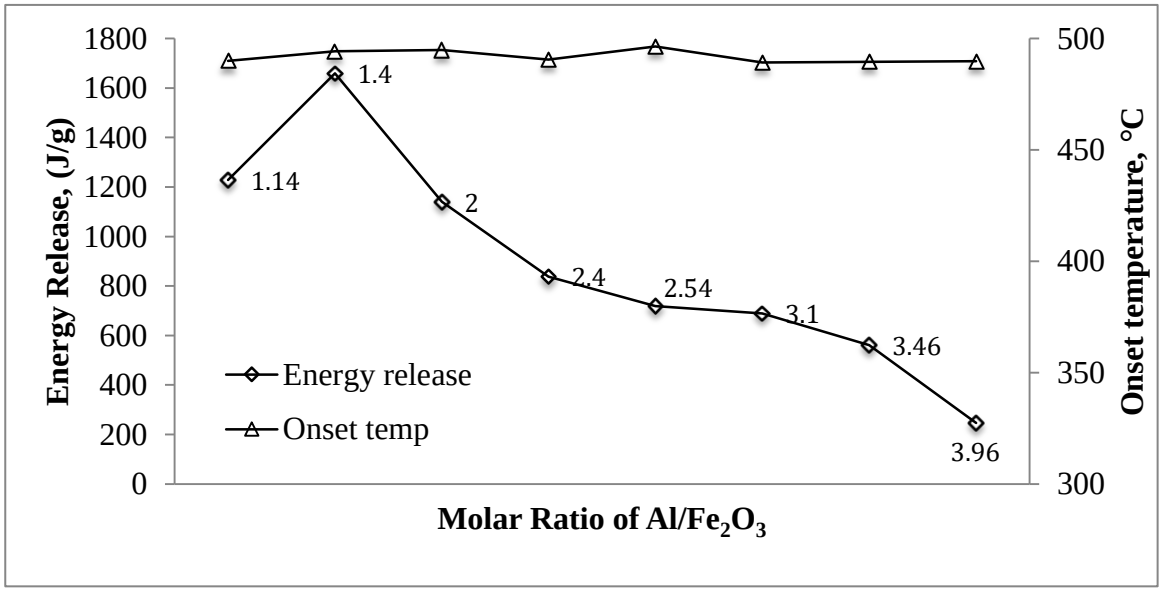

Figure 3.8 Energy release based on Al mass and onset temperature as the function of molar ratio of Al/Fe_2O_3. The molar ratios of each sample are shown in the figures as 1.14, 1.4, 2, 2.4, 2.54, 3.1, 3.46, and 3.96, respectively

Figure 3.8 demonstrates as well the change of onset temperatures with the molar ratio of Al/Fe_2O_3 in the layered compositions. It shows that there is little change of the onset temperature with increasing the molar ratio from 1.14 to 3.96. This confirms the same ignition mechanism of all layered composition which emphases the role of oxygen, generated from the thermal decomposition of Fe_2O_3, during ignition. Secondly, it confirms the EPD process is a satisfying fabrication method to make layered nano-thermite composites with uniform and immediate contacts between two reactive components.

3.4.4.2 Influence of Al nanoparticle size on onset temperature and energy release

In order to investigate the effects of the Al nanoparticle size on the energetic properties, the 18 nm and 40 nm Al nanoparticles were deposited on the Fe_2O_3 coated electrodes. In comparison, as shown in Fig 4. 9, the layered composite with 40 nm Al nanoparticles demonstrates a slightly higher onset temperature (504.8℃ for 40 nm Al nanoparticles vs. 494.3℃ for 18 nm Al nanoparticles). Meanwhile, the DSC curve corresponding to the composite with 40 nm Al nanoparticles presents a small endothermic peak at 630 °C which is close to the melting point of bulk Al (660 °C), which indicates the melting of unreacted Al content in this composite.

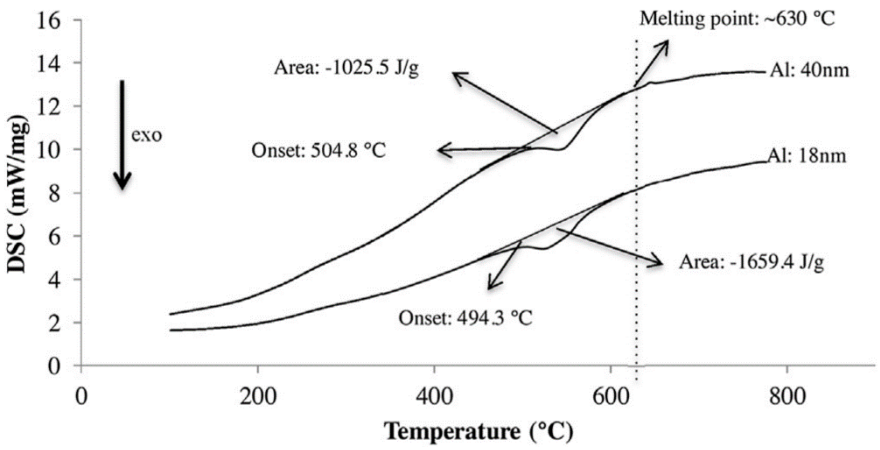

Figure 3.9 TGA/DSC results of a layered composite by using 40 nm and 18 nm of Al nanoparticles

The influence of the Al nanoparticle size contained in the layered composites on their distinct energetic properties can be twofold. First, larger nanoparticles are generally less

reactive than smaller nanoparticles, likely due to their reduced surface energy. Secondly, with the specified oxygen partial pressure and temperature profile during TGA/DSC, the diffusion of oxygen requires a higher activation energy on larger nanoparticles and takes a longer time. Therefore the degree of thermite reaction completion is lower for the composite made from 40 nm Al nanoparticles in comparison with that made from 18 nm nanoparticles. The unreacted 40 nm nanoparticles are melted, which produces the small endothermic peak. Secondly, larger nanoparticles may contribute to the formation of relatively nonuniform interface between two layers. The diffusion path of oxygen becomes longer before it reaches the reactive Al content in the composites with 40 nm Al nanoparticles, which slightly reduces the onset temperature. Further investigations, probably with the help of environmental SEM technology, are needed to reveal the insights of these effects.

3.5 Conclusion

In this study, Al and Fe_2O_3 nanoparticles were deposited on the stainless steel electrode, via EPD process, to form layered structures. Analysis of the active content of Al nanoparticles before and after deposition confirms no additional oxidation was introduced during EPD process. SEM images demonstrate the formation of separated Al and Fe_2O_3 layers within the composites and the direct contact between two reactive components at the interface. TGA/DSC data reveals the energetic characteristics of the layered composite. The consistent onset temperatures of layered composites with different molar ratios of Al/Fe_2O_3 suggest the validity of a previously proposed ignition mechanism of the Al/Fe_2O_3 nano-thermite system

which addresses the role of oxygen in ignition, following the thermal decomposition of Fe_2O_3. Energy release per unit mass decreases with increasing the molar ratio of Al/Fe_2O_3 for thicker layered structures, which suggests the incompletion of the thermite reaction during TGA/DSC. The size of Al nanoparticles in the composites affects their onset temperatures and degree of reaction completion. More experimental effort is expected to address these effects.

Chapter 4: Reaction mechanisms of nano-thermite composites with multi-layered structure

4.1 Overview

The reaction mechanisms and microstructures of various layered nano-thermite composites were investigated through characterization of their energetic properties. Migration of reactive components across the reaction zone was analyzed, which plays a significant role in determining the process initiation, reaction propagation, and chemical stability at low temperatures. Distinct types of nanoparticles were deposited onto filter paper in a sequence, using the vacuum filtration method, which promotes intimate contact between neighbouring reactive layers. Scanning Electron Microscopy (SEM) images demonstrate a well-defined contact region between the two layers in the Al/CuO or Al/NiO composites. Differential Scanning Calorimetry (DSC) data shows that the thermite reaction occurred below the melting temperature of Al, resulting in rapid heat release and improved reaction initiation. Elemental mapping results reveal the migration of Al, Ni/Cu and oxygen before and after the thermite reaction which was arranged during thermogravimetric analysis (TGA). This analysis indicates the dominant pathway of the thermite reaction in each composite, through either decomposition of the CuO nanoparticles in the Al/CuO composite or through direct migration of reactive components across the conducting surface within the Al/NiO composite. Energy-dispersive X-ray Spectroscopy (EDAX) data suggests that the Al and NiO nanoparticles cross-migrate into the counter layers without experiencing decomposition of NiO, which indicates this is a condensed phase reaction.

4.2 Literature review and introduction

The vacuum filtration method has been developed in other applications, such as fabrication of graphene and carbon nanotube based electrodes,[148] but it has not been widely studied for the preparation of nano-energetic material or composites. This study investigates the thermochemical properties and reaction mechanisms of Al/CuO and Al/NiO thermite systems. The Al/CuO thermite system possesses a reaction enthalpy of 4.07 kJ/g and a gas production amount of 0.54 mol/100g, compared to other thermite systems such as Al/Fe_2O_3 (3.96 kJ/g and 0.14 mol/100g) and Al/WO_3 (2.91 kJ/g and 0.14 mol/100g), which promotes its applications for developing propellants and explosives [23]. On the other hand, the Al/NiO system (3.44 kJ/g and 0.01 mol/100g) produces a small amount of gaseous products, showing a potential application in welding [22].

This thesis chapter focuses on the fabrication of layered composites of Al/CuO and Al/NiO nano-thermites via vacuum filtration and the characterization of their morphology, microstructures, and corresponding thermite reaction mechanisms. In order to form multi-layered structures, Al/CuO and Al/NiO nanoparticles are dispersed and mixed in solution. Then, thin films are formed through vacuum filtration on a filter paper, following a layer-by-layer procedure. The microstructures of the layered nano-thermite composites are examined using SEM images and the fuel content of Al nanoparticles is estimated using TGA. The produced energy and initiation temperature of the nano-thermite composites are measured with DSC. Energy-dispersive x-ray spectroscopy (EDAX) and elemental mapping are

employed to study the migration of elements across the layers in the composites. In this work, the difference in the reaction mechanisms of the Al/CuO and Al/NiO nano-composites is directly addressed through the fabrication of layer-by-layer composites, characterization of their micro-structures, and comparison of their elemental mapping, before and after the thermite reaction.

4.3 Methodology

4.3.1 Material and vacuum filtration apparatus

Al nanoparticles, with a size range of 40-60 nm, and 99.8% purity (the percentage of Al nanoparticles compared to other impurities in the sample), were chosen for this experiment. The Al nanoparticles were provided by *Microbonds Inc*. The CuO and NiO nanoparticles were purchased from *Skyspring Inc.* and both had a rated diameter of 50 nm. To fabricate the layered composites with a controllable thickness, a vacuum filtration apparatus, as shown in Figure 4.1, was used. Filter paper (Whatman quantitative filter paper, ashless, Grade 44) was placed onto the porous screen support that was installed in a glass funnel. The bottom of this funnel was connected to the vacuum pump. The nanoparticle suspension was added into the funnel. When the vacuum pump was turned on (at 25 psi), a pressure difference was created between both sides of the filter paper, causing a thin film of nanoparticles to be deposited.

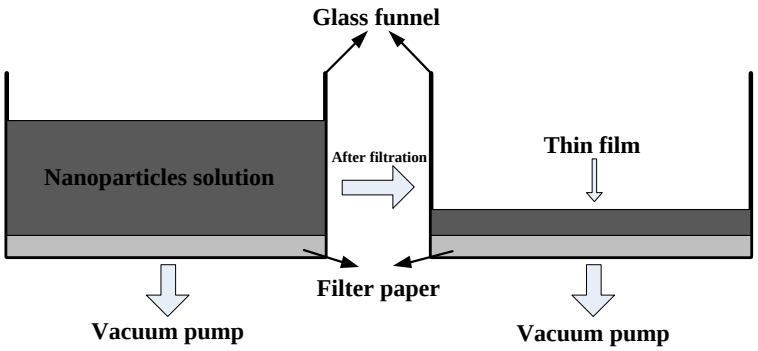

Figure 4.1 Schematic diagram of the experimental setup

4.3.2 Experimental procedure

The Al and CuO nanoparticles were dispersed in ethanol, with a loading of 1 % and 3 % by weight, respectively, and sonicated for 30 min. The loading ratio was chosen to produce a composite with the Al and CuO layers that have a comparable thickness after vacuum filtration. To avoid the accumulation of nanoparticles at the bottom of the container, the suspension was kept under sonication until used for vacuum filtration. The solution containing the nanoparticle suspension was added to a funnel and it was temporarily held above the filter paper. The system was then vacuumed using the vacuum pump and the nanoparticles were deposited on the filter. To produce the Al/CuO composite, the Al nanoparticle suspension was added into the glass funnel to form the first layer. As the solvent was removed by the vacuum pump, an Al thin film was formed with a porosity that allows solvent to pass through. Then the CuO suspension was added and the CuO nanoparticles were deposited on the surface of the Al thin film to form the second layer. The same procedure was repeated to fabricate a composite with multiple layers. The layered thin film was dried in a furnace at 200 °C for 5 min. During the drying process, cracking could occur on the thin

film. To avoid this, a pressure of 500 psi was applied to the thin film as it was dried. The thin film was then detached from the filter paper entirely. Acetone was chosen as the solvent to disperse the NiO nanoparticles for the fabrication of the Al and NiO multi-layer composite. The NiO nanoparticles were dispersed with a 3 % weight loading, and sonicated for 30 min. The main procedure for producing the Al and NiO composite was similar to that of the Al and CuO multi-layer composite, as described above.

The dispersion quality of the nanoparticles was evaluated in different solvents using the following criteria: 1) the nanoparticles should be well dispersed to eliminate agglomeration of these particles, and 2) the solution should provide an air-free environment that allows the dispersed nanoparticles to be stored for a few days. In addition, it was important to choose a solvent that has no reaction with the Al and oxidizer nanoparticles, which is why ethanol and acetone were considered. However, the difference in the viscosity of these two solvents was found to impact the sample preparation times and various microstructures. Because ethanol has a higher viscosity, it was found to cause a long vacuum filtration time for the NiO nanoparticles. Therefore, it was replaced by acetone during the deposition of the NiO nanoparticles.

4.3.3 Characterization

To quantify the fuel content, Al nanoparticles were heated in TGA/DSC (NETZSCH STA model 449F3A-0918-M Jupiter) under an oxygen atmosphere. The heating rate was set to 10 °C/min and the temperature was increased from room temperature to 800 °C. More details

about this process may be found in the reference [149]. The initiation temperature and produced energy of the layered composites were characterized with TGA/DSC. Furthermore, The TGA/DSC measurements were conducted in an argon atmosphere for characterizing the energetic properties of the Al/CuO and Al/NiO composites.

To fabricate a multi-layer composite with controllable thicknesses of the individual layers for different types of nanoparticles, the densities (g/cm^3) of these individual layers should be controlled. More specifically, the density of a layer with the same type of nanoparticles should be kept as constant. In order to achieve this goal, a two-step procedure was developed. At this first step, a single layer containing a specified type of nanoparticles was fabricated using vacuum filtration with a variable thickness. The solution with a fixed nanoparticle loading (in mg/ml) was added into the glass funnel and the derived thickness of the layer is dependent on the amount of the solution (in ml). The following equation was used to calculate the density of the single layer film

$$\rho = \frac{4V \times C}{\pi D\hat{}2T} \qquad \text{(Eq. 4.1)}$$

where *V* and *C* are the volume of solution added into the funnel (ml), and the nanoparticle loading of the solution (mg/ml), respectively. *D* and *T* denote the diameter and the thickness of the thin film, respectively. Due to the brittle nature of the produced multi-layer composites, it was difficult to measure the film thickness using calipers. The film was placed between two glass discs with the same diameter of the film and the distance between the surfaces of these glass discs was measured as the thickness of the film. At the second step when these multi-layers were fabricated, the volume of each solution was determined for every filtration

process, based on the desired thickness of the corresponding layer and the calculated density values of single layer nanoparticle films.

The energetic properties of layered Al/CuO and Al/NiO composites were investigated with TGA/DSC. The detailed procedure and conditions can be found in our previous publication.[149] In short, the layered composite samples were placed into a crucible, and were then loaded into the TGA/DSC reactor. The reactor was then vacuumed to remove air, and then it was filled with argon with 1 bar. The microstructures of the produced composites were investigated with SEM (Zeiss Merlin). These samples were coated with gold to provide a needed electrical conductivity. The elemental mapping and EDAX tasks were performed on the same SEM.

4.3.4 Reaction mechanisms with a multi-layered structure

The reaction mechanisms between Al and oxide nanoparticles are investigated in this thesis. As discussed above, the nano-thermite composites with network structure form complex interfaces between reactants, which makes it difficult to investigate the reaction mechanisms. With preparation methods using EPD and VF techniques, the nano-thermite composites formed with multi-layered structure can be achieved. The advantage of this unique structure is the uniform interface between reactive layers. The thermite reaction can be initiated on the interface area and proceed via mass transfer through the interface area.

Regarding different types of oxides, the major reaction mechanisms are gas-solid and condensed phase reaction. In the gas-solid reaction mechanism, the oxides undergo

decomposition to release oxygen in gas phase that further migrates to reach Al nanoparticles. Due to the onset temperature of the reaction occurring below the melting point of aluminum, the Al nanoparticles remain in solid phase. The oxygen migrates and surrounds the Al nanoparticles, which further diffuses through the Al_2O_3 shell and reaches the Al core. The nano-thermite reaction occurs between the gas phase of oxygen and solid phase of aluminum, which is known as a gas-solid reaction mechanism. On the other hand, the oxide does not undergo decomposition to release oxygen in the condensed-phase reaction, whereas the oxide nanoparticles form direct contact with Al nanoparticles. Then, the thermite reaction occurs between solid-solid phases, known as the condensed-phase reaction.

With the complex and network structure of nano-thermite composites, it is impossible to investigate the migration of either oxygen or oxide nanoparticles. The investigation into the reaction mechanisms can only be conducted by using the mass spectrum method to detect the produced gas phase. However, the fast nano-thermite reaction produces a significant amount of energy, which increases the local temperature of nano-thermite composites. It is possible that the gas phase is produced after the thermite reaction. Meanwhile, the other possibility is that the gas phase produced by the decomposition of oxide is absorbed by Al nanoparticles to generate the thermite reaction, leading to a misunderstanding of the reaction mechanism. Under these considerations, the nano-thermite composites with a multi-layered structure including the uniform interface are formed with EPD and VF.

An uniform interface is formed between Al and oxide layers. The thermite reaction can be initiated from the interface and proceed by mass transfer between the two layers. Assuming

the gas-solid reaction mechanism, which suggests the decomposition of oxide before the thermite reaction occurs, the oxygen produced from the oxide can migrate from the oxide layer to the Al layer. In this case, the oxygen atoms are the element that migrates from the oxide layer to the Al layer. On the other hand, the condensed-phase reaction mechanism requires the direct contact between nanoparticles. Here, the oxide does not undergo decomposition to release oxygen that migrates to the Al layers. After the thermite reaction is initiated at the interface of the reactive layers, the sintering effect is able to form intervals to allow nanoparticles to migrate to the opposite layer and form a direct contact between reactants. Then, the thermite reaction occurs between solid-solid phases of Al and oxide nanoparticles.

As shown in the previous section, EDX is able to trace the migration of elements between layers. In the case of the gas-solid reaction mechanism, the oxygen migrates from the oxide layer to the Al layer, which increases the concentration of oxygen in the Al layer. On the other hand, the metal does not move from the oxide layer to the Al layer. However, both oxygen and metal migrate to the Al layers in the condensed-phase reaction mechanism. The Al nanoparticles may also move to the oxide layer. In this case, the elements of Al, metal, and oxygen should appear in both layers.

This multi-layered structure, which is able to separate two reactants: fuel and oxide, can be used for the investigation of the function of CNTs in the nano-thermite reaction. The CNTs can mix with either Al nanoparticles or oxide nanoparticles, forming an interfacial contact between Al and CNTs, or oxide and CNTs. The interaction of CNTs with Al or oxide can be

controlled via fuel and oxide separation. Using a multi-layered structure can clearly show the reaction between Al and CNTs, or oxide and CNTs. The details regarding the investigation of the function of CNTs in thermite reactions will be revealed in a later chapter.

4.4 Results and discussion

4.4.1 Fuel content of Al nanoparticles (as-delivered and vacuum-deposited)

Figures 4.2(a) and 4.2(b) show the TGA results using the 40-60 nm Al nanoparticles before and after being vacuum-deposited onto the filter paper, respectively. The data from 300 ºC to 1200 ºC was collected to investigate the mass change of the samples. In both cases, the TGA curve shows a slight increase in mass at approximately 400 ºC, together with a significant mass increase at approximately 500 ºC, which agrees with the mass diffusion mechanism [104]. Moreover, the mass increase of vacuum-deposited Al nanoparticles (57.69 %) is slightly larger than that of the as-delivered nanoparticles (53.81 %). This finding is attributed to the following considerations. The sonication process and subsequent vacuum filtration can eliminate the agglomerated nanoparticles in the sample, which reduces the amount of un-reacted Al mass. In addition, the layered film creates more intimate contact between oxygen and Al nanoparticles, which reduces the diffusion path of oxygen during TGA/DSC and increases the oxidation rate. Furthermore, the oxidation curves of both the as-delivered and vacuum-deposited Al nanoparticles demonstrate a rapid oxidation process with a sharp mass gain at 500 ºC, which is below the melting point of Al.

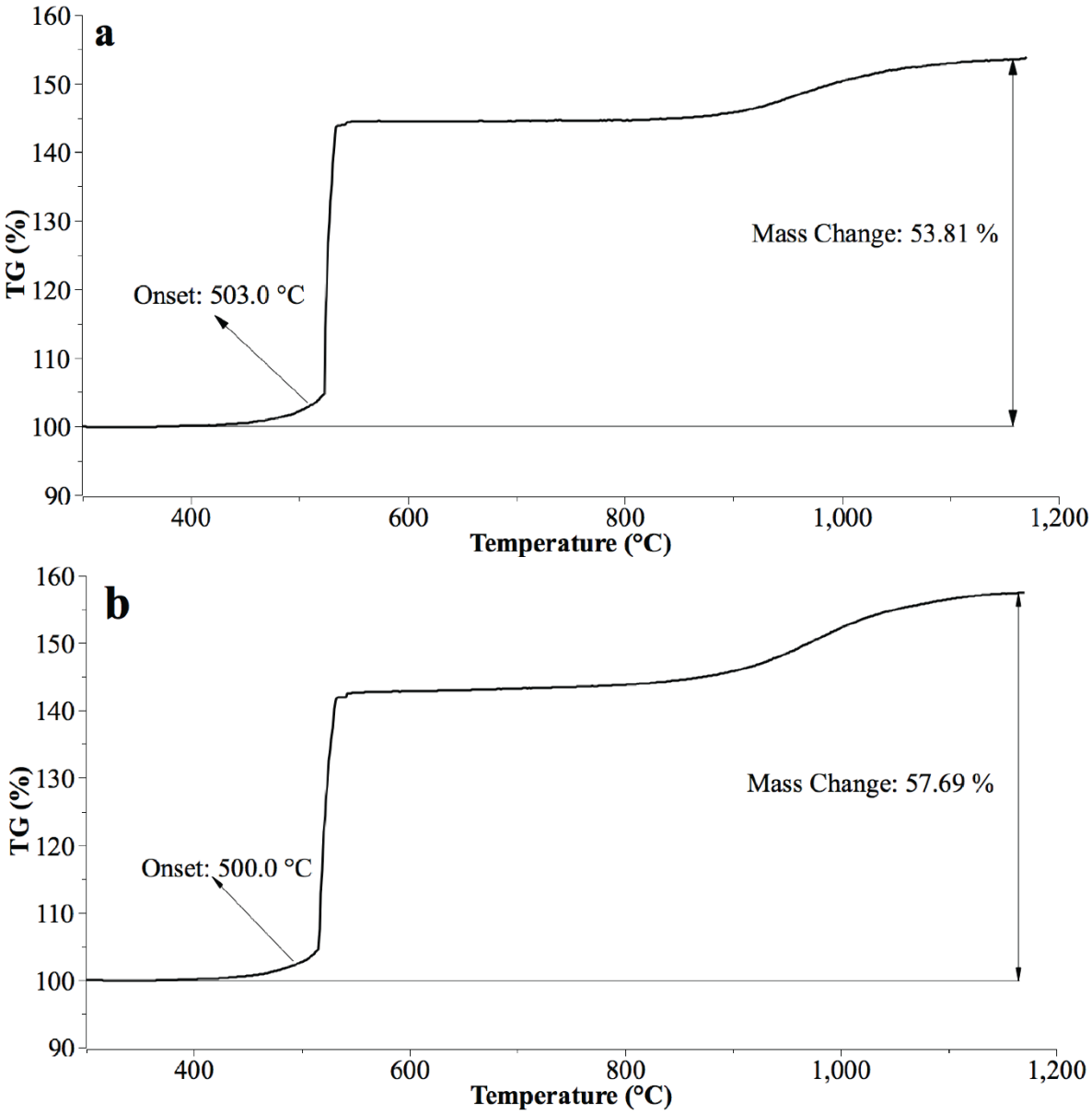

Figure 4.2 TGA results of (a) as-delivered and (b) vacuum-deposited 40-60 nm Al nanoparticles, with 10 ºC/min heating rate, in the temperature range of 300 ºC to 1200 ºC, under air atmosphere

The TGA results confirm that the vacuum filtration process did not change the fuel content of the Al nanoparticles. After their oxidation in TGA, individual Al nanoparticles were found to be able to retain their morphology and size, which suggests that sintering of the Al or

Al_2O_3 nanoparticles is not significant for the vacuum deposited film. In order to reduce experimental error, TGA measurements were performed three times for each sample, as shown in Table 4.1. The oxidation of Al nanoparticles is described by Reaction 4. 2

$$4Al + 3O_2 = 2Al_2O_3 \quad \text{(Eq. 4.2)}$$

The fuel content of the Al nanoparticles can be calculated by

$$F_a = \frac{108p}{96} \quad \text{(Eq. 4.3)}$$

where F_a is the active content of Al nanoparticles and p is the percentage of mass change in the TGA results, respectively. The average fuel contents for the as-received and vacuum-deposited nanoparticles are 60.28 % and 64.46 %, respectively. These analyses, based on TGA/DSC, as shown in Table 4.1, confirm that the vacuum filtration and sonication processes did not have a negative impact on the fuel content of the Al nanoparticles.

Table 4.1 Mass change of as-delivered and vacuum-deposited 40-60nm Al nanoparticles from TGA measurements

	Mass change from TGA			
	1	2	3	Average
As-delivered	53.81 %	55.01 %	51.91 %	53.58 %
Vacuum-deposited	57.69 %	56.67 %	57.53 %	57.30 %

4.4.2 Density variation of the Al, CuO and NiO nanoparticle multi-layers

In order to control the density variation within the as-produced multi-layers, the first task was to determine the densities of these single layers made of different types of nanoparticles.

Table 4.2 demonstrates the densities of the Al, CuO, and NiO nanoparticle single layers. The weight loadings of Al, CuO and NiO nanoparticles in the solution were set to 1 %, 3 %, and 3 %, respectively. In order to produce the single layer with a different thickness, the volume of the solution was changed from 5 ml to 15 ml. Each process was repeated for three times.

Table 4.2 Thin film densities of layered samples with the Al, CuO and NiO nanoparticles, respectively

Amount of solution (ml)	Density (g/cm^3)			Average density (g/cm^3)
Al thin film				
5	1.24	1.06	1.20	1.17
10	1.21	1.12	1.23	1.19
15	1.19	1.12	1.16	1.16
CuO thin film				
5	2.34	2.39	2.34	2.36
10	2.35	2.32	2.40	2.36
15	2.35	2.32	2.37	2.35
NiO thin film				
5	2.42	2.42	2.43	2.42
10	2.43	2.45	2.40	2.43
15	2.41	2.41	2.43	2.42

Table 4.2 shows that these densities of the single layer films of Al, CuO and NiO nanoparticles keep almost constant, under the same operation pressure of the vacuum pump. The averaged densities listed in Table 4.2 were used at the second step, as illustrated before,

to determine the volume of the solution at each deposition step for fabricating of the multi-layer composites. Equation 4. 4 was used to determine this volume according to the desired thickness of an individual layer.

$$V = \frac{T\rho\pi D\hat{}2}{4C} \qquad \text{(Eq. 4.4)}$$

where V and C are the volume of the solution added into the glass funnel and the nanoparticle loading of that solution, respectively.

4.4.3 Energetic properties

The TGA/DSC results of these representative samples of the layered Al/CuO and Al/NiO composites are shown in Figures 4.3(a) and 4.3(b), respectively. These curves were obtained when the composites were heated from the room temperature to 800°C in argon. A small mass change of around a few percentages was observed, which should be counted as an equipment error. Since the TGA tests were performed in argon, the total mass should remain the same. As shown in Figure 4.3(a), the DSC curve exhibits a single exothermic peak with an initiation temperature of approximately 507 °C for the Al and CuO composite. This exothermic peak belongs to the thermite reaction between Al and CuO nanoparticles. The reaction energy release was calculated to be 1.06 kJ/g.

Figure 4.3(a) brings about the following observations on the properties of the layered Al/CuO composite. First, the thermite reaction occurs below the melting point of Al (which is shown in the figure by the melting peak of remaining Al in Figure 4.3(a)), indicating that oxygen diffusion through the Al_2O_3 shell is the dominant mechanism in the thermite reaction

[102, 150]. The outward diffusion of Al, as suggested in the reference [24] for micro-scale Al particles, seems to play a less significant role. Secondly, the energy release from the multi-layered composite with the 40-60 nm Al nanoparticles (~1.06 kJ/g) was found to be greatly lower than the theoretical reaction heat of the Al/CuO system (4.0 kJ/g) [23]. Note that the measured heat release values from these samples can be significantly different from the theoretical values of heat of reaction of the corresponding thermite systems. This derivation may be attributed to the following two factors. First, for the Al nanoparticles being investigated, their Al_2O_3 shells can account for approximately 40% of the mass of these particles. Secondly, due to the geometrical characteristics of these layered composites, some reactants were left unreacted due to the incomplete thermite reaction.

Figure 4.3(b) displays the TGA/DSC results of the multi-layered composite formed with the 40-60 nm Al and 50 nm NiO nanoparticles, and shows a similar exothermic peak when compared with the Al/CuO system. The initiation temperature of the layered nano-composite is around 516.0 ºC with an energy release of approximately 1.01 kJ/g. This lower energy release, compared with the theoretical data (~3.44 kJ/g), can be explained with similar reasons, as was described above. The TGA/DSC result from these two different layered composites gives some insight on their reaction mechanisms. First of all, the initiation temperature (516 ºC) for the Al/NiO system is higher than the initiation temperature (507 ºC) of the Al/CuO system, which indicates the improved performance of the Al/CuO system (discussed later). Secondly, both curves of these composites exhibit the melting peak of Al.

This indicates an incomplete reaction due to the limited diffusion length of reactive species which restricts the size of the reaction zone.

Figure 4.3 (c) shows the TGA results obtained by heating up CuO and NiO nanoparticles without the presence of Al nanoparticles. The solid line displays the data for CuO nanoparticles, which demonstrates the mass drop starting from approximately 870 °C. Oppositely, the dashed line is the result for NiO nanoparticles, which presents that the mass of NiO nanoparticles does not have change during the heating up procedure. The TGA data indicates that the CuO nanoparticles release gas phase to the atmosphere to reduce the total mass upon heating up to ~870 °C. The mass drop in CuO nanoparticles can be caused by the decomposition of CuO to form O_2 gas phase. On the other hand, the NiO nanoparticles has no mass change, which suggest that the NiO nanoparticles did not undergo decomposition to release O_2 to the atmosphere.

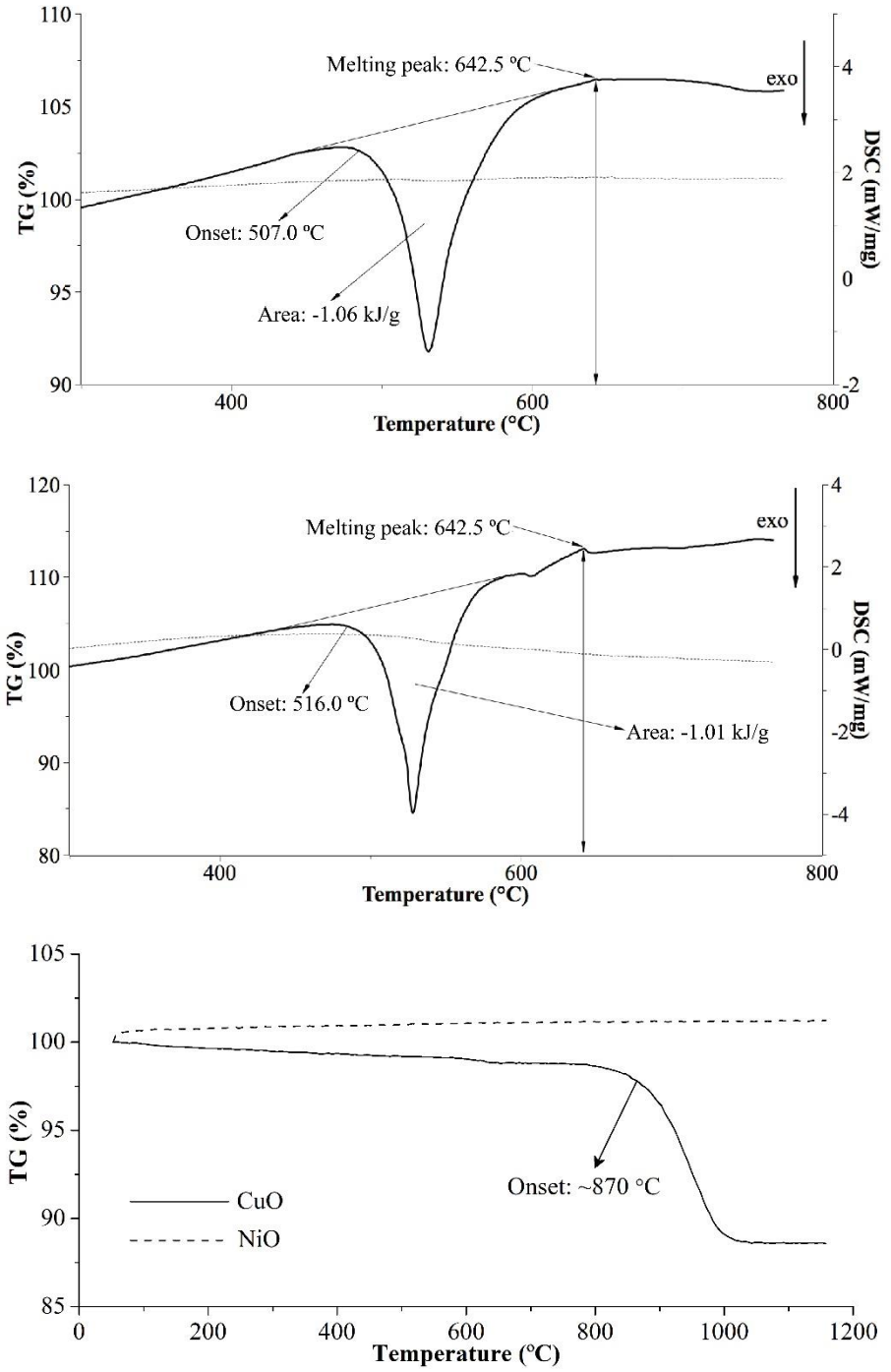

Figure 4.3 TGA/DSC results for the multi-layered a) Al/CuO and b) Al/NiO composite heated up to 800 °C, with a heating rate of 10 °C/min, using 40-60 nm Al NPs. The solid curve: DSC result. The dotted curve: TGA result. c) Heating up CuO and NiO without the presence of Al to 1200 °C

4.4.4 Microstructures and reaction mechanism of the Al/CuO system

Initiation of the thermite reaction within the composite is primarily affected by the physical and chemical stabilities of its reactive components. The TGA/DSC results show that the initiation temperature of the Al/CuO composite is below the melting point of Al, which indicates that the diffusion of oxygen through the Al_2O_3 shell occurs [149]. Therefore, the stability of the oxidizer dominates the reaction mechanism of the Al/CuO composite. The oxidizers are generally categorized into different groups based on whether the oxidizers can decompose into oxygen and metal [151]. The thermite reactions are subsequently categorized into gas-solid reactions or condensed phase reactions. If the solid-solid reaction is the dominant process between the Al and CuO nanoparticles, Cu and oxygen should co-exist with Al across the reaction zone. On the other hand, if the gas-solid reaction prevails, oxygen can reach all composite layers without Cu being present.

SEM images were used to analyze the microstructures and shapes of nanoparticles at the intersection of the vacuum-deposited multi-layers. The intersection view of the multi-layers shows the interfacial contact between reactive components. The SEM images of the as-fabricated multi-layers of the Al and CuO composite are shown in Figure 4.4. The direct contact of the Al and CuO layers is clearly demonstrated and the Al and CuO layers contact intimately without forming gaps or cracks. The direct contact between Al and CuO nanoparticles at the contacting surface facilitates the initiation of the Al-CuO thermite reaction. The thicknesses of these layers were approximately 20-40 μm.

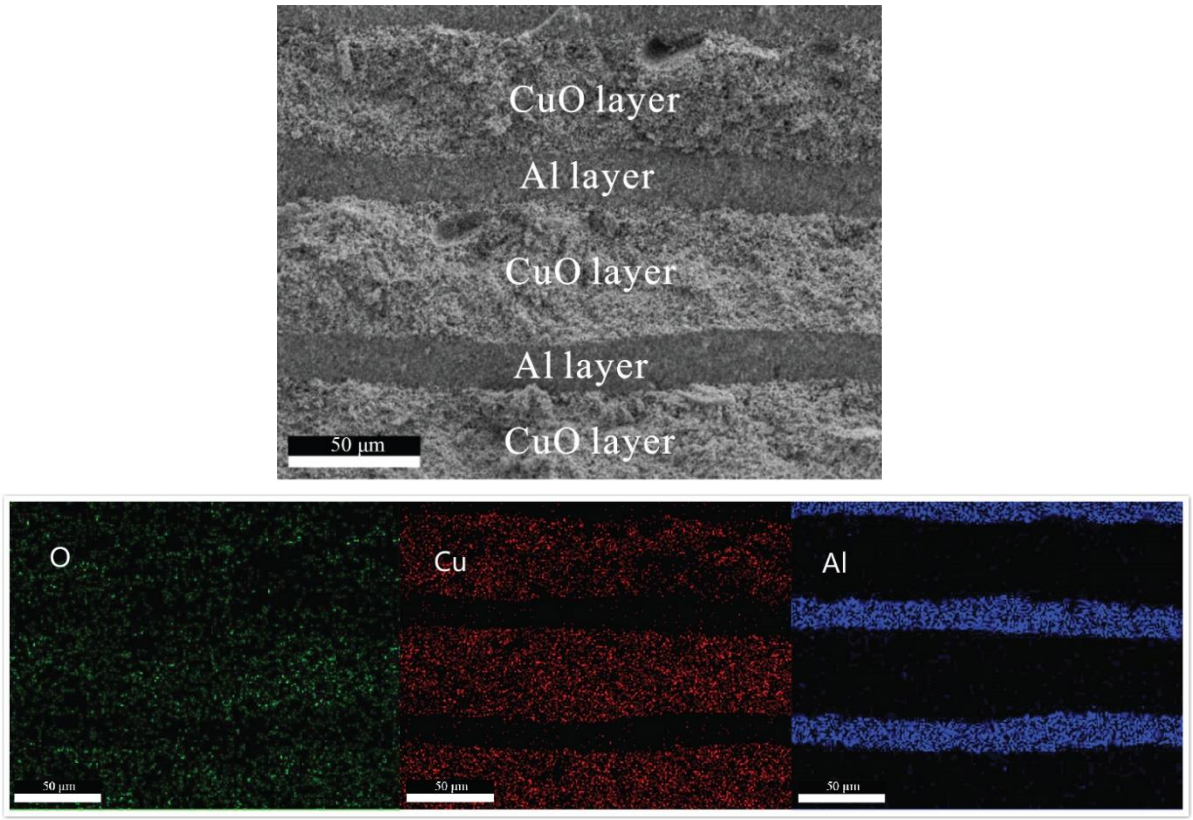

Figure 4.4 SEM images and corresponding elemental mapping of the vacuum-deposited multi-layer of Al/CuO composite before thermite reaction

Furthermore, the elemental mapping images shown in Figure 4.4 indicate the distribution of Al, O, and Cu around the contacting surface of the as-produced composite. The oxygen distributes throughout these layers, although its concentration is relatively low in the Al layers. The presence of oxygen in the Al layers is due to the formation of an Al_2O_3 shell on the Al core, which accounts for approximately 35 % of the total mass of the Al nanoparticles, as previously discussed. The signals from Cu and Al give evidence supporting that the CuO and Al nanoparticles do not diffuse into the opposite layer. This indicates that the thermite reaction was only initiated on the contacting surface of the neighboring CuO and Al layers upon heating up to the initiation temperature.

The SEM images of the microstructures of the reacted composites are presented in Figure 4.5. A gap is visible between the neighboring layers and the element distributions are different from the images in Figure 4.4. In Figure 4.5, the concentration of oxygen is greatly increased in the Al layer, in comparison to Figure 4.4. The contacting surface and reaction zone are visible in Figure 4.5 due to the obvious differences in oxygen concentration in the product layers. The Cu and Al remain in their original layers without migrating into the opposite layers.

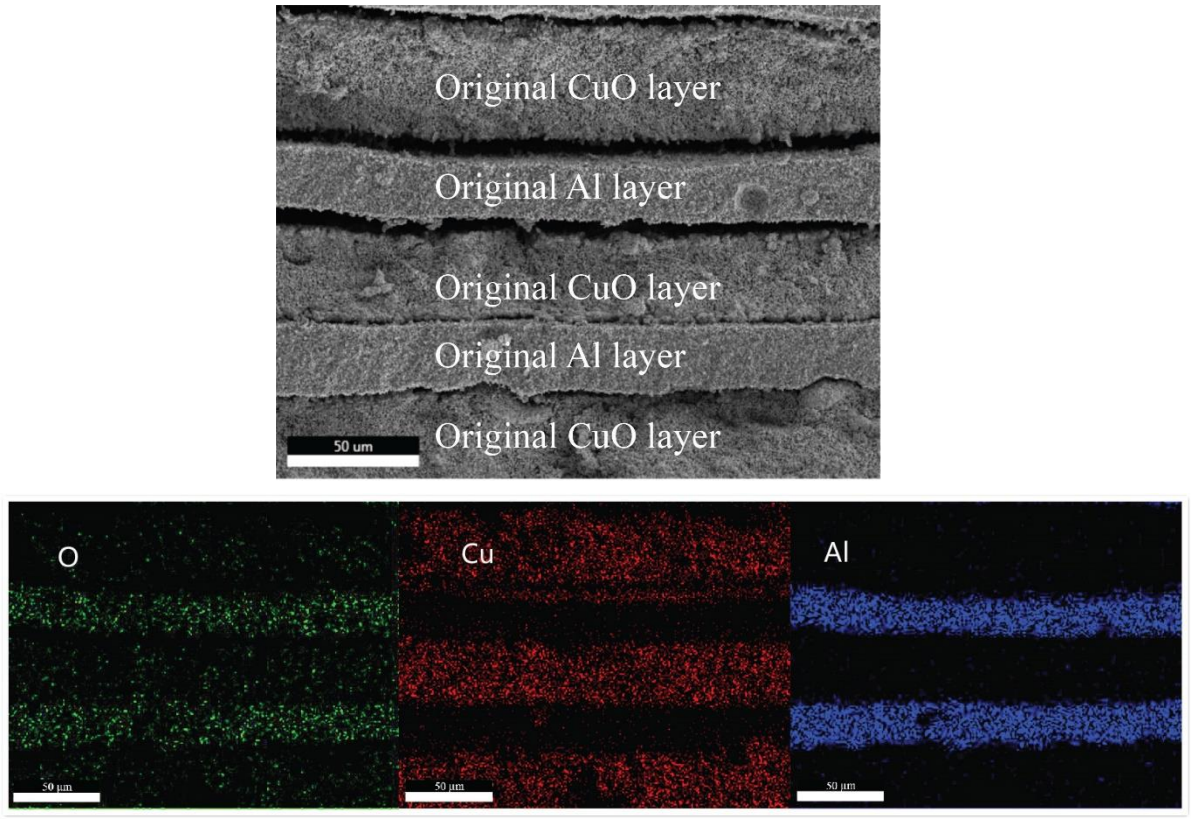

Figure 4.5 SEM images and corresponding elemental mapping of the vacuum-deposited multi-layer of Al/CuO composite after thermite reaction

It is important to discuss the possible pathways of the thermite reaction upon heating the composites to the onset temperature. Before reaching the onset temperature, there was no significant change in the mass of the composite and no heat release was observed. When the temperature reached the onset temperature, it was suspected that the thermite reaction between Al and CuO was initiated through the direct interaction of Al and CuO nanoparticles at the contacting surface of these two reactive layers. Since the onset temperature was quite low, it seems impossible to achieve the thermal decomposition of CuO at this stage. After the reaction was initiated, however, the local temperature increased dramatically and the decomposition of CuO to oxygen became possible. Oxygen subsequently diffused into the Al layer and it oxidized the Al nanoparticles. The production of oxygen from the original CuO layer was supported by the formation of the gap near the contacting surface of these two layers. Meanwhile, diffusion of oxygen into the original Al nanoparticle layer was evidential, thanks to the distribution of separated Al and CuO species in different product layers.

4.4.4.1 Gaps between two reactive layers

Figure 4.6 shows the gap between the reactive layers and the microstructure of the CuO layer after the reaction. Areas “a” and “b” in Figure 4.6 represent spots in the CuO layer that are at different distances from the contacting surface of the reactive layers. The direct contact of reactive layers on their contacting surface causes a faster heat production event at the initiation temperature. This is a result of the short diffusion path for mass transfer, due to direct contact of Al and CuO nanoparticles. The heat increases the local temperature and

causes the decomposition of the CuO nanoparticles. As shown in Figure 4.6, at area “a”, the decomposition of CuO produces a porous structure, which allows decomposed gas to diffuse into the Al layers. Oppositely, the SEM image exhibits a structure without porosity in area “b”. This can be explained by the faster heat release at the contacting surface between the two layers, which melts the products and fills the holes within the porous structure to reduce the volume of the CuO layers. These processes cause the shrinking of the reaction zone and lead to the separation of the CuO and Al layers. At the same time, the increasing local temperature induces thermal stress, which strengthens the separation effect of the Al and CuO reactive layers.

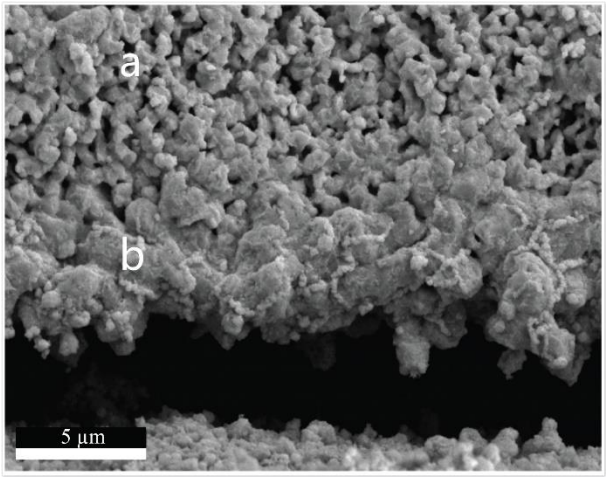

Figure 4.6 SEM image of the contacting area of two layers after heating up to 800 °C using nano-composites of 40-60 nm Al nanoparticles and 50 nm of CuO. a: the area of CuO having not direct contact with Al layer. b: the area of CuO having direct contact with Al layer

4.4.4.2 XRD analysis for the Al/CuO composite before and after the thermite reaction

The XRD analysis was conducted to characterize the chemical compositions of the derived samples before and after the thermite reaction.

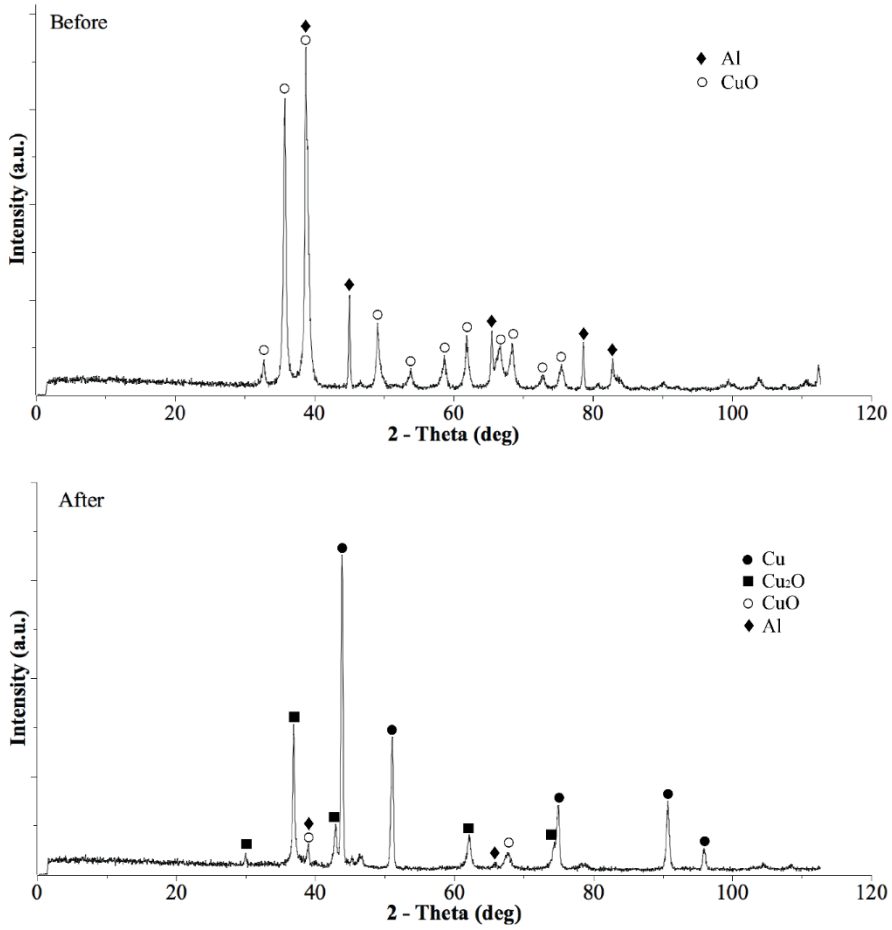

Figure 4.7 XRD patterns of samples before and after the thermite reaction for Al/CuO nanocomposite

Figure 4.7 shows the XRD spectra and it reveals a significant change in the chemical composition after the thermite reaction occurs. Thanks to the amorphous nature of the Al_2O_3 shell on these original Al nanoparticles, only Al and CuO diffraction lines are present for the unreacted composite. After the thermite reaction occurs between the Al and CuO

nanoparticles, however, clear and sharp Cu and Cu_2O diffraction lines show the formation of products from the thermite reaction. Additionally, small CuO and Al peaks exist, which suggests some reactants have not been fully consumed. This agrees with the TGA/DSC results shown in Figure 4.3, which demonstrates a small melting peak of remaining Al in the sample. XRD peaks corresponding to Al_2O_3 are relatively small, which suggests fewer large Al_2O_3 crystalline structures were produced from the reaction of layered energetic composites.

4.4.5 Microstructures and reaction mechanism of the Al/NiO system

The layered composite, composed of Al and NiO nanoparticles, was fabricated through vacuum filtration with a similar procedure to produce the layered Al/CuO composite. The morphology and microstructures of these composites were then investigated with SEM images, as shown in Figure 4.8. These images show intimate contact between the Al and NiO layers at their contacting surface. Similar to the contact conditions of the Al and CuO layers, the direct contact between two types of reactive nanoparticles is clearly visible.

The elemental mapping results show the element distribution of the as-produced Al/NiO multi-layers. The distribution of O, Ni and Al are displayed, respectively, from left to right in Figure 4.8. Oxygen is present in both the NiO and Al layers, whereas the Al and Ni elements are present in separate layers and do not mix. After the composite was heated up in the TGA/DSC to 800 ºC, the SEM images were collected to show the microstructure of the product.

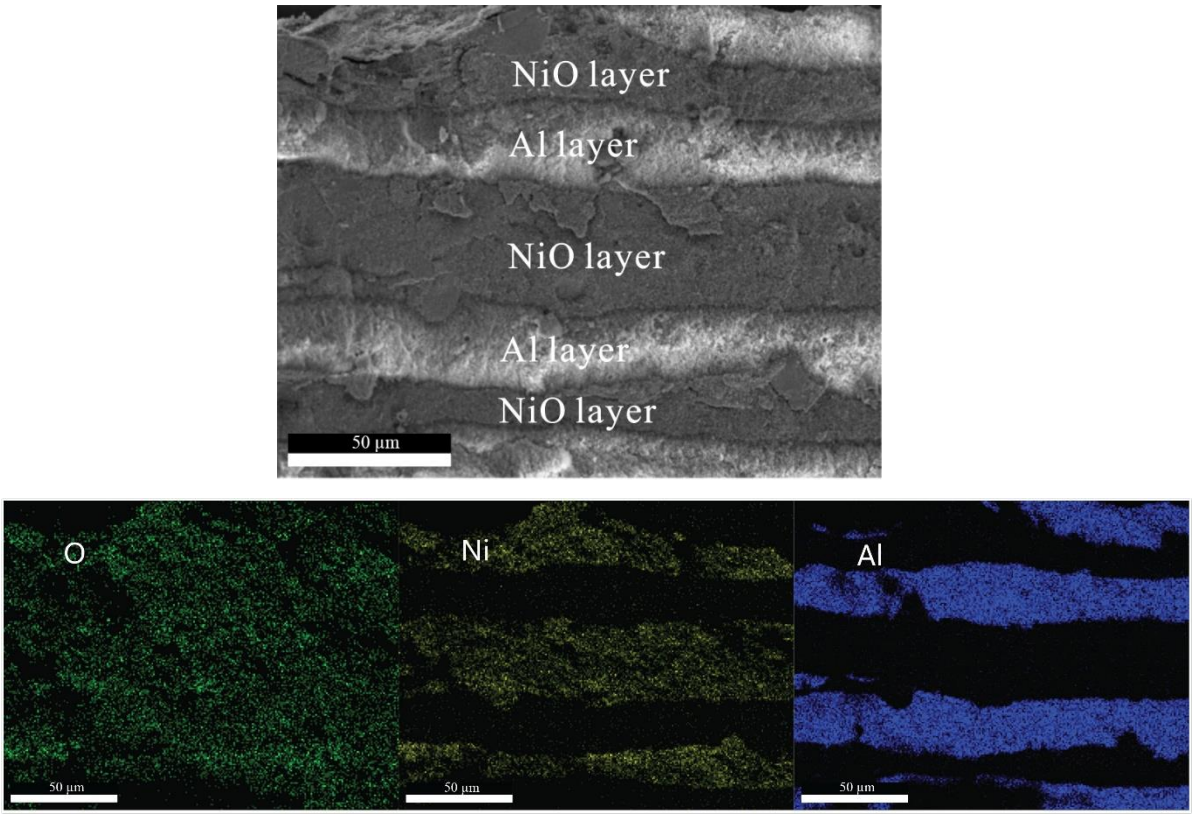

Figure 4.8 SEM images and corresponding elemental mapping of the vacuum-deposited multi-layer of Al/NiO composite before thermite reaction

Figure 4.9(a) is the SEM image of the reacted Al/NiO composite. Comparison between Figures 4.8 and 4.9 supports the following. First of all, the NiO layers underwent shrinking during the reaction, while the Al layers remained in a condensed condition. The reactive layers remained in contact even though the original NiO layer shrunk. Secondly, the shrinking that occurred within the NiO layer can be attributed to the sintering of the Ni metal which was produced in the NiO layer [152].

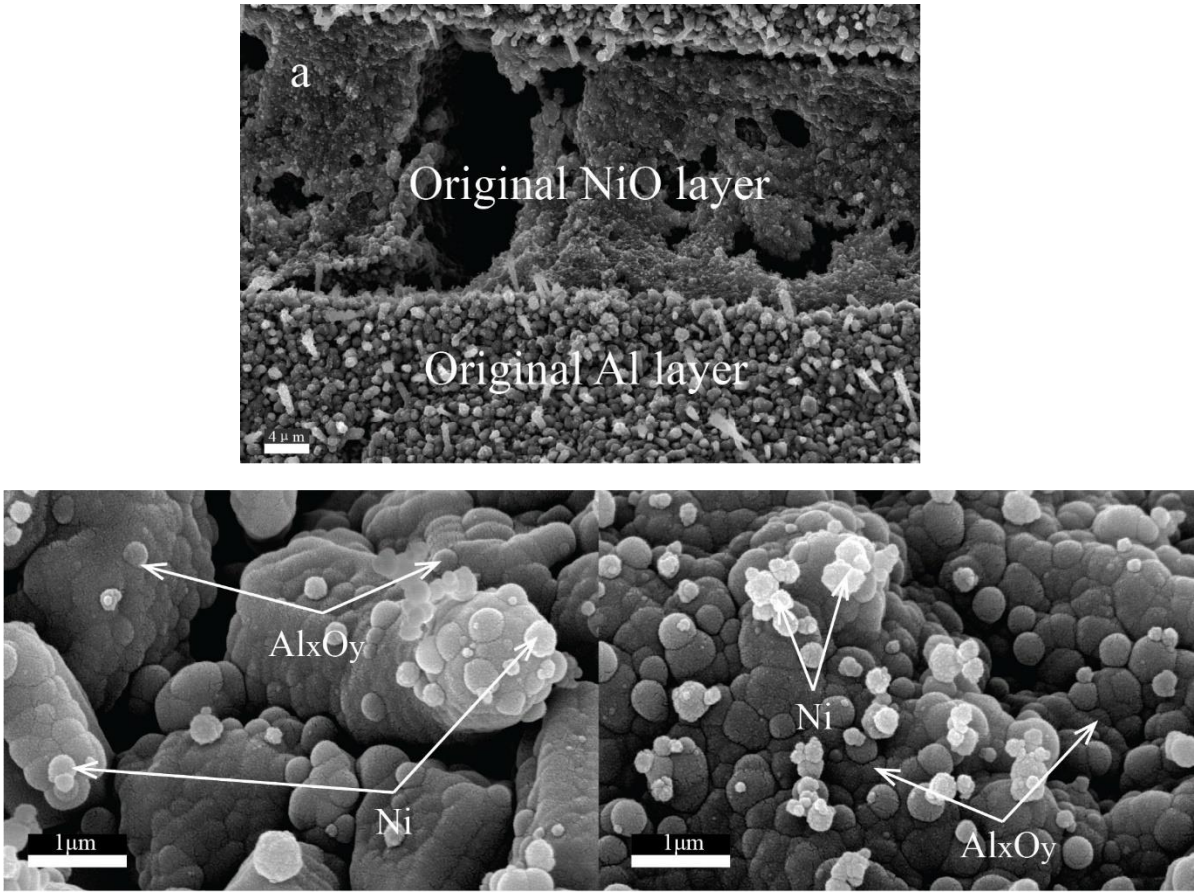

Figure 4.9 SEM images of the products formed from the thermite reaction between Al and NiO nanoparticles. a) Interfacial view of reactive layers with 5,000×; b) Al layer with 100,000×; c) NiO layer with 100,000×

In order to acquire the detailed information from both layers shown in Figure 4.9(a), 4. 9(b) and 4. 9(c) demonstrate each layer with a higher magnification (100,000x). Figure 4.9(b) shows the Al layer, while Figure 4.9(c) shows the NiO layer, respectively. The SEM images suggest that, after the reaction, the particle sizes were increased from the original 50 nm to more than 1 µm. This supports the previous statement that the produced Ni metal melted and this caused large metal particles to form. These images in Figure 4.9 also demonstrate the co-

existence of Ni and Al in both layers. This suggests that Ni and Al migrated from their original locations into both layers. Oxygen is also widely distributed in both layers.

4.4.5.1 XRD analysis for the Al/NiO composite before and after the thermite reaction

The XRD analysis was conducted to reveal the chemical compounds before and after the thermite reaction and Figure 4.10 shows the XRD results.

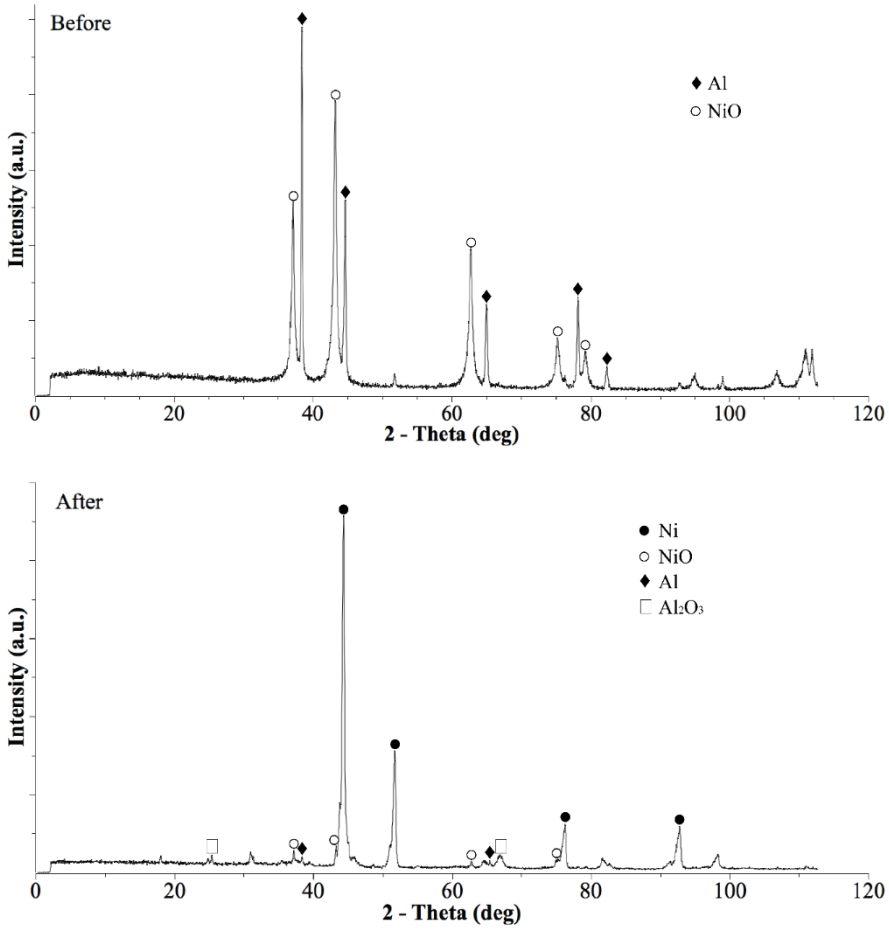

Figure 4.10 XRD patterns of samples before and after the thermite reaction for Al/NiO nanocomposite

Only Al and NiO diffraction lines are visible in the XRD pattern before the thermite reaction, which is due to the fact that the amorphous phase of the Al_2O_3 shell cannot be detected with XRD. The XRD patterns from the reacted composite show clear and strong Ni diffraction lines. Additionally, NiO, Al, and Al_2O_3 chemical compounds are present with small peaks. These weak peaks of Al and NiO can be explained by the degree of reaction completion, which also agrees with the TGA/DSC results shown in Figure 4.3.

4.4.5.2 EDAX point scan and line scan

EDAX point scans and line scans were conducted to trace the elements migration within the contacting layers upon the thermite reaction. Figure 4.11 shows the point scan in the Al and NiO layers, respectively. Selected area "1" displays the elements present in the Al layer where Al, Ni, and O are all present. The Au element comes from the gold coating that was applied before conducting the EDAX measurements. In selected area "2", the three elements of Al, Ni, and O are also present. The point scan results provide the following information with regards to the migration of elements. First of all, after the reaction Ni becomes available in the Al layer. Supported by the XRD and SEM images, this observation suggests: 1) NiO nanoparticles migrate into the Al layer after the thermite reaction is initiated on the contacting surface of the reactive layers. NiO then reacts with the Al nanoparticles to produce Ni metal; 2) the produced Ni metal undergoes melting and it merges into larger particles. Secondly, the Al element is present in the NiO layer, suggesting the following processes: 1) Al nanoparticles migrate across the contacting surface between the two layers and go into the

NiO layer. Al reacts with the NiO nanoparticles to produce Ni metal and Al_2O_3; 2) the Ni metal is melted and sintered into larger particles, as shown in Figure 4.9(c).

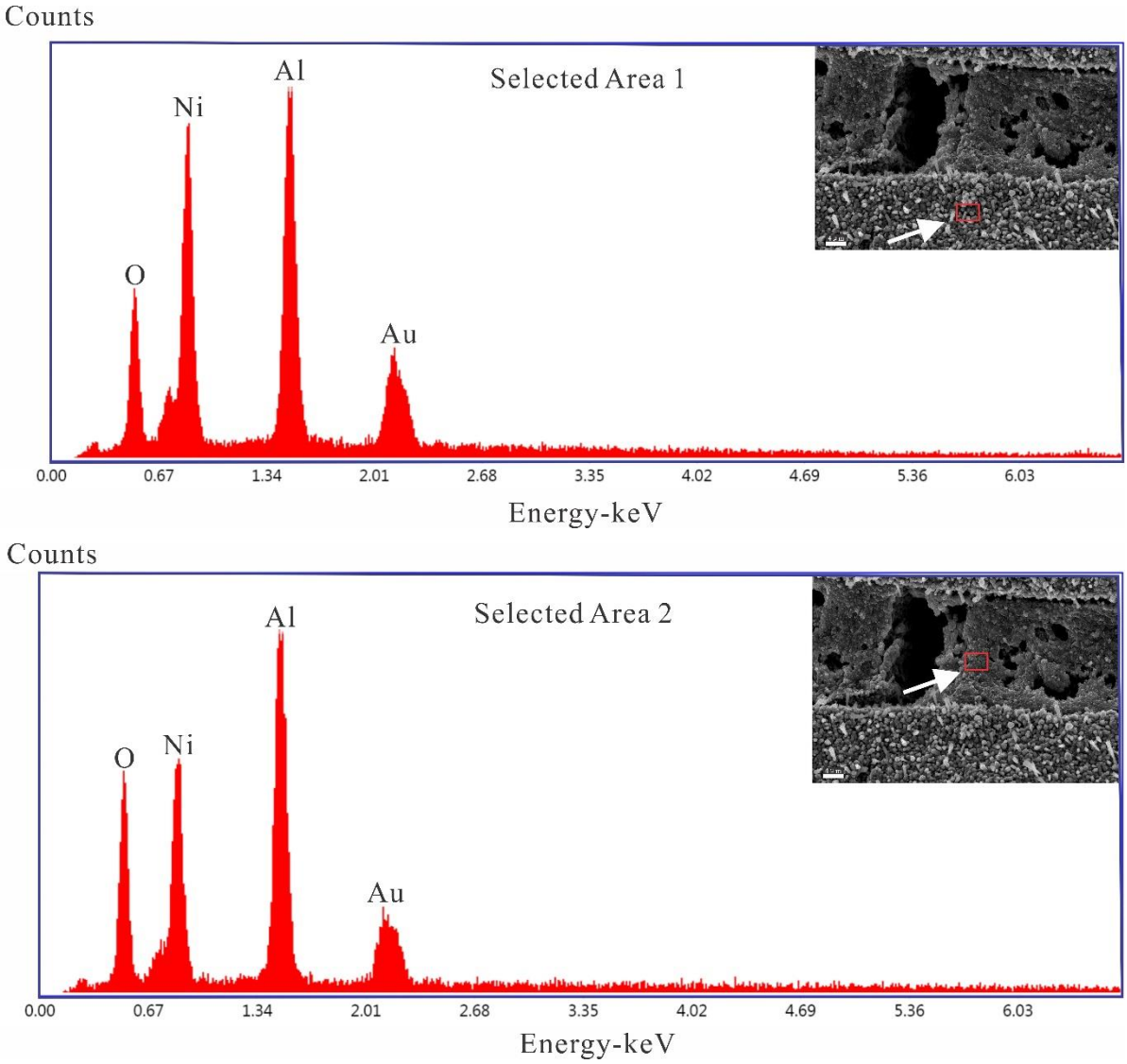

Figure 4.11 Point scans of EDAX on the original Al (area 1) and NiO (area 2) layers

To further investigate the distribution and migration of the Al and NiO nanoparticles, a line scan was conducted across the contacting surface of the reactive layers, as shown in Figure 4.12. The solid line is the distribution of O from the NiO layer to the Al layer, while the dash

line and dotted line show the signals of Ni and Al in the same direction, respectively. It can be seen that O, Al, and Ni possess a similar trend throughout these layers, indicating that these three elements are all involved in the thermite reaction. This suggests that a condensed phase reaction occurred.

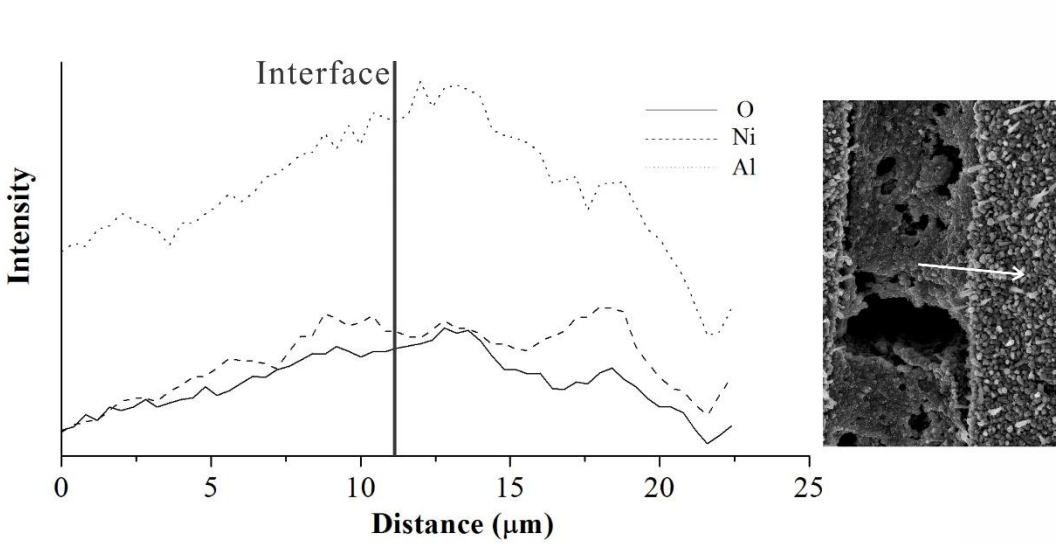

Figure 4.12 Line scan in EDAX from the NiO to Al layer, across the contacting surface of the two reactive layers

4.4.5.3 Elemental mapping of reacted Al/NiO layered composite

Elemental mapping was performed on the reacted Al/NiO composite to further examine the proposed reaction mechanism, as shown in Figure 4.13. First, in comparison with Figure 4.8, the clearly separated distributions of Al, Ni and O in the individual layers of the original sample are replaced by the unseparated distributions of these elements in all layers of the product. A further comparison with Figure 4.5 suggests that, decomposition of NiO to form O did not happen when the thermite reaction between Al and NiO layers was initiated.

Secondly, all three elements distribute almost evenly across the examined volume, though less of them exist in the porous layer.

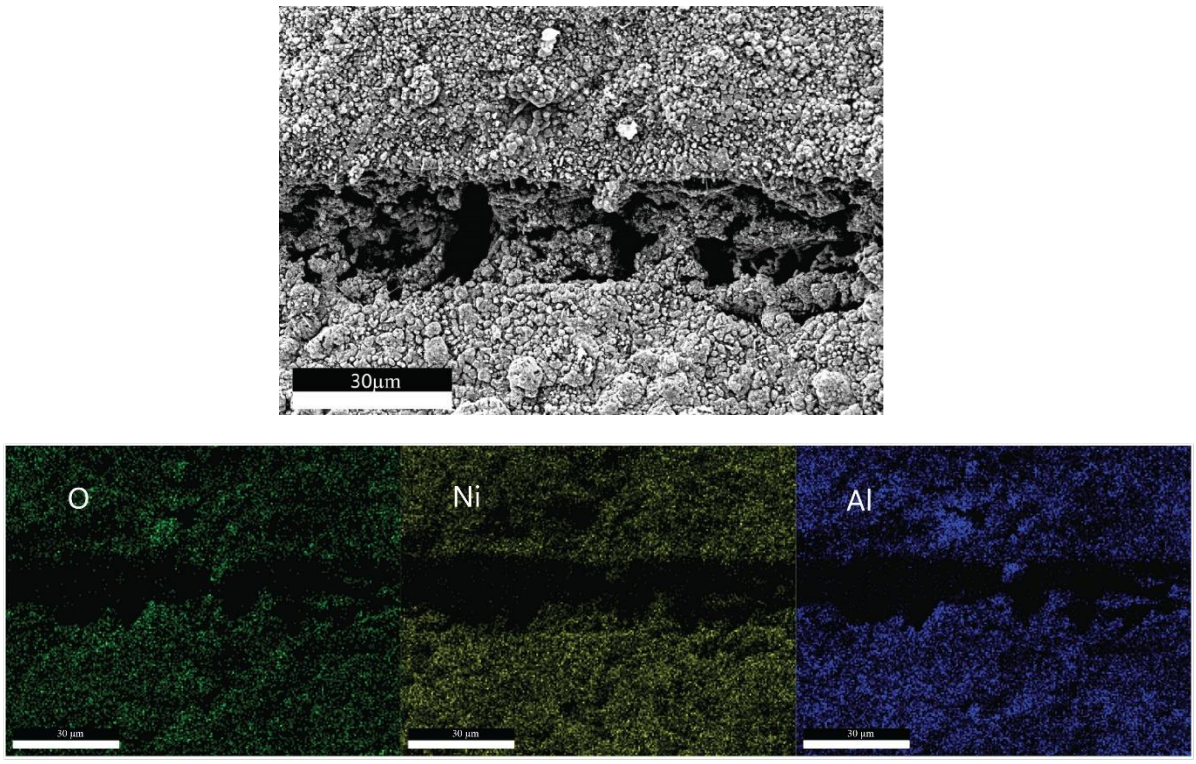

Figure 4.13 SEM images and corresponding elemental mapping of the vacuum-deposited multi-layer of Al/NiO composite after thermite reaction

This observation confirms the solid-solid reaction between Al and NiO and it supports the cross-migration of NiO and Al into the opposite layers. The difference between the reaction mechanisms of Al/CuO and Al/NiO systems is mainly attributed to their distinct thermochemical stability and increase of nanoparticles' mobility with temperature. The standard enthalpies of formation for Al_2O_3, CuO, and NiO are 1669.8 kJ/mol, -155 kJ/mol, and -244.3 kJ/mol, respectively. A larger standard enthalpy of formation indicates a more

stable chemical compound. Since the standard enthalpy of CuO is smaller than that of NiO, it can decompose into Cu and O at a lower temperature, which agrees with the findings in this study. On the other hand, the mobility of nanoparticles increases with the temperature. When the sample is heated to an intermediate temperature, before reaching the onset temperature of the thermite reaction, the CuO nanoparticles would decompose and form Cu and O while the NiO nanoparticles migrate to the Al layer. These two processes lead to the different reaction mechanisms of the layered Al/Cu and Al/NiO nano-composites studied in this work.

4.4.6 Strategy to improve the ignition properties and reaction completion

According to the aforementioned experiment results, Al/CuO and Al/NiO systems demonstrate diverse reaction mechanisms. For the Al/CuO system, the thermite reaction is initiated on the contacting surface of the reactive layers through the direct contact of the reactive components. Next, the CuO nanoparticles undergo decomposition to release oxygen, which further diffuses into the Al layer. The oxygen passes through the Al_2O_3 shell to reach the Al core, which agrees with the gas-solid reaction mechanism.

In the case of the Al and NiO nanoparticles, the NiO oxidizer does not undergo decomposition, and the thermite reaction occurs through the direct contact of the Al and NiO nanoparticles after the thermite reaction is initiated at the contacting surface of two reactive layers. With increasing temperature, the NiO and Al nanoparticles migrate into the opposite layers and form contact between the solid-solid compounds. After this stage, oxygen diffuses

from NiO into the Al nanoparticles, according to the bond order simulation, which presents the fact that the Al-O bond forms after reaching the onset temperature. Because of the fast energy release from the thermite reaction, the heat is absorbed by the Ni metal and causes it to melt, resulting in larger Ni particles. The released energy, captured by the Ni product, is not sufficient to cause the phase transformation of amorphous Al_2O_3 into a crystalline structure. This agrees with the solid-solid reaction mechanism.

4.5 Conclusion

In this study, thermite composites consisting of one Al nanoparticle layer and a CuO or NiO nanoparticle layer were fabricated via vacuum filtration. SEM images showed that there was intimate contact between these two reactive layers before the thermite reaction was initiated. The energetic properties of Al/CuO and Al/NiO composites were investigated using a TGA/DSC device, showing 507 °C and 516 °C as the onset temperatures of the corresponding thermite reactions, respectively. Microstructures of these composites were examined using SEM before and after the thermite reaction. A comparison of these images revealed that, after the reaction had occurred, there was a gap formed between the two layers of the Al/CuO composite. In contrast, the two layers of the Al/NiO composites remained attached, but both became highly porous. Further analysis based on elemental mapping and scanning (point and line) suggested that, after the thermite reaction Al and Cu were present separately within the different layers for the Al/CuO composite. In the products of the Al/NiO composite, however, Al and Ni were found to be widely distributed in both the layers. These

observations support the following reaction mechanisms of the Al/CuO and Al/NiO composites. The thermite reaction between Al and CuO nanoparticles is initiated, at the onset temperature, by the interactions of Al and CuO nanoparticles at the contacting surface of the two reactive layers. Then, the thermal-decomposition of CuO occurs, followed by the subsequent migration of oxygen into the Al layer. The thermite reaction is maintained by the gas-solid reaction between Al and oxygen. On the other hand, upon heating the Al and NiO composite to the onset temperature, their reaction is initiated at the contacting surface of the two layers. Next, both nanoparticles migrate towards each other within the composite, which leads to energetic processes. These processes include solid-solid reactions, melting, and sintering, which produces a porous structure in both layers. A future study to investigate the migration of related nanoparticles under a specified temperature gradient is highly desirable.

Chapter 5: Nano-thermite reaction with multi-layered structure tuned by CNTs

5.1 Overview

Single walled carbon nanotubes (CNTs) were added into layered Al/NiO nano-thermite composites, to tune their energetic and reaction properties. Scanning Electron Microscopy (SEM) images showed a direct contact between the Al and NiO layers, where the presence of CNTs in a designated layer was clearly visible. Thermal-chemical data obtained from Differential Scanning Calorimetry (DSC) demonstrated these composites, although modified with CNTs in either the Al or the NiO layer, exhibited a nearly constant onset temperature, implying comparable reaction initiation mechanisms. However, different amounts of energy release, accompanied with formation of distinct layer composition and microstructures of their products, was produced. It was further revealed that, by means of mass spectrometry, SEM and X-ray Diffraction (XRD) analysis, upon the initiation of the thermite reaction between Al and NiO at the interface layer, the reaction between CNTs and NiO nanoparticles produced CO and CO_2, which promoted the gas-solid chemistry and gas diffusion within the microstructure of the composite. Both increased the energy release and resulted in less agglomerated reaction products. In comparison, adding CNTs into the Al layer did not bring a significant change to the condensed-phase reaction mechanism which was proposed previously for the Al/NiO composite.

5.2 Introduction and literature review

Recently carbon nano-tubes (CNTs) were tested for their influence to the thermo-chemical properties of certain types of composites. When mixed into the CL-20 (a nitroamine explosive) composite, it was found CNTs could increase the overall thermal conductivity of the composite, which subsequently reduced the impact sensitivity of CL-20 [153]. The enhanced thermal conductivity was attributed to the formation of a three-dimensional heat-conducting network structure of CNTs. In another study [154], it was found hybridising CNTs with metal oxide nanoparticles could lead to low-temperature oxidation of CNTs, when the catalyst (metal oxide) was able to provide its lattice oxygen directly to CNT. Interestingly enough, the products from this reaction, i.e., CO or CO_2, can react with Al nanoparticles [155, 156]. Adding CNTs into the Al/CuO nano-thermite composites was found, indeed, to change their energetic properties including an increased exothermic enthalpy with increasing the CNT content, the lowered ignition temperature of the thermite reaction by 71°C [157]. There is no such report focused on the roles of CNTs in the Al/NiO nano-composite in the literature. The distinct reaction mechanisms of the Al/CuO and Al/NiO systems, plus the missing mapping of interactions between CNTs and metal oxide nanoparticles during the thermite reaction, highly suggest a new study on energetic properties of the CNTs modified Al/NiO nano-thermite composite.

This work focuses on a layered Al/NiO nanoparticle composite, which was modified with CNTs in its individual layers. Since the Al and NiO nanoparticles were patterned in separated layers, which reduced the direct particle-to-particle interaction within these layers, the interface between these neighboring layers played a dominant role in reaction initiation. This

arrangement facilitated the study of reaction mechanisms. Secondly, CNTs were added into either the Al or the NiO nanoparticle layer, which provided suitable conditions to investigate the different interactions between CNTs and two reactive components. The microstructures and thermo-chemical properties of these layered composites, modified by CNTs, were investigated, with the objective of revealing the roles of CNTs during reaction initiation and propagation. The energy release and onset temperature were measured with simultaneous thermogravimetry (TGA) and differential scanning calorimetry (DSC). The chemical compositions of the products were studied by x-ray diffraction (XRD) and energy dispersive x-ray spectroscopy (EDS).

5.3 Experimental method

In this work, the nano-thermite composites were fabricated with a multi-layer structure via vacuum filtration. The detailed procedure of vacuum filtration can be found in our previous publication [158].

5.3.1 Sample preparation

The Al (size range: 40-60 nm) and NiO (average size: 50nm) nanoparticles, with 99% purity, were purchased from *Skyspring Inc*. The single-walled carbon nanotubes (1.1 nm in the average diameter and 5~30 μm in the length) were obtained from *US Research Nanomaterials Inc*. Before vacuum filtration, the nanoparticles and CNTs were dispersed in acetone and sonicated to eliminate agglomeration. The sonication times of Al and NiO

nanoparticles were set to 20 min, in order to eliminate the chance of nanoparticle-solvent reaction. The sonication time of CNTs was set to 90 min. Two types of samples were fabricated. To produce Sample 1 (the Al/NiO+CNT composite), the solution with CNT suspension (0.5 ml) were mixed with the solution containing NiO nanoparticles (0.5 ml). Then this new solution was added into the glass funnel of the vacuum filtration apparatus. Driven by a vacuum pump, a single layer of mixed NiO and CNT nanostructures was produced on a filter paper. Then the solution containing Al nanoparticles (1 ml) was deposited on the top of the NiO+CNT layer, which completed the preparation of one interface for Sample 1. The same procedure was repeated, until a multi-layered composite containing 9 interfaces was obtained. To produce Sample 2 (the Al+CNT/NiO composite), the CNT solution (0.5 ml) was mixed with the Al nanoparticle solution (0.5 ml) to form the first layer. Then the NiO nanoparticle solution (1 ml) was added, to deposit a NiO nanoparticle layer on the top of the Al+CNT layer. For a bilayer of these two samples, the Al layer contained 7.84 mg of Al nanoparticles and the NiO layer contained 23.52 mg of NiO nanoparticles. In addition, 1 mg of CNT was added to the corresponding layer. The mass ratio of Al and NiO composite was then calculated as 0.33. Taking into account of the active content (57.30%) of Al nanoparticles, as determined previously for the sample batch of nanoparticles [158], the mass ratio between Al and NiO reactants in a bilayer was calculated as 0.19. It has to be noticed that the mass ratio of 0.33 refers to the global ratio of Al and NiO nanoparticles, including the Al_2O_3 shell presenting in the Al nanoparticles. The ratio between active content of Al nanoparticles and NiO is calculated as $0.33\times57.30\%=0.19$, which excludes the natural

Al_2O_3 shell. The stoichiometric ratio can be calculated according to the reaction equation between Al and NiO, which is 0.42 in regard to the global stoichiometric ratio and 0.24 excluding the Al_2O_3 shell. The same procedure was repeated, until a multi-layered composite containing five Al/NiO bilayers was produced. The global stoichiometric ratio was estimated to be the same as that of each bilayer. The produced samples were hence fuel-lean. A detailed description of these prepared samples is shown in Table 5.1. It has to be mentioned that the global ratio in Table 5.1 considers the mass of CNT in either Al or NiO layer, which results in the different value of the global stoichiometric ratio in Al/NiO+CNT and Al+CNT/NiO composites. Following vacuum filtration, Sample 1 features direct contact between the NiO nanoparticles and CNTs within the same layer, while Sample 2 highlighted the direct contact between the Al nanoparticles and CNTs within a same layer.

Table 5.1 Specification of prepared samples using vacuum filtration

Sample 1 (Al/NiO+CNT)				
Al layer		NiO+CNT layer		Stoichiometric ratio[2]
7.84 mg ± 0.43 mg (4.49 mg)[1]		NiO	23.52 mg ± 0.59 mg	0.404
		CNT	1 mg	
Sample 2 (Al+CNT/NiO)				
Al+CNT layer		NiO layer		Stoichiometric ratio[2]
Al	7.84mg (4.49 mg)[1] ± 0.33 mg	NiO	23.52 mg ± 0.67 mg	0.448
CNT	1 mg			

[1]Active content of Al nanoparticles, based on the calculation in [158].

[2] Global Stoichiometric ratio.

5.3.2 Characterization

The microstructures of the multi-layered nano-thermite composites were examined with a SEM (Model LEO 1550 Zeiss) under the 20 kV electron beam voltage. EDS equipped on this SEM was used to study the element distributions of Ni, O, C, and Al throughout the layered structure. Due to the high operation voltage of SEM and to produce a high electric conductivity, the samples were coated with a gold layer via a UHV sputter system under 20 mA for 120 seconds. The initiation temperature and energy release data was collected from each sample using DSC (NETZSCH STA model 449F3A-0918-M Jupiter) with a heating rate of 10 °C/min, when the temperature was increased up to 1000 °C under an argon atmosphere. XRD (XRG 3000, Philips) was utilized to identify the chemical compositions of reactants and products. To investigate the gases produced during the thermite reaction, a tube reactor equipped with a mass spectrometer (CATLAB-PCS) was used. The target sample was placed on a porous bed of the reactor when its temperature was increased from room temperature to nearly 900 ºC. A carrier gas (ultra & high purity 5.0 argon, Praxair Canada Inc.) with a flow rate of 20 ml/min was fed into the reactor. At the beginning of the experiment, the argon was allowed to flow through the reactor and mass spectrometer for 30 minutes, to purge the system. When the reading values of measured gases became stable, the tube reactor was heated with 10 ºC/min and the collection of gas concentrations was started.

5.4 Result

5.4.1 Microstructures and elemental compositions

The SEM images of the nano-thermite composites, produced from vacuum filtration, are shown in Figure 5.1. In order to demonstrate the difference microstructures of the cross sections of these samples, secondary electron and backscattered electron images are also presented. From Figure 5.1, the interfaces which separate the neighbouring Al and NiO reactive layers are clearly visible. The overall 9 interfaces were formed, as shown in Figures 5.1(a) and 5.1(b). Figure 5.1(a) shows in Sample 1 (Al/NiO+CNT), the region near each interface exhibits a darker color which is distinguishable from the neighbouring Al and NiO+CNT layers. In Figure 5.1(b), the produced microstructures of Sample 2 (Al/CNT/NiO) are less distinguishable from one another. Different morphologies of Samples 1 and 2 are believed to result from the corresponding interaction between CNTs and the hosting nanoparticles. In general, NiO nanoparticles have a greater density and therefore it is more difficult to disperse them into a solution. During the vacuum filtration, heavy NiO nanoparticles intend to form agglomerates. Adding CNT into the NiO layer can help fill in pores among NiO nanoparticles, which results in a smooth boundary between two reactive layers (Figures 5.1(a) and 5.1(g)). The SEM images with the secondary electron and backscattered electron detection are shown in Figures 5.1(c) and 5.1(d) for Sample 1 and Figures 5.1(e) and 5.1(f) for Sample 2. For Sample 1, the gran sizes in the Al layer are much smaller than the grain sizes in the NiO+CNT layer. Interestingly, these three domains found in Sample 1 (Al/NiO+CNT) by secondary electron imaging (in Figure 5.1(c)) are not shown in Figure 5.1(d). Considering the backscattered electrons reflect the elemental contrast, the

comparison between Figures 5.1(c) and 5.1(d) suggests the slightly dark region at the interface actually locates in the Al layer. For Sample 2 (Al+CNT/NiO), its microstructure shown in the secondary electron image (Figure 5.1(e)) and in the backscattered electron image (Figure 5.1(f)) is similar, with larger agglomerates in the NiO layer. Figure 5.1(g) shows the higher resolution image of the region near the interface of one Al/NiO+CNT bilayer. The interface is highlighted by a dash line. It confirms the existence of these three domains in Sample 1: the Al layer with smaller grain sizes, the darker region in the Al layer, and the NiO+CNT layer with larger grain sizes. The insert in Figure 5.1(g) demonstrates the presence of CNTs in the NiO+CNT layer. Figure 5.1(h) shows the higher resolution image of the region near the interface of one Al+CNT/NiO bilayer. The interface is also highlighted by a dash line. The insert in Figure 5.1(h) demonstrates the presence of CNTs in the Al+CNT layer.

It is important to mention, due to the limitations of solvent dispersion and vacuum filtration which were applied in this study, mixing of CNTs with hosting nanoparticles (Al or NiO) is not homogeneous. Some nanoparticles are agglomerated but the sizes of these agglomerates are still below 100 nm (see the inserts in Figures 5.1(g) and 5.1(h)). Nevertheless, at least in some area, CNTs form a 3D network to which nanoparticles are attached. The length of CNTs become shorter due to vibration and cutting during sample preparation. It is worth to mention that the length of CNT is specified by the manufacturer to be 5 ~ 30 μm and these CNTs are able to connect the hosting nanoparticles and subsequently increase the heat conductivity of the sample.

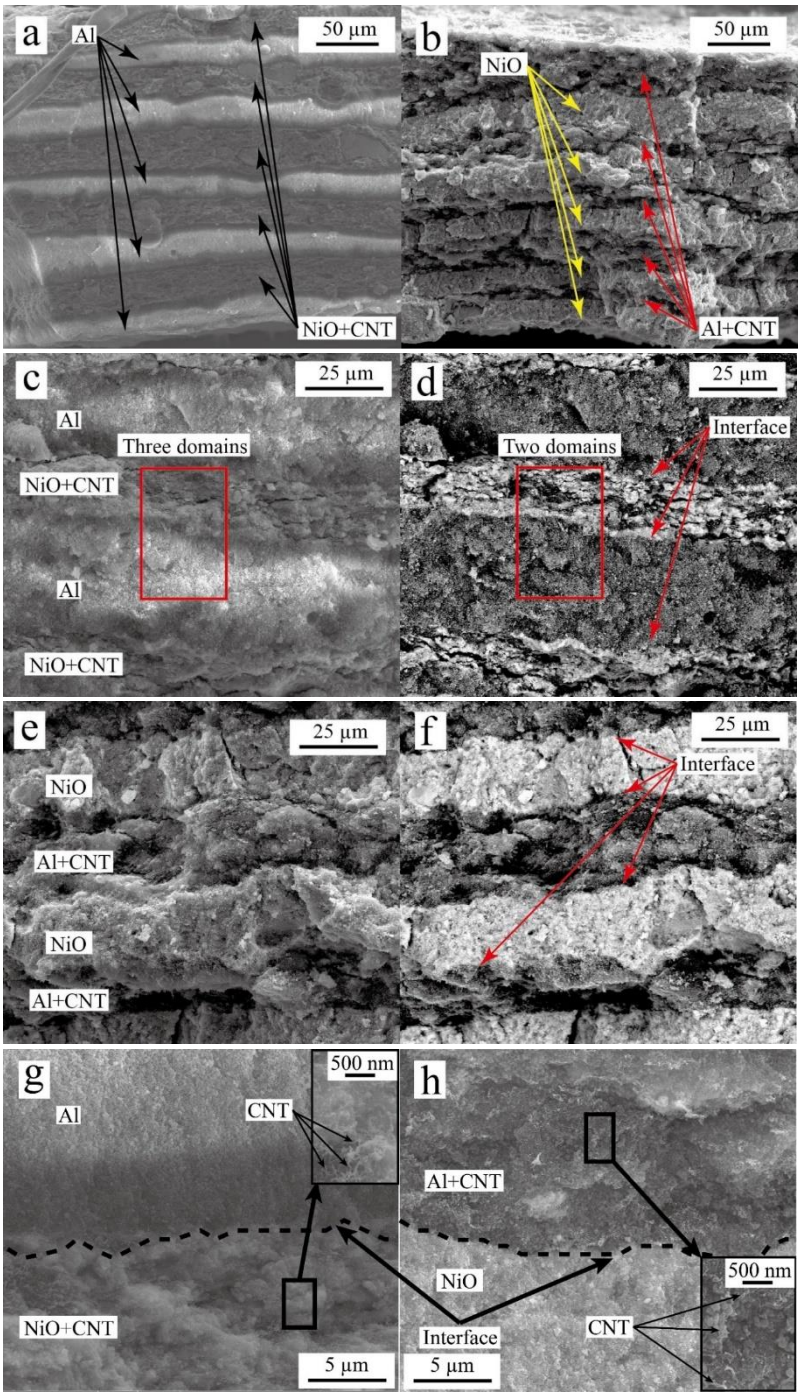

Figure 5.1 SEM images of the overall view of 10 layers of Sample 1 (a) and Sample 2 (b); Sample 1 with secondary electron imaging (c) and backscattered electron imaging (d); Sample 2 with secondary electron imaging (e) and backscattered electron imaging (f); the zoom-in view of Sample 1 (g) and Sample 2 (h)

The elemental distributions of C, O, Ni and Al within the individual layers are shown in the EDS results Figure 5.2. The inserts show the EDS scanning areas on the corresponding SEM images. In Figure 5.2(a), the scanning area in the Al layer contains Al and O, and a trace of Ni (the amount of C is negligible). The Ni element may come from the sample preparation procedure, during which the vacuum draws a small amount of NiO nanoparticles into the Al layer. In Figure 5.2(b), Ni, C, and O are present in the NiO+CNT layer with a trace of Al. Figures 5.2(c) and 5.2(d) show the elemental distributions in Sample 2. In Figure 5.2(c), C, O, and Al are present in the Al+CNT layers, with a trace of Ni element. In Figure 5.2(d), Ni and O are dominant in the NiO layer, with a trace of Al.

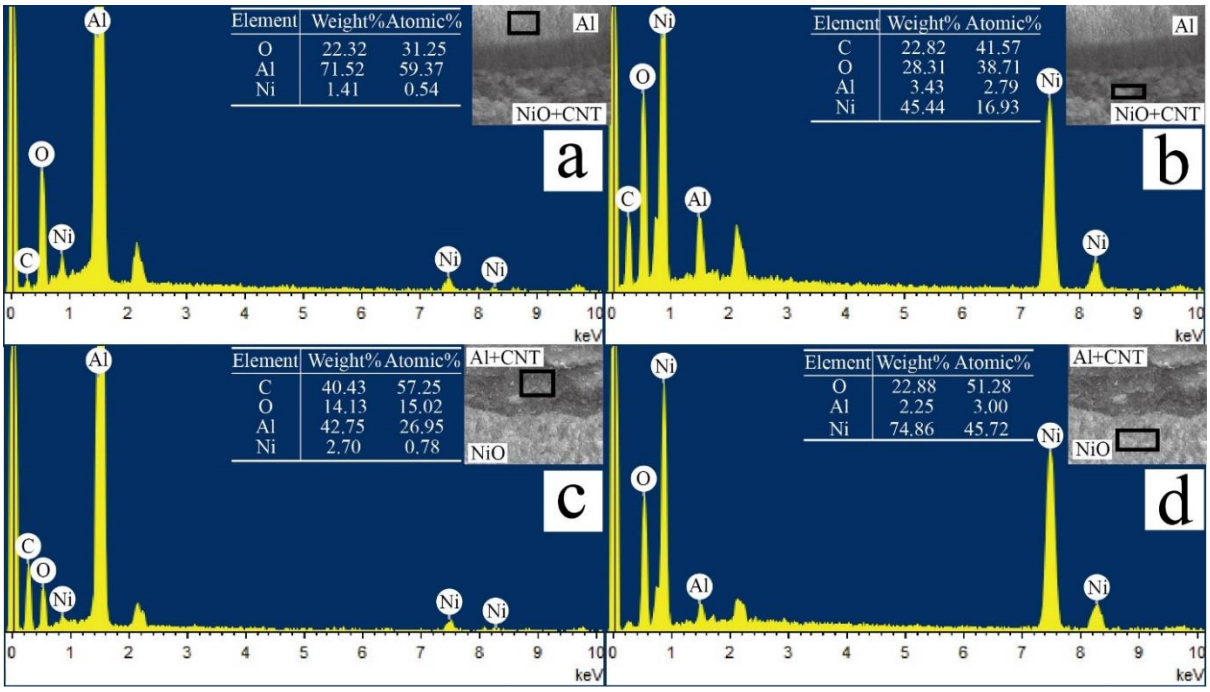

Figure 5.2 EDS results showing the elemental compositions in the Al and NiO+CNT layers of Sample 1: (a) and (b), and the Al+CNT and NiO layers of Sample 2: (c) and (d), before thermite reaction

The SEM and EDS results provide the needed information on their layered structures of Al/NiO nano-composites and the degree of mixing between CNTs and reactive nanoparticles. CNTs are successfully added into a specific layer of Al or NiO, with satisfying contacts with the surrounding nanoparticles. Meanwhile, an interface between the fuel and oxidizer layers is produced for each Al/NiO system. Intimate contacting between reactive nanoparticles is achieved in this interface range. Moreover, despite of some traces of unexpected elements in these individual layers, CNTs are primarily located in the desired Al or NiO layers.

Samples 1 and 2 are treated in TGA/DSC from room temperature to 1000 °C, with a heating rate of 10 °C/min in argon atmosphere. Due to direct contacting of these reactive nanoparticles near the interface, the thermite reaction is initiated when the temperature reaches the onset temperature. The reaction further propagates into the microstructure of these samples, driven by the mass and heat transfer, until the fuel nanoparticles are nearly consumed. The reaction products are collected from the DSC equipment and their SEM images are analyzed.

Figure 5.3 shows the SEM image of the product microstructure derived from Sample 1 (Al/NiO+CNT). In Figure 5.3(a) a continuous gap is clearly visible between two reacted layers, with a thickness of around 1 μm. The formation of this gap can be attributed to the gas formation during the reaction, which will be discussed later. The zoom-in view of the region near the interface is shown in Figure 5.3(b), showing that these nanoparticles in the original Al layer still remain their spherical shapes. The produced particles (composed of

mainly Ni, see later) in the original NiO+CNT layer however have a much large size of around 1-2 microns compared to the sizes of original NiO nanoparticles. The particles in the original Al layer are much smaller and in the range of a few hundred nanometres. In addition, it is hard to find CNTs in the products.

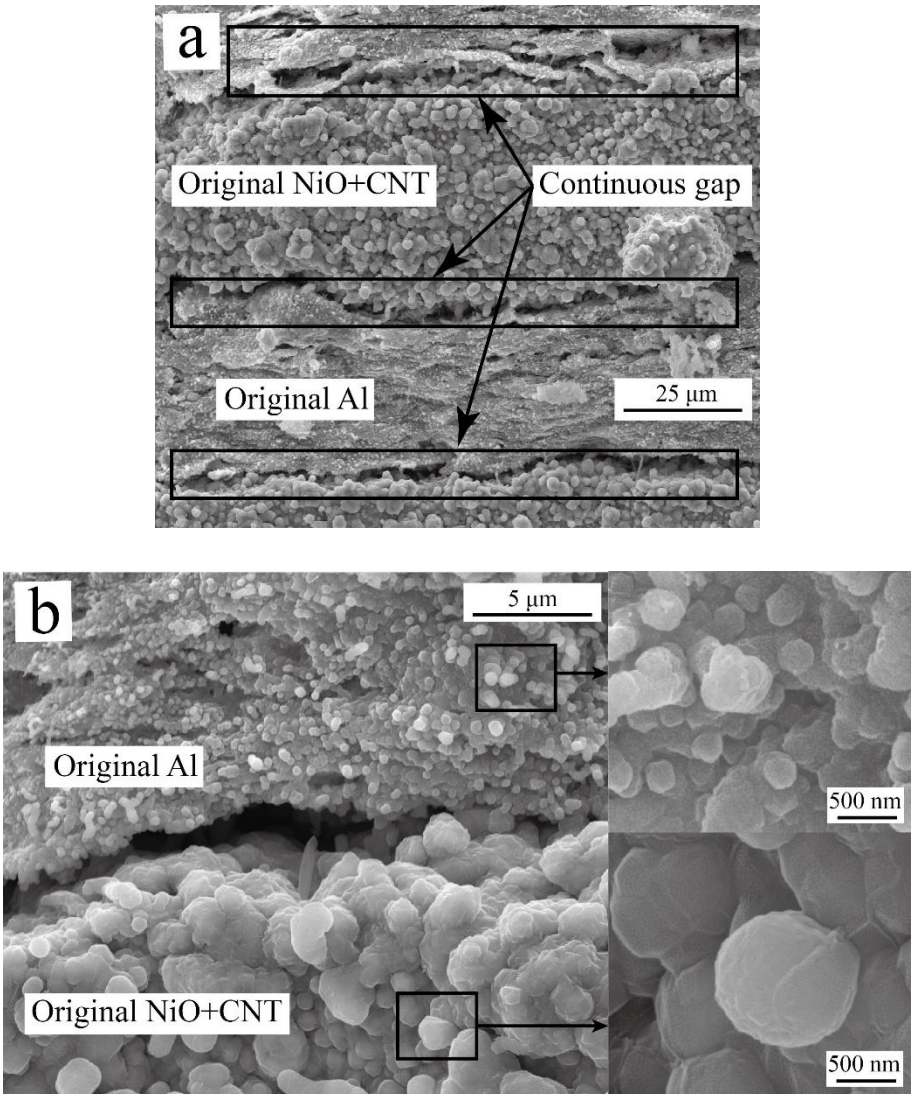

Figure 5.3 SEM images of Sample 1 after thermite reaction: (a) the original Al and NiO+CNT layers with a continuous gap; (b) zoom-in view near the interface

Figure 5.4 shows the reacted structure of Sample 2 (Al+CNT/NiO). For Sample 2, although the original NiO layer becomes more porous, no obvious gap is visible between two reacted layers. When CNTs cannot be found in Figure 5.4(b), the morphologies of these products of Sample 2 are quite different from these of Sample 1. Most interestingly in the original NiO layer, a well-organized crystalline structure has been produced (see the insert of Figure 5.4(b)), implying the history of a high reaction temperature. In the original Al+CNT layer, particles are found with wide ranges of sizes and shapes.

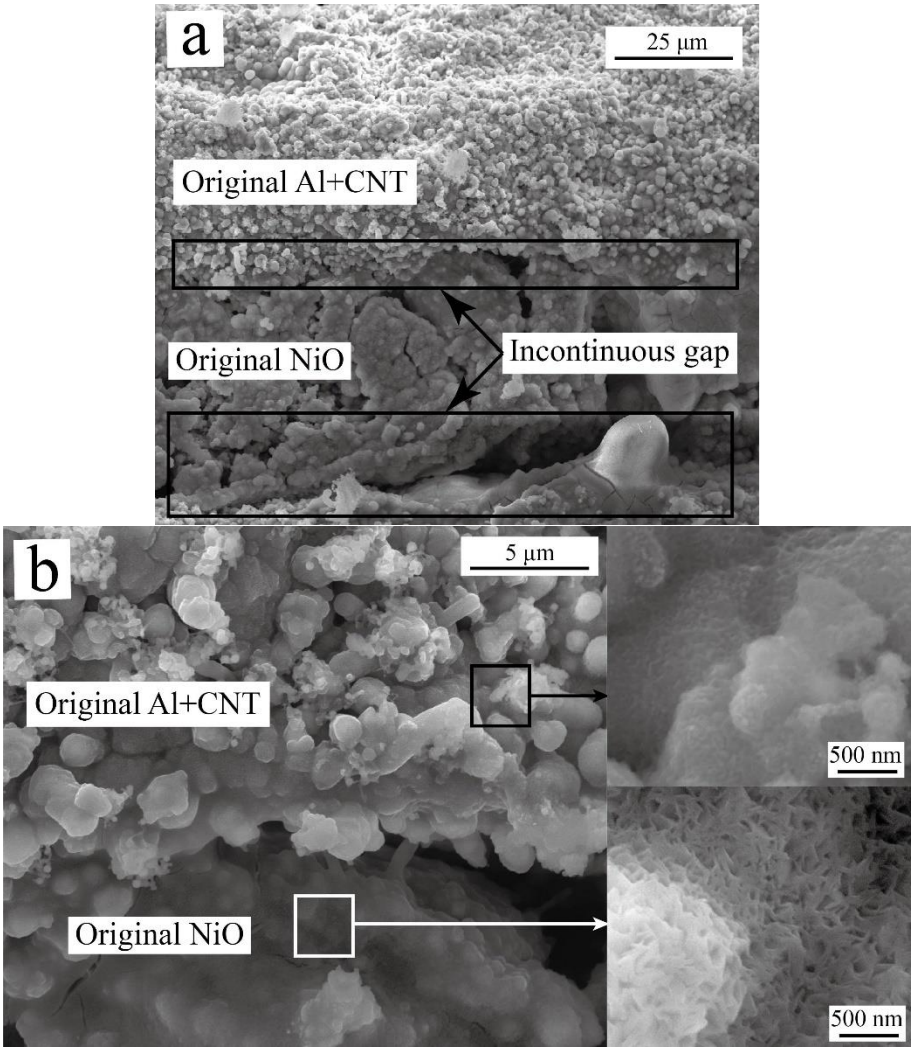

Figure 5.4 SEM images of Sample 2 after thermite reaction: (a) the original Al+CNT and NiO layer; (b) zoom-in view near the interface

In order to identify the chemical composition of these products, EDS results are shown in Figure 5.5. Figures 5.5(a) and 5.5(b) show the product element distributions in the original Al and NiO+CNT layers of Sample 1, respectively.

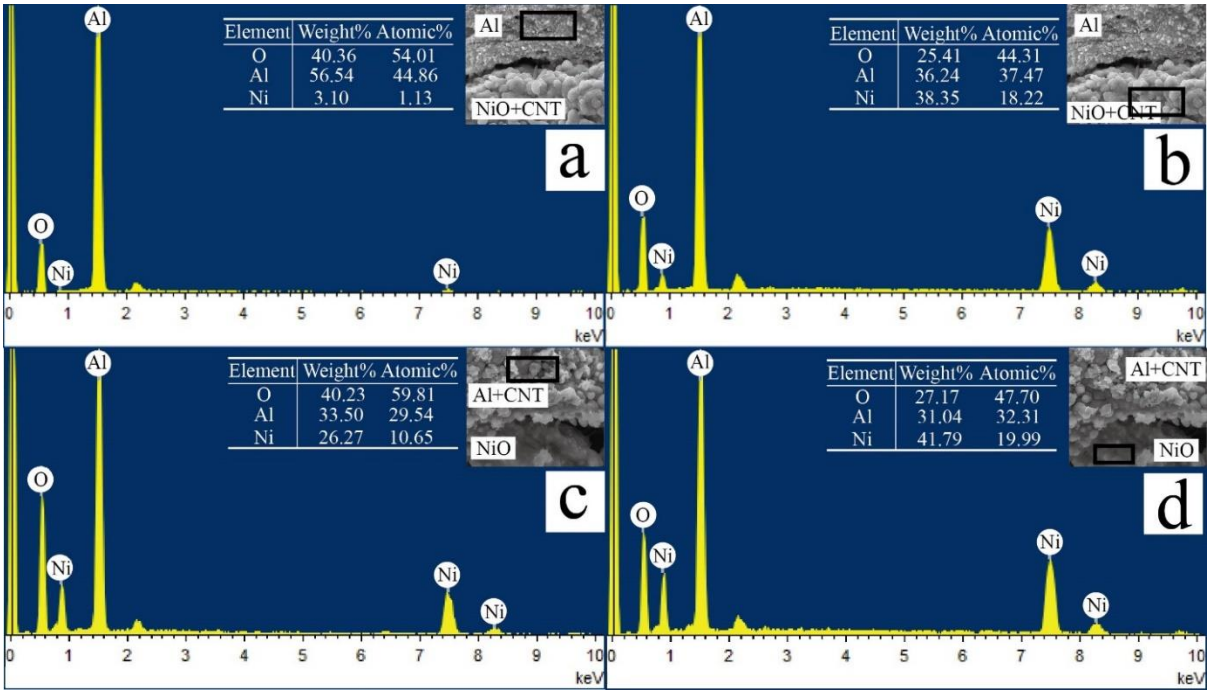

Figure 5.5 EDS result showing the elemental compositions in the Al and NiO+CNT layers of Sample 1: (a) and (b), and the Al+CNT and NiO layers of Sample 2: (c) and (d), after thermite reaction

In Figure 5.5(a), O and Al are present in the original Al layer, whereas a very small amount of Ni may be found in the same layer, indicating the diffusion of Ni element into the Al layer is negligible. Figure 5.5(b) shows, O, Al, and Ni are all present in the original NiO+CNT layer, with comparable concentrations. This suggests the migration of Al nanoparticles into

the NiO+CNT layer. Figures 5.5(c) and 5.5(d) show the element distributions in the original Al+CNT and NiO layers of Sample 2, respectively. As demonstrated, all three elements (O, Al, and Ni) are present in both reacted layers of Sample 2, which is similar to our previous study where layered Al and NiO nano-composites were investigated [158]. In that study, cross-migration of Al and NiO nanoparticles into the opposite layer was found to sustain the thermite reaction. CNTs are not present in the products of Sample 2.

5.4.2 Onset temperature and energy release

During the TGA/DSC measurement, the samples are heated, with a constant heating rate, to the onset temperature from which an energy evolving process is started. The DSC curves of Samples 1 and 2 are shown in Figure 5.6. It shows the onset temperatures for Samples 1 and 2 are 517.3 °C and 518.5 °C, respectively. A previous study reported the onset temperature of the layered Al/NiO nano-composite as 516 ºC [158]. There is apparently no significant change among the onset temperatures of these samples, which implies a similar reaction initiation process. The area of the major exothermic peak of the DSC curve can be used to derive the heat release from the reaction. The reaction heat of Sample 1 is calculated as 1.512 kJ/g, whereas that of Sample 2 is 1.268 kJ/g. Both values are higher than the reaction heat found from the layered Al/NiO nano-composite (1.01 kJ/g) [158], thanks to the reaction involving CNTs. The amount of energy release from Sample 1 is increased by approximately 20%, compared to that of Sample 2. In addition, a small DSC peak corresponding to the melting point of Al nanoparticles exists on each DSC curve, which implies some unreacted

Al nanoparticles were left in the sample. This behavior is common to layered nanothermite composites [158].

In order to examine the thermo-chemical properties of individual layers, the NiO+CNT and Al+CNT layers are produced separately from vacuum filtration, following the same procedure to make other samples. They are tested in the same TGA/DSC instrument with the same conditions. Their TG and DSC curves are shown in Figures 5.7(a) and 5.7(b), respectively.

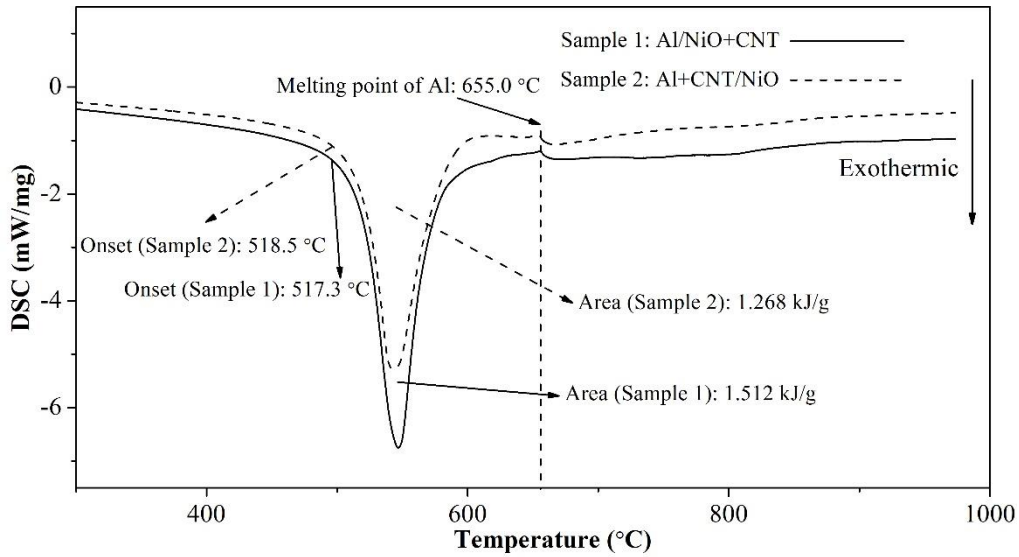

Figure 5.6 DSC result of Sample 1 (Al/NiO+CNT) and Sample 2 (Al+CNT/NiO) up to 1000 °C with a heating rate of 10 °C/min

As shown in Figure 5.7(a), the onset temperature for the NiO+CNT layer, corresponding to the maximum mass reduction accompanied with an endothermic process, is approximately 698 °C, which is much higher than the onset temperatures of Samples 1 (517.3 °C) and 2

(518.5 °C) for their exothermic reactions. Note this onset temperature can be misleading, if a multi-stage oxidation happens. Indeed, the TG curve shows a noticeable reaction between NiO and CNTs at approximately 400 °C, followed by a more significant oxidative reaction of CNTs at about 530 °C.

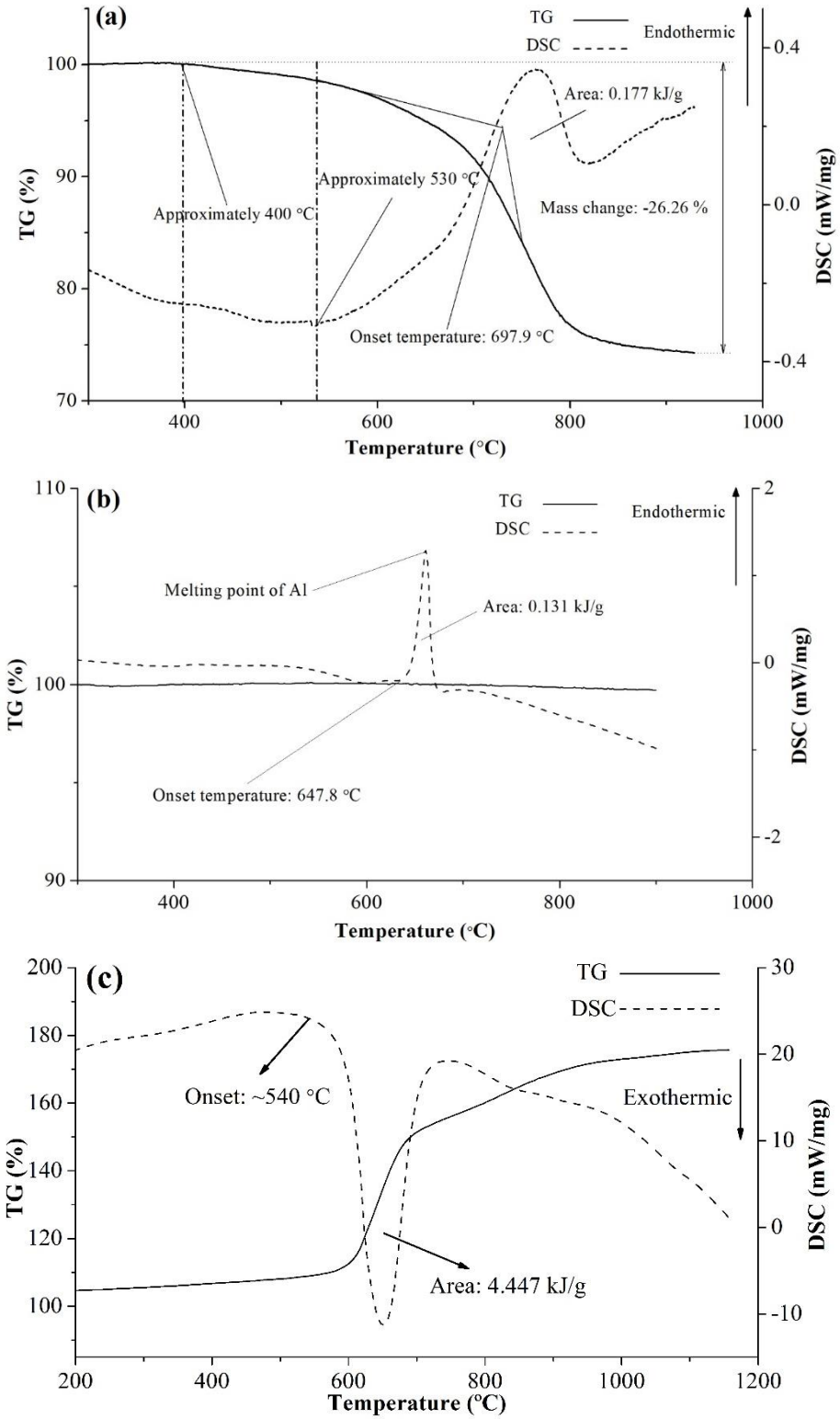

Figure 5.7 TGA/DSC result of (a) NiO nanoparticles and CNTs, (b) Al nanoparticles and CNTs mixture and (c) Al nanoparticles under CO_2 atmosphere up to 1000 °C with a heating rate of 10 °C/min

This two-staged oxidation of CNT by NiO is further studied by mass spectrometry, which will be described later in this paper. The mass change between 400 °C and 530 °C is only 1.6%, indicating an insignificant process. It is interesting to find this oxidative process (which may contain more than one reaction, supported by its broad DSC curve over a large temperature range) is endothermic, with a small energy need of 0.177 kJ/g. In Figure 5.7(b), the only significant peak of the DSC curve is the endothermic peak caused by the melting of Al nano-particles. No reactions between Al and CNTs are observed. Due to its endothermic nature, the oxidation reaction between NiO nanoparticles and CNTs in the composite may occur when the thermite reaction between Al and NiO nanoparticles is able to provide the needed energy to initiate the NiO-CNT oxidation. Before this process, CNTs mainly act as an inert network which may enhance the mass and heat transfer. As showing in Figure 5.7(c), the Al nanoparticles have reactivity with under CO_2 atmosphere. The DSC result shows the exothermic reaction with an energy release of 4.447 kJ/g. The mass increase in TGA data suggests that the Al nanoparticles absorb gas phase, indicating that Al nanoparticles react with CO_2 gas with an onset temperature of approximately 540 °C.

5.4.3 Phase identification using X-ray diffraction

In order to examine the chemical composition and crystalline structures of unreacted samples, as-delivered NiO, Al nanoparticles and CNTs are mixed and investigated using XRD. As shown in Figure 5.8, crystalline structures have been identified in the NiO and Al

nanoparticles, while CNTs are not shown in the XRD patterns. A trace of Ni metal is also found, which is believed to come from the manufacturing process of NiO nanoparticles. After the TGA/DSC measurements, the reaction products of Samples 1 and 2 are further characterized using XRD.

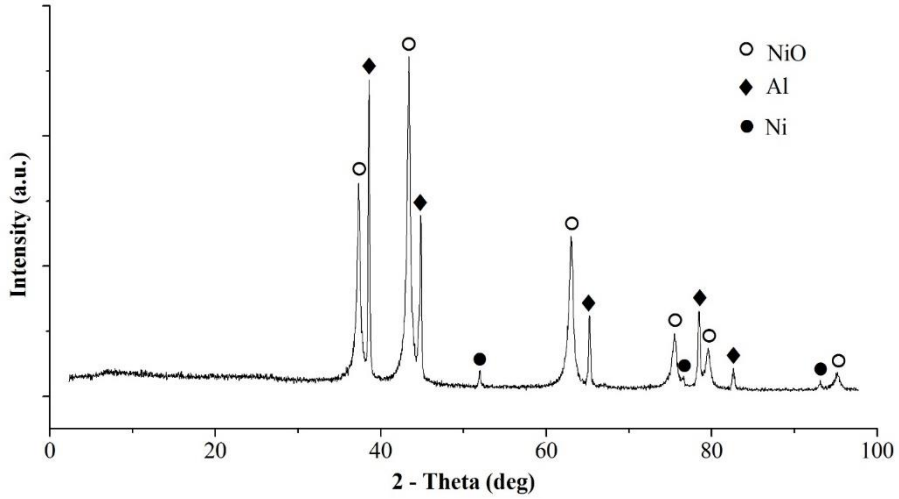

Figure 5.8 XRD result of the mixture of Al, NiO nanoparticles, and CNTs before thermite reaction

As shown in Figure 5.9(a), the reacted Sample 1 contains predominantly Ni(111), mixed with other crystal phases such as Ni(200), Ni(220), Ni(311) and Ni(222). This indicates a series of complex phase transformation processes occurs with Ni during and following the thermite reaction. Some distorted Ni grains are detected in the products of Sample 1, supporting the same reason. The distorted peaks belong to the crystal structure with strain and tensile deformation that forms a lattice with different lattice constants. No sharp peaks of crystalline Al_2O_3 are observed in the reacted Sample 1. The crystalline structures of the

products of Sample 2, shown in Figure 5.9 (b), are similar to these corresponding to Sample 1, except for the weakened signals of these distorted Ni grains. These results will be elaborated in the discussion section when the reaction mechanism is addressed.

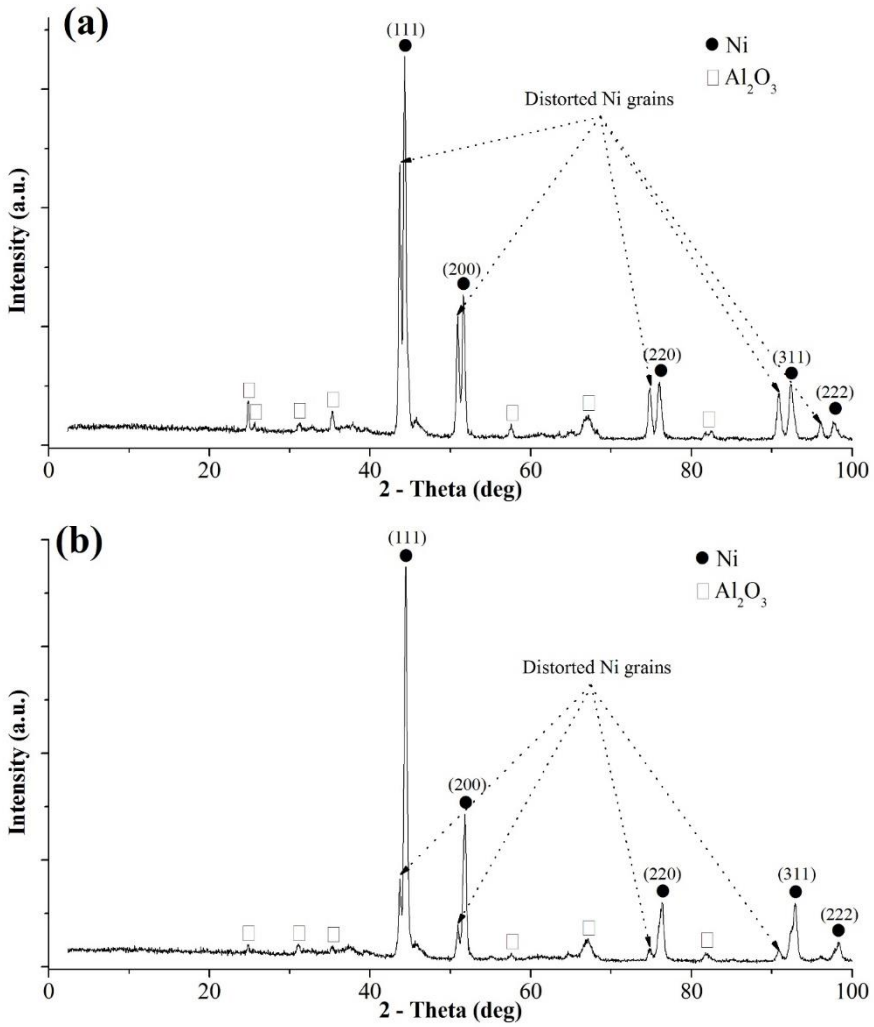

Figure 5.9 XRD result of the products of (a) Sample 1: Al and NiO+CNT layers, and (b) Sample 2: Al+CNT and NiO layers after thermite reaction

5.4.4 Gaseous species studied by mass spectrometry

Both SEM and EDS results suggest, CNTs in the original composites are consumed during the reaction, most likely through formation of gaseous species, such as CO_2 or CO. In order to obtain some qualitative understanding on the type(s) of gases produced, which helps explain the role of CNTs during the thermite reaction, a few as-produced composites (NiO, NiO+CNT, NiO+CNT/Al, and Al+CNT/NiO) were placed in a tube reactor where argon was used as the carrier gas. When the sample was heated with a specific heating rate, the reaction products were examined by a mass spectrometer.

Figure 5.10 shows the relative intensity of gaseous species detected by this mass spectrometer. Note that all these experiments are conducted in a tube reactor with a moving fluid, background noise is therefore expected for gaseous species measurements. Figures 5.10(a) and 5.10(d) show that the NiO and Al+CNT/NiO composites, when being heated from the room temperature to 880 °C, do not produce any significant amount of gases such as O_2, CO or CO_2. This eliminates the possibility of direct thermal decomposition of NiO. Moreover, the Al nanoparticles do not react with CNT in the interested temperature range. Figures 5.10(b) and 5.10(c) exhibit a similar gas formation characteristic. First, there is no O_2 formation during the process. Secondly, the major products from the reactions between NiO and CNT are CO_2 and CO, while the peak concentration of CO_2 is about three times of that of CO. Thirdly, the formation of CO_2 from the reactions between NiO and CNT is a multi-staged process, which exhibits two major steps at about 440 °C and 565 °C, respectively.

It is believed CNTs react with NiO nanoparticles through the following procedure, as illustrated by the Mars-van Krevelen (MvK) mechanism, to produce CO_2 and CO [154]. First, at a moderate temperature (e.g., 200-400 °C) the carbon atom of CNTs reacts with the lattice oxygen of NiO nanoparticle, at the interface of CNT and NiO nanoparticle, to form surface CO or absorbed CO on the surface of NiO nanoparticle, which leaves a vacancy of oxygen on the surface of NiO nanoparticle. This vacancy is then filled by other lattice oxygen through its bulk or surface diffusion. The surface CO can react with another lattice oxygen to form surface CO_2, which desorbs from the nanoparticle and forms a gaseous CO_2 molecule. At an elevated temperature (e.g., 500 °C) and when the lattice oxygen is depleted, surface CO may desorb from the nanoparticle and form the gaseous CO molecule. Noticeably, in comparison with the pure NiO+CNT sample, the NiO+CNT composite produces CO_2 at slightly higher temperatures (at the first stage: 460 °C vs. 420 °C; at the second stage: 580 °C vs. 550 °C).

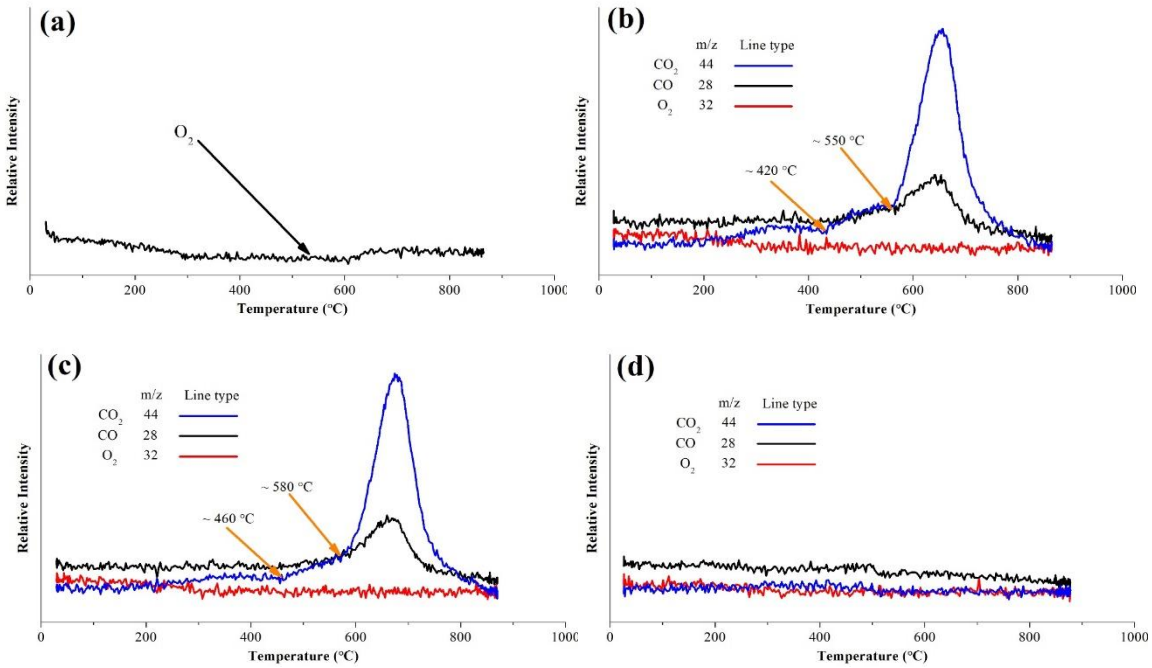

Figure 5.10 Mass spectrometry results of (a) NiO; (b) NiO+CNT; (c) Al/NiO+CNT and (d) Al+CNT/NiO composites during heating in a tube reactor which was fed with argon. The heating rate was 10 ºC/min and the argon flow rate was 20 ml/min

5.5 Discussion

Analysis based on the SEM and EDS results (Figs. 1 and 2) indicates CNTs are relatively immobile, at room temperature, in the specified layers when mixed with either NiO or Al nanoparticles. A continuous NiO-Al interface is formed between these two reactive layers, as shown in the SEM images of both low and high resolutions. The high-magnification SEM images demonstrate the intimate contact between Al and NiO nanoparticles before the reaction is initiated. Some NiO nanoparticles however migrate into the oppose layer during vacuum filtration. After Samples 1 and 2 are heated up to 1000 ºC in argon atmosphere, different morphologies and chemical compositions are produced from these samples. For Sample 1 (Al/NiO+CNT), data shown in Figures 5.3, 5.5(a) and 5.5(b) support the following discussions. First, the products in the original Al layer remain spherical shape and exhibit the smaller sizes than these nanoparticles in the original NiO+CNT layer. This observation agrees with the previous finding on gas-solid reactions between oxygen and Al nanoparticles under a moderate heating rate. In that case oxygen diffuses through the shell of Al nanoparticles and oxidizes them to Al_2O_3 nanoparticles. The EDS data shows the content of oxygen in the original Al layer changes from 22.32 wt% to 40.36 wt%, indicating more oxygen atoms come from the NiO+CNT layer. Secondly, there is no Ni element detectable

in the original Al layer. This observation, together with the first point, suggests the reduction of NiO nanoparticles into Ni metal in the original NiO+CNT layer. The EDS data shows in the original NiO+CNT layer, the content of Ni changes from 1.41 wt% to 3.10 wt%, indicating losing oxygen to the Al layer. Thirdly, some Al nanoparticles are shown to migrate across the interface between two layers and enter into the NiO+CNT layer where they are oxidized into Al_2O_3 nanoparticles. This finding is supported by the EDS results. For Sample 1, the Al content in the original NiO+CNT layer increases from 3.43 wt% to 36.24 wt%. Finally, all CNTs are consumed. Considering the small adding ratio of CNTs (around 4-5%), these CNTs are oxidized by oxygen atoms which are originated from the NiO nanoparticles (as the only source of oxygen in the system). The above elaboration suggests the following reaction pathways for Sample 1. Some reaction between NiO nanoparticles and CNT causes the reduction of NiO into Ni, accompanied by the formation of gaseous species, which is most likely CO_2 and CO, according to the early mass spectrometry study. CO_2 and CO diffuse into the Al nanoparticle layer and oxidize these nanoparticles to Al_2O_3 nanoparticles. A recent study supports the reaction kinetics between CO_2 and Al, showing the formation of CO and AlO as the products [156, 159].

For Sample 2 (Al+CNT/NiO), these products in the original Al+CNT layer, shown in Figures 5.4, 5.5(a) and 5.5(b), exhibit a complex morphology which includes spherical particles and sintered agglomerates. In this layer, the content of Ni changes from 2.7 wt% to 26.27 wt%. Existence of a significant amount of Ni in this layer suggests NiO nanoparticles migrate into the Al+CNT layer and then react with Al nanoparticles. During TGA/DSC, Al

nanoparticles get oxidized into Al_2O_3 nanoparticles and retain their spherical morphology [158], while sintering of Ni metal causes the formation of larger agglomerates. In the original NiO layer, a bulk 3D crystalline structure (mainly Ni(111)) is observed. This structure requires an intensive heat evolving process, which becomes possible after some Al nanoparticles migrate into the NiO layer and react with NiO nanoparticles there. This explanation is supported by the EDS data which shows in the original NiO layer, the content of Al increases from 2.25 wt% to 31.04 wt%. Finally, no CNTs are found in the product, suggesting they are oxidized into CO or CO2. The above analysis suggests the counter-migration of Al and NiO nanoparticles in Sample 2 leads to the thermite reaction which occurs in both layers. After NiO nanoparticles migrate into the Al+CNT layer, they also react with CNTs and consume them.

In addition to tuning the reaction pathways, adding CNTs into different nano-composite layers causes the release of different amounts of energy from the thermite reaction, though the onset temperature remains nearly constant. Since the same amount of CNTs is added and all these CNTs are consumed, this change in energy release unlikely comes from the reactions involving CNTs. In fact, the increased energy release from Sample 1 is believed to result from the gas-solid reaction mechanism, which is more efficient than the condensed-phase reaction mechanism for Sample 2. Production of gaseous oxidizers such as CO and CO_2 from the reactions between NiO and CNTs in Sample 1 produces gases, facilitates effective mass transfer within the microstructure of the layered composite and causes more Al nanoparticles being oxidized. This process leads to the increased total energy release from Sample 1. In

Sample 2 the thermal reactions are mainly maintained by migration of Al and NiO nanoparticles, which leaves some Al nanoparticles unreacted. More unreacted Al nanoparticles in the produce indicate a reduced energy release. The distorted Ni peaks of the XRD curve from the products of Sample 1 are stronger than those from Sample 2, indicating a higher density of dislocation of Ni atoms in the lattice. The distorted peaks are also known from other publications [160]. The gas-solid reaction mechanism found for Sample 1, which brings about a larger energy release and enhanced reaction rate, should be the major contributor to these heavily distorted Ni peaks from Sample 1. As a secondary factor, adding CNTs into the composite can certainly increase the heat conductivity of the sample and provide a network for easier mass transfer, which can change the reaction rate. This factor however needs further investigations on correlation between the microstructure and reaction kinetics, which is not the focus of the current study.

Based on the aforementioned discussions, the roles of CNTs in the layered Al/NiO nano-composite, when they are added to different reactive layers, are summarized in Figure 5.11. When CNTs are added into the NiO nanoparticle layer which is next to the Al nanoparticle layer, the thermite reaction starts at the interface between these two layers upon reaching the onset temperature. Activated by the reaction heat produced at the interface, catalytic oxidation between NiO nanoparticles and CNTs happens in the NiO+CNT layer, which produces CO and CO_2. During this oxidation of CNTs, NiO is reduced to Ni. Then the gaseous species, mainly CO_2, will reach Al nanoparticles in the oppose layer. Al nanoparticles react with CO_2 to form Al_2O_3 and CO, following the gas-solid reaction route.

Driven by the energy released from the exothermic reaction, some Al nanoparticles migrate into the NiO layer and react with NiO nanoparticles directly. Eventually the gaseous products leave the composite and the final products include Ni and Al_2O_3.

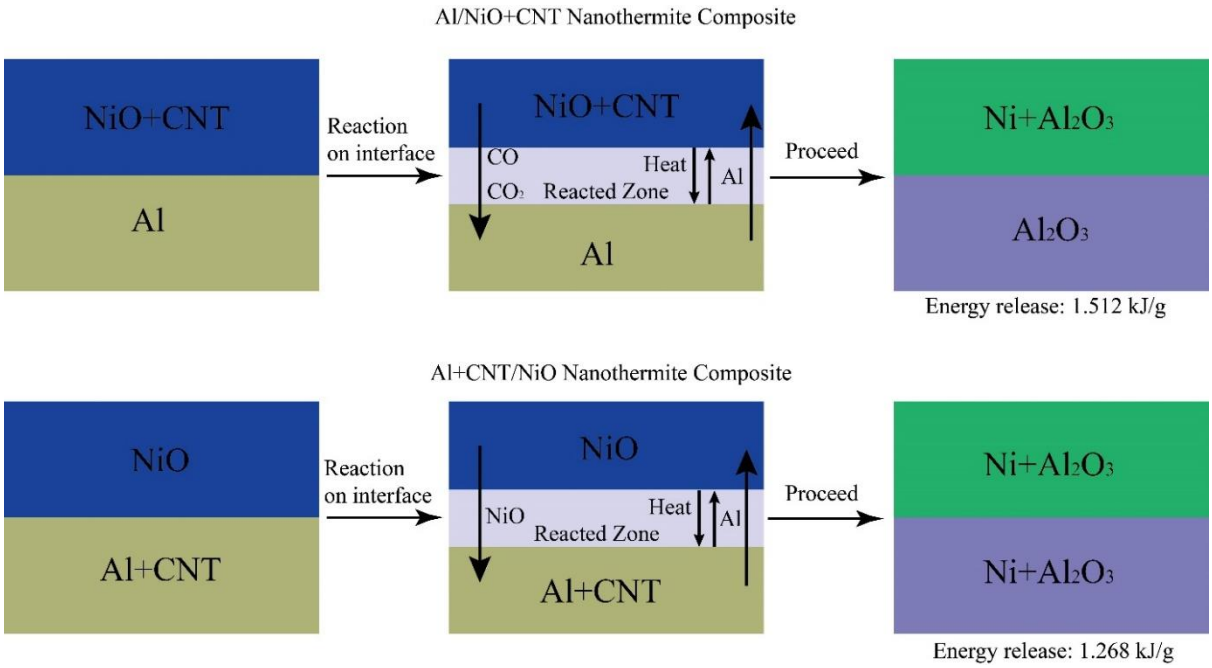

Figure 5.11 Proposed reaction mechanisms of Al/NiO+CNT and Al+CNT/NiO nano-thermite composites

The morphologies of the products are determined by the reaction kinetics and the heat transfer rate. When CNTs are added into the Al nanoparticle layer which is next to the NiO nanoparticle layer, the thermite reaction also starts at the interface between these two layers upon reaching the onset temperature. There is no chemical reaction between Al nanoparticles and CNTs. Driven by the reaction heat produced at the interface, both Al and NiO nanoparticles migrate, in the opposed direction, across the interface and enter into the other

layer. The thermite reaction then occurs between these two nanoparticles in both layers, mainly though a condensed-phase reaction mechanism. Due to the heterogeneous nature of solid-solid reactions, the products possess a wide range of sizes and morphologies.

5.6 Conclusion

Single walled carbon nanotubes (CNTs) have been added into different layers of a multi-layered Al/NiO nano-thermite composite, to investigate the role of CNTs in modifying the reaction routes and subsequently energetic properties of the composites. Adding CNTs into different layers of the composite affects the microstructures of the products, their chemical composition, distributions of Ni elements in the composite, and energy release from the reaction. When the CNTs are added to the NiO nanoparticle layer, chemical reactions between CNTs and NiO nanoparticles occur and form gaseous CO and CO_2. The gas diffuses into the Al nanoparticle layer and oxidizes then into Al_2O_3 nanoparticles. This process is governed by the gas-solid reaction route. When the CNTs are added to the Al nanoparticle layer, on the other hand, there is no chemical reaction detectable between CNTs and Al nanoparticles. The thermite reaction is achieved by the direct contact between Al and NiO nanoparticles, which can be described by the condensed phase reaction mechanism. Further studies are suggested to investigate the influence of micro-scale heat and mass transfer, modified by the creation of a 3D network of CNTs, to the reaction kinetics of the target nanothermite composites.

Chapter 6: Joining of silicon wafers welded with Al/NiO nano-composites

6.1 Overview

The Al/NiO nano-thermite composite, fabricated via a vacuum filtration method, was investigated as a heat source for joining of silicon wafers, via an aluminum interlayer. Energy production and the reaction kinetics of the nano-thermite composite were controlled by modifying the composite by a specified amount of Al powder (average size of 5 μm) or Ni powder (average size of 1 μm). Scanning Electron Microscopy (SEM) was utilized to reveal the microstructures of the welded zone between two silicon wafers. Energy-dispersive X-ray Spectroscopy (EDX) were employed to analyze elemental compositions across the interface of these two welded wafers. Energy production from the Al/NiO nano-thermite composites with different mixing ratios of the additive was measured by Differential Scanning Calorimetry (DSC) and the apparent activation energy was then calculated. Experimental data shows, the nano-thermite composite with the additive of Al micro-powder (60%) or Ni micro-powder (30%) was able to join the silicon wafers. The micro-hardness of the welded zone was measured as 158.9 HV and 56.0 HV for the Al and Ni modified nano-thermite composites, respectively. The reduced joining quality produced by the Ni modified nano-thermiate composite is due to the decreased energy release from the thermite reaction. The Al micro-powder modified Al/NiO composite exhibited a two-step energy release process which highlights the pilot reaction between Al and NiO nanoparticles and the subsequent reaction between Al micro-powder and NiO nanoparticles. This unique reaction sequence

was found being critical to deliver the needed energy to the joining zone which is necessary to achieve a superior joining quality.

6.2 Introduction and literature review

Welding technologies based on combustion synthesis have been used for joining of several types of materials, such as C_f/Al composites and TiAl intermetallic [140, 161, 162], carbon/carbon composite [138, 139], aluminum alloy [163], and SiC ceramic to Ni-based superalloy [164]. According to previous research, the reactive layers including Al/Ni [138, 165-167], Al-CuO-Ni [161, 163], Al/Ti [162] provide heat to melt metals for joining. The reactions of Al/Ni and Al/Ti composites produce the alloys with relatively lower temperatures. The main drawback of the Al/Ni (1.38 kJ/g) and Al/Ti (1.00 kJ/g) composites is the low reaction enthalpy, which results in incomplete combustion due to the heat loss effects [23]. Meanwhile, the theoretical adiabatic temperature of Al/Ni (1637 ºC) and Al/Ti (1324 ºC) limits the selection of joining materials. Usually a preheating procedure is required to increase the temperature of surrounding environment and materials to be joined [138, 161, 163], which requires a complex apparatus. On the other hand, thermite reactions between Al and metal oxidizers possess greater reaction enthalpies and higher adiabatic temperatures, e.g., Al/CuO (4.08 kJ/g and 2570 ºC), Al/Fe_2O_3 (3.96 kJ/g and 2862 ºC), and Al/NiO (3.44 kJ/g and 2914 ºC) [23]. Al and metal oxidizer composites can provide sufficient energy and the needed temperature to join either refractory or non-refractory materials. One of the major

concerns exists, the ceramic product (Al_2O_3) is difficult to be removed from the interlayer of joining parts, which drastically deteriorates the welding quality.

In order to join materials without introducing impurities and to provide sufficient energy with an appropriate reaction rate, a new nano-thermite composite modified by its additives is investigated in this paper. To prevent the formation of impurities, an interlayer of Al foil is added between the two silicon wafers to be joined together. Then the thermite composites act as the heat source which is placed away from the interlayer, without introducing Al_2O_3 in the welded zone. Meanwhile, the energy production rate is controlled by choosing the Al and NiO composite and tuning its chemical compositions. Joining is a compulsory technology in the industry and these methods of adding surface coating and interlayer material are beneficial to improve the weldability [168-171].

In this work, the Al/NiO nano-thermite composite which usually exhibits a solid-solid reaction mode is selected, to prevent the oxygen production from the decomposition of the oxidizer [158]. A challenge exists when the Al and NiO nano-thermite composites react rapidly and undergoes explosion, thanks to its low onset temperature and shortened mass diffusion path. To overcome this effect, additives of Ni powder (1 μm) or Al powder (5 μm) are added with the two purposes: 1) reducing the thermite reaction rate trough the heat sink effect of Ni micro-powder and Al micro-powder, and 2) increasing the heat conductivity to enhance the energy propagation mechanism during combustion. Two types of composites are fabricated, consisting of :1) Al (40 nm)-Al (5 μm)-NiO (50 nm), and 2) Al (40 nm)-Ni (1 μm)-NiO (50 nm).

Nano-thermite composites have been utilized for decades [44, 163, 172]. Due to their nano-sized constituents, the surface to volume ratio of reactants is greatly increased compared with the micron-powder. Several methods have been developed to reduce the agglomeration of nano-particles [76, 149, 158, 163, 173]. In this work, the vacuum filtration method is applied to form nano-thermite mixtures with a thin film structure. Three heating rates of 10 ºC/min, 20 ºC/min, and 30 ºC/min are used in DSC measurements to increase the temperature up to 1000 ºC. The apparent activation energy is calculated from the DSC results, using the well-known Kissinger equation [128, 174]. The controllable energy release and reaction rate contribute to formation of different material phases in the welded zone. The microstructures and elemental distributions at the joint interlayer are investigated with the scanning electron microscopy (SEM) and energy-dispersive X-ray spectroscopy (EDS) analyses. Finally, the micro-hardness tests are conducted to estimate the joining qualities.

6.3 Experimental method

6.3.1 Nano-thermite composite preparation and joining apparatus

40 nm Al and 50 nm NiO particles (99% in purity), provided by *Skyspring Inc.*, are used as the raw material to produce the thin-film nano-thermite composites. The Al (5 μm) and Ni (1 μm) micro-powders, acting as the additive, are provided by *US Research Nanomaterials, Inc.* and *Sigma-Aldrich*, respectively. In the preparation of the Al (40 nm)-Al (5 μm)-NiO (50 nm) nano-thermite composite, the equivalence ratio of fuel (Al) and oxidizer (NiO) remains 2, which means that the mass of 40 nm and 5 μm Al particles accounts for 32.52 %

of the total mass of the prepared composites. The mass ratio of Al (40 nm) to Al (5 μm) is 2:3. This sample is labeled as Sample A or the 60%-Al sample. For the Al (40 nm)-Ni (1 μm)-NiO (50 nm) composite, the equivalence ratio of Al and NiO remains 2, while 1 μm Ni particles are added with 30 % of the total mass. This sample is denoted as Sample B or the 30%-Ni sample. Furthermore, a pure Al (40 nm) and NiO (50 nm) composite is made with the equivalence ratio of 2. This sample is labelled as Sample C or the No-additive sample. The detailed information on these samples and their preparations is summarized in Table 6.1.

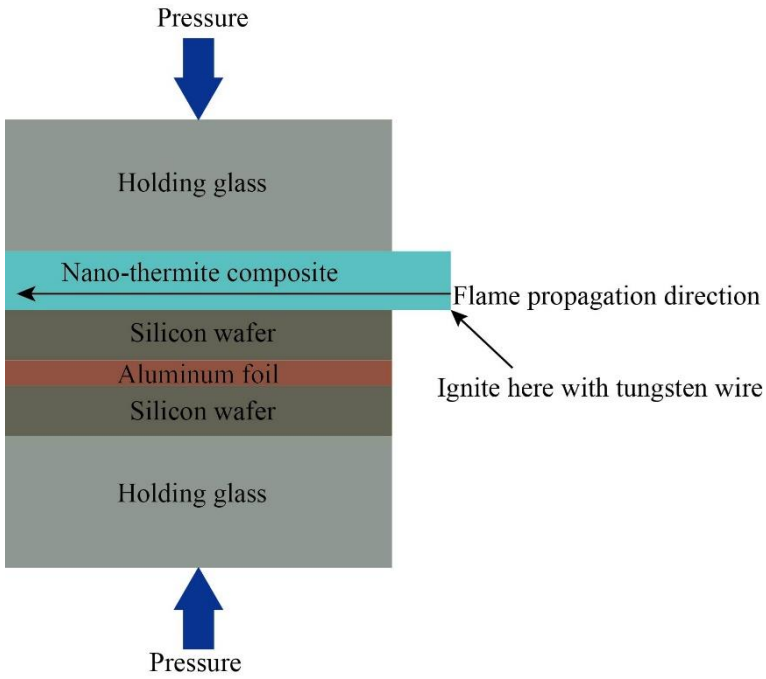

Figure 6.1 Schematic view of joining apparatus. Heat produced by the nano-thermite composite is transferred, through the top silicon wafer, to the aluminum foil interlayer, which results in successful joining

The procedure of vacuum filtration to produce the thin-film composites are documented in

the literature [149, 158]. The nanoparticles and micro-powder are dispersed in acetone and sonificated for 20 min. The sonificated solution is then gradually added on the filter paper for vacuum filtration. After the subsequent drying procedure, the filtrated particles are detached from the filter paper to form a freestanding thin film.

Table 6.1 Nano-thermite compositions and thermochemical properties

	Sample A (60%-Al)	Sample B (30%-Ni)	Sample C (No-additive)
Al (40nm)	64 mg	160 mg	160 mg
NiO (50 nm)	332 mg	332 mg	332 mg
Al (5 μm)	96 mg	-	-
Ni (1 μm)	-	210.86 mg	-
Peak temperature (°C), 10 °C/min	1st 564.9 2nd 634.8	558.7	551
Peak temperature (°C), 20 °C/min	1st 578.6 2nd 655.6	564.3	556.4
Peak temperature (°C), 30 °C/min	1st 588.6 2nd 666.4	567.7	560.3
Onset temperature (°C), 30 °C/min	1st 567.3 2nd 665.3	566.5	558.6
Energy release (kJ/g), 30 °C/min	1st 0.33 2nd 1.56	1.06	1.65
Apparent activation energy (kJ/mol)	332.96	696.09	663.81

To achieve joining, an aluminum foil is inserted between two silicon wafers as an interlayer.

Then the thin film of nano-thermite composite is placed on the back of the top silicon wafer. The schematic view of the welding apparatus is shown in Figure 6.1. The nano-thermite composite is ignited at one end with a tungsten wire at room temperature (25 ºC). The flame propagates across the entire thin film and provides heating for joining.

6.3.2 Characterization

Thermodynamic and kinetic properties of nano-thermite composites are measured with a DSC device (NETZSCH STA model 449F3A-0918-M Jupiter). The energy release is obtained by recording the energy divided by the total mass of the thermite systems. In order to derive the apparent activation energy, three different heating rates of 10 ºC/min, 20 ºC/min, and 30 ºC/min are used to heat up to 1000 ºC in argon atmosphere. The microstructure and elemental contrast of nano-thermite composites before and after combustion are investigated with SEM (Model LEO 1550, Zeiss) by secondary and back-scattered electron beams, respectively. The x-ray diffraction (XRD) analysis (XRG 3000, Philips) is employed to study chemical compositions of the as-prepared and combusted nano-thermite composites. The interface between the joint silicon wafers is observed with the SEM. The EDS installed on the same SEM is applied to measure chemical compositions and the elemental mapping at the interface, which determines the phase formation on the welded zone. A micro-hardness testing machine (Wilson Hardness VICKERS 402 MVD) is used to measure the hardness on the welded zone between joint silicon wafers.

6.4 Results

6.4.1 Onset temperature and energy release

In this experiment, three types of nano-thermite composites shown in Table 6.1 are used in the joining procedure. The 60%-Al (Sample A) and 30%-Ni (Sample B) samples are successfully ignited with the tungsten wire and the produced flames achieve self-propagation. The reaction heat generated from the combustion of these samples is able to weld the two silicon wafers. For the No-additive (Sample C), the tungsten wire is able to trigger the reaction which further develops itself into an explosion. The silicon wafers are damaged and the joining is not successful. Thermodynamic and kinetic properties of the No-additive sample are measured as a benchmark. Thermochemical properties such as the onset temperature and energy release are then measured with the DSC device under argon atmosphere when the samples are heat up to 1000 °C with the heating rate of 30 °C/min.

The DSC results of the 60%-Al, 30%-Ni, and No-additive samples are shown in Figure 6.2 (a)-(c). The 60%-Al sample shows two distinguished exothermic peaks, whereas the 30%-Ni and No-additive samples demonstrate a single exothermic peak. The 60%-Al sample contains Al particles with 40 nm and 5 μm, which exhibit distinct thermite reaction mechanisms. The melting points of the Al micro-powder and nanoparticles are measured using DSC and the results are shown in Figure 6.2 (d).

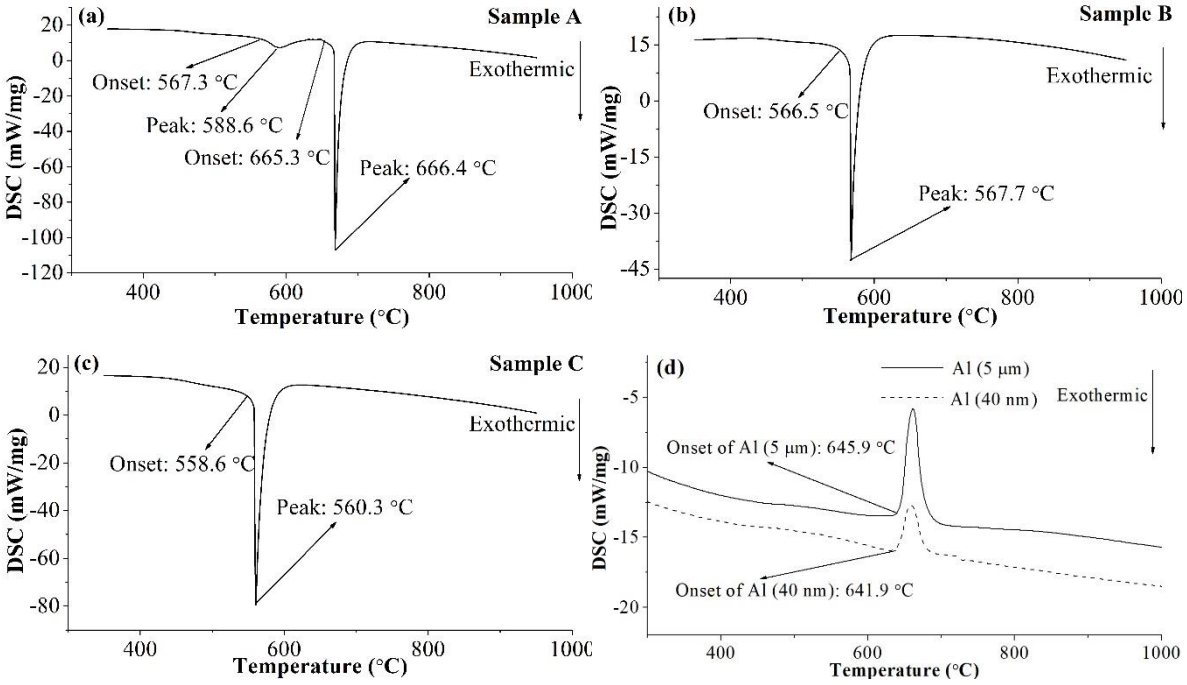

Figure 6.2 DSC results of the 60%-Al (a), 30%-Ni (b), and No-additive (c) samples in argon atmosphere, up to 1000 ºC with the heating rate of 30 ºC/min. The melting points of Al nanoparticles and micro-powder are shown in (d)

A slightly lower melting point of 40 nm nanoparticles (641.9°C) is measured, compared to 645.9°C for the 5 μm micro-powder. The reaction below the melting point is controlled by oxygen diffusion into the Al particle, usually indicating the solid-solid reaction mode between Al and NiO nanoparticles. The reaction occurring above the melting point suggests that the melted Al core diffuses through the Al_2O_3 shell to reach outer oxidizer, which is true for Al micro-powder. The 30%-Ni sample shows a single thermite reaction peak, indicating the reaction happens between Al and NiO nanoparticles. There is no separate peak observed for the possible reaction between Al nanoparticles and Ni powder (1 μm). In the No-additive sample, the single exothermic peak corresponds to the thermite reaction between Al and NiO

nanoparticles. The detailed information of the thermochemical properties is also listed in Table 6.1.

The 60%-Al sample possesses the highest total energy release (1.89 kJ/g) among the three composites, which is slightly higher than that of the No-additive sample (1.65 kJ/g), due to thicker Al_2O_3 shells on Al nanoparticles [4]. The energy release of the 30%-Ni sample is 1.06 kJ/g, which is attributed to the inert and heat sink effects of Ni powder. There are two exothermic peaks of the 60%-Al sample. The first one with an onset temperature of 567.3 ºC, similar to that of the exothermic peak of the 30%-Ni sample (566.5 ºC). Both are believed to belong to the reactions between Al (40 nm) and NiO (50 nm). The onset temperature of the No-additive sample (558.6 ºC) is slightly lower, which is caused by the more intimate interfacial contact between nanoparticles. Agglomerated nanoparticles can also enhance the heat conductivity, which promote the reaction propagation.

6.4.2 Microstructures of as-prepared and reacted 30%-Ni samples

In the 30%-Ni sample, the Ni micro-powder is added into the nano-thermite of Al/NiO composite. The Ni micro-powder is supposed to serve as an inert, but a heat sink material to absorb heat produced by the thermite reaction, which reduces the reaction rate. Potentially Al particles can react with Ni powder, which produces the AlNi compounds [175]. In order to understand the role of Ni micro-powder in the nano-thermite composite, the SEM images with secondary and back-scattered electron beams are studied using Figure 6.3.

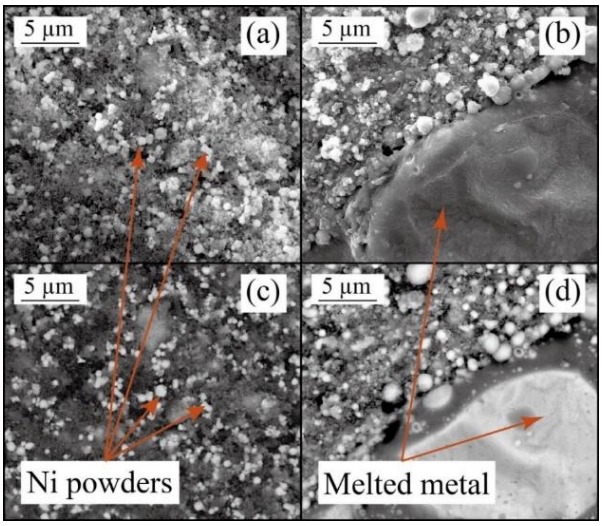

Figure 6.3 SEM images with secondary electron beams of a) as-prepared and b) products, and with back-scattered electron beams of c) as-prepared sample and d) products

Figure 6.3 (a) and (b) show the SEM images with secondary electron beams for the as-prepared 30%-Ni sample and its products after reaction, respectively. Figure 6.3 (c) and (d) show the corresponding SEM images with back-scattered electron beams. The secondary electron beams reveal the surface morphology, while the back-scattered electron beams show the elemental contrast (a heavier element demonstrating a brighter signal). In Figure 6.3 (a), the larger particles are Ni powder (~1 μm in diameter), which are more visible in Figure 6.3 (c) as the brighter particles. Figure 6.3 (b) shows the morphologies of products after reaction. In addition to nano-sized particles, large size (20 ~ 30 μm) particles are formed, which is the sintered Ni metal. The source of those large Ni particles are the newly formed Ni from the reaction between Al and NiO nanoparticles and the added Ni micro-powder in the reactants. Figure 6.3 (d) demonstrates the elemental contrast of the products. These SEM images

confirm, thanks to the heat produced from the thermite reaction, large Ni particles are formed and can be utilized for joining.

6.4.3 XRD analysis on the 30%-Ni sample

To investigate on the potential reaction between Ni and Al powders, the XRD measurements are performed on both as-prepared and reacted products. As shown in Figure 6.4 (a), the as-prepared 30%-Ni sample contains Ni, NiO, and Al, which corresponds to the Ni micro-powder, NiO, and Al nanoparticles in the original composite. Figure 6.4 (b) demonstrates the compositions of Ni, NiO, Al_2O_3, and Al in the reacted sample. The XRD data suggests the following information. First, the nano-thermite reaction occurs between Al and NiO nanoparticles, which produces pure Ni metal and Al_2O_3. Secondly, the AlNi alloy cannot be detected with the XRD analysis, indicating that no direct reactions between Ni micro-powder and Al nanoparticles. Thirdly, the reaction mechanism between Al and NiO nanoparticles is considered as condensed-phase reactions [158]. The remaining Al and NiO signals from the reacted sample indicates the incompletion of the thermite reaction, partially due to the heat absorption of Ni micro-powder. Combining with the SEM images, the XRD results confirm the roles of Ni micro-powder as a chemically inert and heat sink additive which modifies the total energy release and the reaction rate.

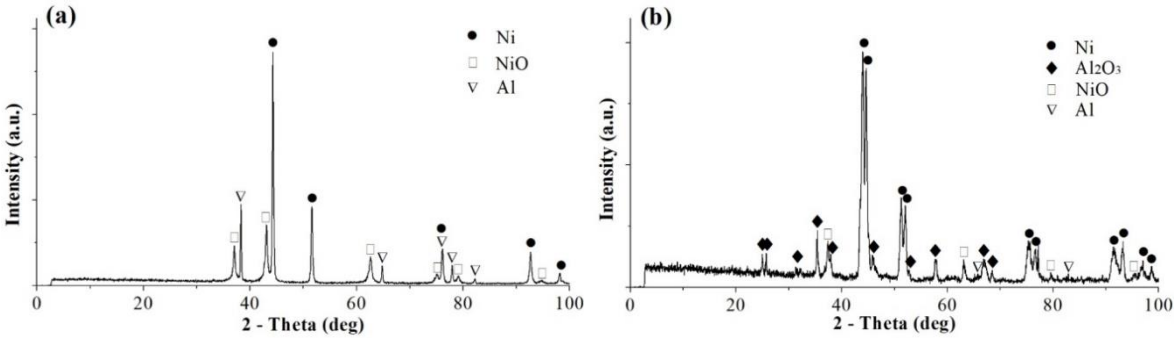

Figure 6.4 XRD data for the chemical compositions of the 30%-Ni sample: (a) as-prepared and (b) products after combustion

6.4.4 Microstructure and EDS analysis of joining zone on interface

The microstructure of the welded zone near the interface area is investigated with SEM images. Figures 6.5 (a) and (b) show the SEM images of the welded zones produced with the 60%-Al and 30%-Ni samples, respectively.

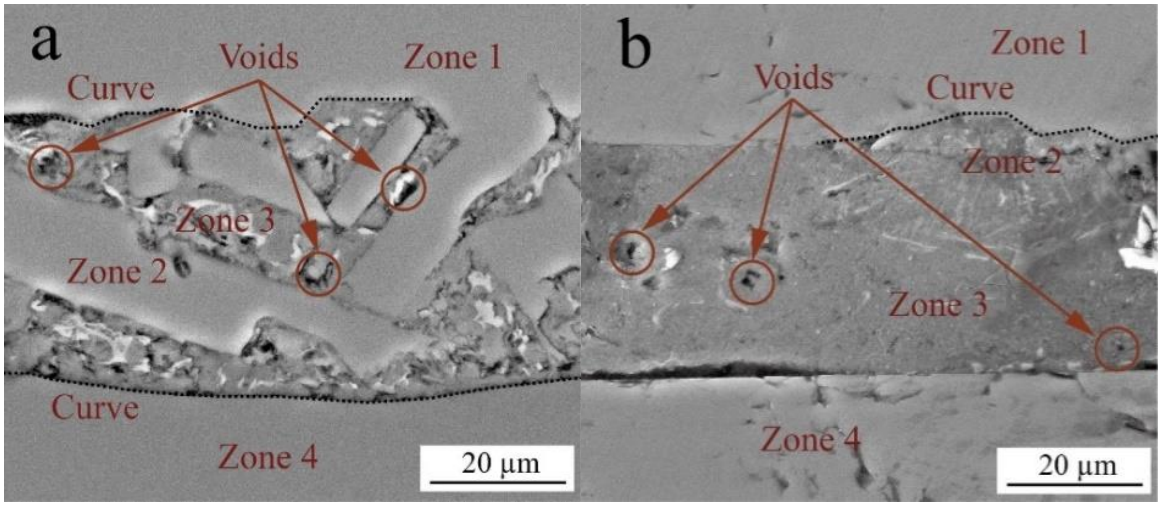

Figure 6.5 SEM images of the welded zone produced with the a) 60%-Al and b) 30%-Ni samples

Figures 6.5 (a) and (b) demonstrate a quite satisfying interfacial bonding between silicon wafers. The welded zones with both samples can be divided into four different areas as shown in these figures. Zones 1 and 4 are the top and bottom silicon wafers, respectively. Zones 2 and 3 are the two different bonding phases. Some voids exist in both zones, which are possibly originated from the gap between silicon wafers and the Al interlayer. Worthwhile to note in Figure 6.5 (a), there is a smooth and curved interface between the bottom silicon (Zone 4) and the welded zone. This curved interface is formed when the local temperature reaches the melting point of silicon (1414 ºC). Subsequently, the edge of the bottom Si wafer is softened and melted. In Figure 6.5 (b), a curved interface exists between the top silicon wafer (Zone 1) and the welded zone. The similar process is expected.

Distribution of various elements in the welded zone is measured using EDS and the results are shown in Table 6.2. It demonstrates for the 60%-Al sample, Al (2.34 wt%) and Si (97.66 wt%) dominate in Zone 2, indicating the diffusion of Al into Si. In Zone 3, Al (74.77 wt%) and Si (25.23 wt%) co-exist in the form of Al-Si alloy with an eutectic composition. Supported by the SEM images, it is concluded that at the bonding interface produced by the 60%-Al sample, there are two distinct phases: a eutectic Al-Si alloy and a Si phase with dispersed Al element. For the welded zone produced with the 30%-Ni sample, the compositions of Zone 2 (30%-Ni) are Al (81.6 wt%) and Si (18.4 wt%), which indicates the diffusion of Si into the Al interlayer. In Zone 3 (30%-Ni), the Si level reduces to 9.8 wt%, which shows a decreased diffusivity of Si in Al at a lower temperature of the lower part of

the welded zone (this location is far from the heating source which is the nano-thermite composite being placed on the top of the top wafer).

Table 6.2 Elemental Mapping of the welded zones produced with Sample A (60%-Al) or Sample B (30%-Ni)

Welded zones		Sample A	Sample B	Silicon wafer
Zone 2	Al (wt %)	2.34	81.6	N/A
	Si (wt %)	97.66	18.4	N/A
Zone 3	Al (wt %)	74.77	90.2	N/A
	Si (wt %)	25.23	9.8	N/A
Micro-hardness (HV)	Point 1	157.1	46.9	819.8
	Point 2	166.2	62.5	836.2
	Point 3	153.3	58.6	825.4
Average (HV)		158.9	56.0	827.1

The elemental mapping is conducted to provide a direct view to the distributions of interested elements across the base materials and welded zone. The silicon wafers and welded zone produced with the 60%-Al sample are presented in Figure 6.6 (a), while these produced with the 30%-Ni sample are shown in Figure 6.6 (b). In Figure 6.6 (a), the Al and Si elements are distributed in two separate areas: an Al-rich zone and a Si-rich zone. It is believed that, due to the heat produced by the thermite reaction, Si diffuses into the Al interlayer and forms the Si-rich zone. According to the previous EDS result, this Si-rich zone contains eutectic Al-Si alloy. Some Si element is visible in the Al-rich zone. In Figure 6.6 (b), the welded zone

mainly contains Al element, indicating the remaining Al interlayer. A small amount of Si element can be found in the Al interlayer, which agrees with the EDS result shown previously. Near the interface between the top wafer and the interlayer, there is a region (shown by the arrow) showing a relatively high concentration of Si. These Si species migrate from the top wafer into the Al interlayer, driven by the higher temperature in this region. Near the bottom wafer, diffusion of Si into the Al interlayer is negligible, due to the lower temperature in that region.

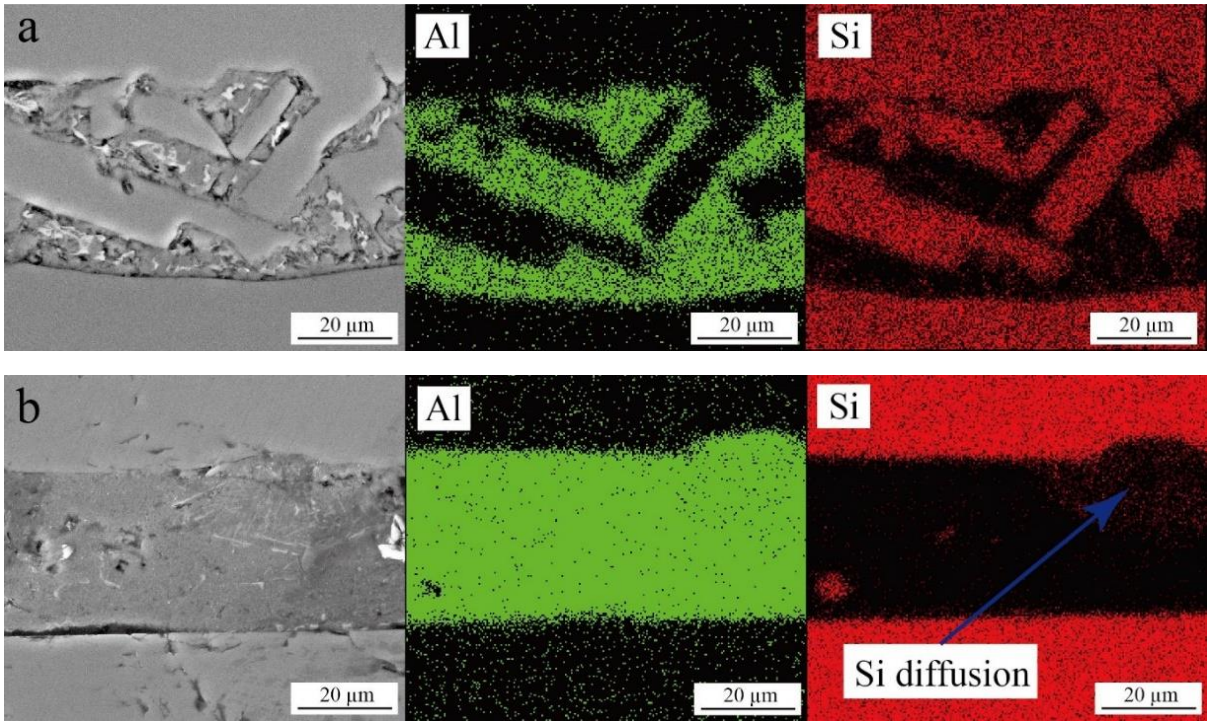

Figure 6.6 Elemental mappings of Al and Si across the base material and welded zones: (a) with the 60%-Al sample; and (b) with the 30%-Ni sample

6.4.5 Reaction kinetics on apparent activation energy of thermite composites

The total energy release, reaction rate of thermite composites, and the thermodynamic and heat transfer properties of the welded zone determine the joining quality. After these thermite composites are ignited, the reaction propagates through the nano-thermite layer, which is accompanied with the heat transfer from the reacting layer to the neighboring Si wafer and the Al interlayer. The energy which is delivered to the welded zone is therefore predominantly dependent on the reaction rate and the heat transfer rate of the joining system. In order to characterize the reaction kinetics of the nano-thermite composites, the apparent activation energy is derived from the DSC measurements. The equations and procedure are provided in the supplemental material. Three heating rates of 10 ºC/min, 20 ºC/min, and 30 ºC/min are selected to obtain the reaction peaks for the 60%-Al, 30%-Ni, and No-additive samples. The measured DSC curves and the plot of calculated apparent activation energy for these samples are shown in Figure 6.7. The activation energy of these samples and the peak temperature under each heating rate are listed in Table 6.1. The apparent activation energy E_a can be calculated from the function of $\ln\left(\frac{\beta_i}{T_{Pi}^2}\right)$ *vs* $\frac{1}{T_{Pi}}$, as shown in Figure 6.7.

The apparent activation energy (E_a) of the 60%-Al, 30%-Ni and No-additive samples are determined as 322.96 kJ/mol, 696.09 kJ/mol and 663.81 kJ/mol, respectively. It should be mentioned that the Kissinger method is valid for the first order reaction (n = 1), for which the reaction rate linearly depends on the conversion rate of one specified reactant. In the 60%-Al sample, there are two non-continuous thermite reactions occurring below and above the melting point of Al, respectively, as shown in Figure 6.2 (a).

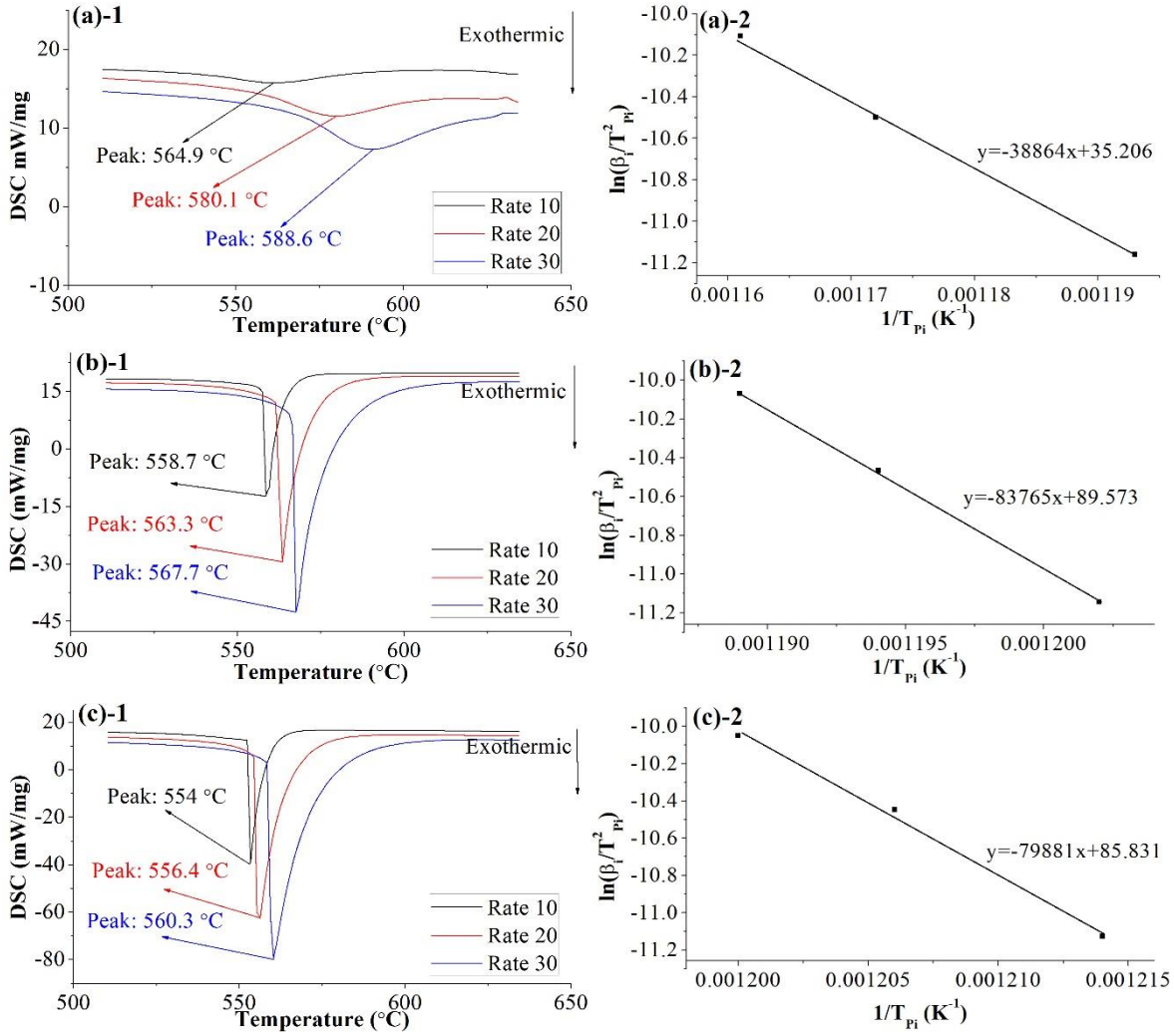

Figure 6.7 DSC curves with three heating rates and plot of fitted curves with calculated apparent activation energy of the (a)-1/2: 60%-Al; (b)-1/2: 30%-Ni; and (c)-1/2: No-additive samples

It is expected that the first exothermic peak corresponds to the dominating initiation which subsequently triggers the second peak. Since the first reaction occurs below the melting point of Al particles, its rate is controlled by the diffusion coefficients of reactive species (i.e., oxygen) within the solid domain (i.e., the Al nanoparticle). The calculated apparent activation energy for the 60%-Al sample, using the Kissinger method, is from the first thermite reaction

of this sample. Figures 6.7 (a)-1, (b)-1 and (c)-1 show the exothermic reaction peaks with different heating rates measured on the three samples, respectively. The reaction of the 60%-Al sample possesses a reduced energy release compared to the No-additive sample, which indicate that the reaction within the 60%-Al sample is not complete, which is attributed to the existence of Al micro-powder in this sample. Note that there is no a direct correlation between the activation energy and the reaction completion. When the external energy succeeds the required activation energy, a reaction will be initiated. Whether this reaction may be complete is however dependent on other parameters such as the fuel/oxidizer ratio, mixing or conducting of reactants, and heat and mass transfer, etc. Moreover, the apparent activation energy measured from the No-additive sample should account for both the chemical reaction energy barrier and the diffusion energy barrier. We believe the apparent activation energy measured from the 60%-Al sample mainly reflects the chemical energy barrier, whereas the activation energy measured from the No-additive sample includes both the chemical and diffusion energy barriers. This is partially demonstrated by the 30%-Ni sample, for which the apparent activation energy is comparable to the No0additive sample, due to the role of Ni powers which absorb the heat and slow down the reaction rate.

6.4.6 Microhardness test results

The micro-hardness in the welded zone is measured to evaluate the mechanical strength of the joints. As shown in the earlier SEM images, the thickness of the welded zone ranges from 30 μm to 80 μm. Three isolated points in each welded zone are selected to measure the micro-

hardness, based on which an average value of the joint micro-hardness is obtained. In addition, the micro-hardness of the base material (silicon wafer) is also measured. The measured micro-harness values are shown in Table 6.2. The base material exhibits the highest average value of micro-hardness (827.1 HV), which agrees with the hardness of crystal silicon [176]. The hardness of the welded zone produced with the 60%-Al sample exhibits an average value of 158.9 HV, which is about three times of that with the 30%-Ni sample (56.0 HV). The improved hardness of the welded zone with the 60%-Al sample is believed to result from the greater penetration of Si in the Al interlayer. When the Al interlayer is almost destroyed by the reaction heat for the 60%-Al sample, the original interlayer shape nearly remains for the 30%-Ni sample.

6.5 Discussion

A successful joining requires the nano-thermite composites to satisfy these three conditions: 1) providing a sufficient amount of energy, 2) propagating the reaction with an appropriate reaction rate and 3) delivering the needed energy to the joining location. The reaction enthalpy of the thermite reaction, subsequently, serves for melting of welding parts in the welded zone. As shown in Figure 6.1, after the heat is produced by the nano-thermite reaction on the top of the silicon wafer, it is transferred (via conduction) to the interlayer and the bottom part. When the interlayer is melted, joining between two components is achieved. However, this energy can be dissipated to the surrounding environment, which slows down the reaction propagation rate and reduces the energy delivered to the interfacial area. It is

hence important to optimize the effects of three aforementioned factors for developing the joining technology.

First of all, a higher energy release from the thermite reaction is desirable. DSC results show, in Table 6.1, the 60%-Al sample possesses a highest energy release (1.89 kJ/g). On the other hand, the energy release of the No-additive sample, containing only Al and NiO nanoparticles, is 1.65 kJ/g which is slightly lower than that of the 60%-Al sample. Although the energy release from the first reaction of the 60%-Al sample is only 0.33 kJ/g, based on the DSC measurement, it is important to initiate the thermite reaction of Al micro-powder in this sample and to provide a large amount of energy. For the 60%-Al sample, its two-step reaction mechanism highlights the initiation role of Al nanoparticles and the energy production role of Al micro-powder. The highest energy release of the 60%-Al sample leads to increasing the delivered energy to its welded zone. This agrees with the SEM and EDS results which show the formation of the silicon phase and the Al-Si eutectic structure in the welded zone produced with the 60%-Al sample. Only the Al-Si alloy is observed in the same zone produced with the 30%-Ni sample. In Table 6.2, the silicon percentage (97.66% and 25.23 wt%) from the 60%-Al sample is much higher than that (18.4 wt% and 9.8 wt%) from the 30%-Ni sample, indicating the greater amount of silicon migration to the welded zone which is driven by the increased energy delivered to the joining region. Furthermore, the enhanced energy delivery to the welded zone results in an improved inter-locking joining mechanism in the silicon wafers, as shown in Figure 6.6 for the 60%-Al sample.

Second, a smaller activation energy is preferred for joining. The 60%-Al sample shows the apparent activation energy of 322.96 kJ/mol, which is calculated from its first exothermic peak below the melting point of Al nanoparticles. It was previously found that Al micro-particles can be oxidized under their melting points [177]. However, due to the long diffusion path within such particles, only a small percentage of the Al content is oxidized below the melting point. It is generally accepted that Al micro-powder reacts more completely above the melting point. In Figure 6.2, the first thermite reaction of the 60%-Al sample occurs below the melting point of Al particles. We expect this peak corresponds to the reaction between Al and NiO nanoparticles via a solid-solid reaction mode, which usually exhibits a low activation energy. The second peak of the 60%-Al sample appears above the melting point of Al particles, suggesting a liquid-solid reaction mode which is initiated by the heat production from the first thermite reaction. The measured activation energy of 322.96 kJ/mol is believed to belong to the thermite reaction between Al and NiO nanoparticles, unlikely involving the reaction propagation to the other unreacted components such as Al micro-powder in the composite. This value is reasonably higher than the previously measured activation energy for the Al nanoparticle and NiO nanowire composite (216.3 kJ/mol) [44], if the structural characteristics of vacuum filtered composites are taken into account [158, 178].

The apparent activation energy corresponding to the only exothermic peak of the 30%-Ni sample is 696.09 kJ/mol, which doubles the value of the 60%-Al sample. Considering the apparent activation energy of a reactive composite which consists of different constituents is

the characteristic which describes the reaction dynamics of the entire composite, it is closely related to the microstructure of the composite. The high apparent activation energy of the 30%-Ni directly reflects the slower reaction rate of its Al nanoparticle constituent than the rate of those nanoparticles in the 60%-Al sample. The following factors in these two samples are therefore important. First, the initial exothermic peak of the 60%-Al sample corresponds to the 'pilot' reaction of Al nanoparticles in this sample, which successfully initiate the subsequent reaction between Al micro-powder and NiO nanoparticles. This pilot 'ignition' process does not require much propagation and therefore its kinetics is similar to the thermite reaction between Al and NiO nanoparticles. It is interesting to show, the Al nanoparticles in the 60%-Al sample are not completely reacted, which release energy of 0.33 kJ/g (vs 0.424 kJ/g from the 30%-Ni sample). Reactions in the 30%-Ni sample require the propagation of heat and mass throughout the composite, in order to consume all reactive Al nanoparticles. The reaction rate of the 30%-Ni sample is considerably slower. Secondly, the Ni powder in the 30%-Ni sample has the heat sink effect that absorbs energy produced by the thermite reaction, which reduces the heat transfer and mass diffusion and slows down its reaction rate.

The apparent activation energy (663.81 kJ/mol) measured from the No-additive sample is comparable to the value of the 30%-Ni sample (696.09 kJ/mol). Since this sample does not contain the Ni powder, its reaction rate is greater than that of the 30%-Ni sample. The completion of the thermite reactions of the No-additive sample requires an appropriate propagation of heat and reactive species throughout its microstructure, which is not the case of the pilot reaction of Al nanoparticles in the 60%-Al sample. Therefore its reaction rate is

significantly smaller than that of the 60%-Al sample, due to lack of the ‘pilot’ reaction in this composite. There is no melting peak of Al observed for the 30%-Ni and No-Additive samples, indicate the dominant solid-solid reaction mode and the similar degree of Al nanoparticle consumption by the thermite reaction.

The No-additive sample cannot joining the Si wafers successfully. The experiment underwent an explosion that damaged the joining apparatus. The failure is largely due to the amount of energy release during a very short period, which is not delivered successfully to the joining zone. Although the energy release of the No-additive sample is comparable to that of the 60%-Al sample, the rate of energy release is faster for the No-additive sample via a single exothermic peak. For the 60%-Al sample, energy release is produced through two steps which correspond to the pilot reaction of Al nanoparticles (the first exothermic peak in Figure 6.2 (a)) and the thermite reaction of Al micro-powder (the second exothermic peak in Figure 6.2 (a)). Because the energy release rate is controlled by the combination of the pilot reaction and the subsequent reaction of Al micro-powder, the needed heat for melting the interlayer is able to reach the weld zone, which results in a successful joining. Another possible reason for the explosion of the No-additive sample goes to its reaction mechanism under the joining condition. The reaction between Al and NiO nanoparticles occurs below the melting point of Al in DSC experiment, which exhibits the solid-solid reaction mode or the diffusion based mechanism [102]. During joining experiment, however, a high heating rate in the No-additive sample is possible, which may causes a melt dispersion mechanism [107, 179-181]. This

phenomenon was proposed previously to address the fast melting of the Al core which expands through the Al_2O_3 shell [104].

The 30%-Ni sample can joining the Si wafers. However, the produced joint has a lower micro-hardness than the one produced by the 60%-Al sample. This is due to the smaller energy release of the 30%-Ni sample. Some energy is delivered to the joining zone. The amount of energy however is not sufficient to fully melt the interlayer to achieve a successful joining (shown in Figure 6.6 (b)). Note that the focus of this work is to develop technologies for joining these thin and brittle silicon components, which are difficult to be welded by traditional methods. The routine approaches such as the tensile stress measurement is not suitable for these components with a small thickness. The micro-hardness experiments are used to assess the joining quality. With increasing the micro-hardness, the welded zone is able to withdraw a greater mechanical stress. As shown in Table 6.2, the 60%-Al sample, which contains both Al nanoparticles and micro-powder and exhibits a two-step reaction mechanism, produces the strongest joint between two Si wafers.

6.6 Conclusion

In this work, silicon wafers are welded using Al/NiO nano-thermite composites containing Al or Ni micro-powder. The Al/NiO thermite composite is selected to achieve gasless reactions. The SEM and EDS analyses show the microstructure and phase transformation in the welded zone. Three nano-thermite composites show distinct energy release values and different reaction kinetics, which result in diverse phases in the welded zone. When a high

amount of energy release is desirable, to provide more heat for melting the interlayer at the joining zone, a quick energy release leads to explosion which fails the task. This is the case for the pure Al/NiO nano-thermite composite. Adding Ni micro-powder into the nano-thermite reduces the energy release and subsequently decrease the heat available in the joining zone. This leads to unsuccessful melting of the interlayer and a poor joining quality.

Adding Al micro-powder into the Al/NiO nano-thermite composite changes the reaction mechanism of the composite. Its two-step energy release process is characterized by the pilot reaction between Al and NiO nanoparticles and the subsequently occurring reaction between Al micro-powder and NiO nanoparticles. While the first reaction, possessing a low activation energy, facilitates the joining process, the second reaction produces the heat which is needed to melt the interlayer and to join Si wafers. SEM and EDS results show a large amount of silicon diffused into the Al interlayer to form the Al-Si alloy. The micro-hardness test confirms the superior joining quality produced by the Al/NiO nano-thermite composite with Al micro-powder.

Chapter 7: Summary and further work

7.1 Contributions of the thesis

This thesis contains two major parts: 1) the fundamental research on the reaction mechanisms of nano-thermite composites, and 2) the attempt to weld silicon wafers for potential applications. The nano-thermite composites contain nanoscale particles, which increase the interfacial contact between reactants. The introduction of nanoparticles improves the reactivity of the thermite system. Due to the shortened mass diffusion path, the reaction rates are significantly improved compared with traditional micron thermite composites. The onset temperatures and reaction mechanisms in nano-thermite composites are different from those of traditional thermite systems. The thermite reactions with aluminum nanoparticles initiate under a solid state without the melting of the Al core, which then leads to the diffusion of oxygen through the Al_2O_3 shells. In this case, the metal oxidizers play significant roles in the nano-thermite reaction. The reaction mechanisms of gas-solid or condensed-phase reaction become the critical points in understanding the reaction routes. However, pre-mixed nano-thermite composites have network structures, which involve uncountable interfaces between the reactive nanoparticles; therefore, the reaction mechanisms cannot be observed on the reactant interfaces. In the gas-solid reaction mechanism, the oxidizers undergo decomposition to release oxygen, which then surrounds the surface of Al nanoparticles at the initial stage of the thermite reaction. The oxygen further diffuses through the Al_2O_3 shell and reacts with the Al core. The critical point of the gas-solid reaction mechanism is the decomposition of oxidizer that occurs in advance of the nano-thermite reaction. On the other

hand, the condensed-phase reaction does not feature the decomposition of oxidizers before the initiation of the nano-thermite reaction. The Al nanoparticles form direct physical contact with the oxidizer nanoparticles. After heating the nano-thermite composites to the onset temperature, the oxygen atoms are released from the oxidizers and they further diffuse through the Al_2O_3 shell. During the process, the reactive nanoparticles migrate towards each other. The reaction mechanisms that are desired determine the required structures of nano-thermite composites and the potential applications. As stated above, the pre-mixed nano-thermite composites possess many interfaces; thus, observation of the interfacial area is impossible.

This thesis began with the development of nano-thermite composites with layered structures via the EPD process, using Al and Fe_2O_3 nanoparticles. In this work, the Al and Fe_2O_3 nanoparticles were formed and separated as different layers. The advantages of the separation are: the formation of a uniform interface and the avoidance of direct particle-by-particle contact. Due to the presence of the interface between the reactive layers, the thermite reaction initiates on the interface area. The initial objectives of the work were to confirm the formation of the nano-thermite composites and to measure their thermochemical properties. The layered Al/Fe_2O_3 nano-thermite has an onset temperature lower than the melting point of aluminum, indicating the contact between the reactants and the solid-status of Al nanoparticles when the thermite reaction initiates. The nano-thermite composites show consistent onset temperature even with different thickness of Al and Fe_2O_3 layers, which suggests the formation of uniform interfacial contacts, where the nano-thermite reactions

initiate. In addition, the energy release data reveals a large amount of energy, indicating the extension of the nano-thermite reaction across the interfacial area. The investigation ensures that the thermite reaction follows the reaction mechanisms by using nanoscale particles. It means that the nano-thermite composites with layered structures exhibit nano-thermite reaction mechanisms. The layered structure can be used to investigate the reaction mechanisms of nano-thermite composites.

The contribution of this work is the investigation of the reaction mechanisms of the typical nano-thermite composites, Al/CuO and Al/NiO. The thermochemical tests show the nano-thermite properties of these two composites. The XRD measurements follow the thermochemical analysis to show the chemical compositions of the reactants and their products. The crystalline structures of the aluminum and the oxidizers are shown in the reactants, whereas the alumina and the pure metal are presented in the products. The changes of chemical compositions specify the thermite reaction between the aluminum and the oxidizers to produce the new metals and alumina. The investigation of the microstructures of the reacted samples was then conducted. The results showed that the products remain as layered structures after the thermite reaction was completed, which provides useful structures to investigate the reaction mechanisms. Before the initiation of the nano-thermite reaction, the Al and oxidizers exist in their layers. For the thermite reaction to proceed, the elements (Al, metal, or oxygen) must move to the opposite layers. The products, which remain in layered structures within the defined interfacial area, can help trace the elements' migration between the layers. Furthermore, the EDS apparatus was used to measure the elements in

each layer. For the Al/CuO nano-thermite composite, the aluminum element was found in the original Al layer, indicating that the alumina exists in the original aluminum layer as revealed by the XRD data. Meanwhile, the copper element was only found in the original CuO layer, which suggests that the copper element did not migrate into the opposite layers. The oxygen element showed increasing concentration in the original Al layer. It is concluded that the oxygen released from the decomposition of CuO component migrates to the Al layer, which further reacts with the Al nanoparticles. This investigation clearly showed that the Al/CuO nano-thermite composite belongs to the gas-solid reaction mechanism. On the other hand, the aluminum and nickel elements exist in both the original Al and the NiO layers. The operation conditions in TGA/DSC ensured a constant temperature for the whole system. Even with the fast thermite reaction, which can increase the local temperature and induce sintering effects, the produced nickel metal cannot migrate to the opposite layer. Therefore, the nickel element found in the original Al layer indicates the migration of NiO nanoparticles into the original Al layer. Then, the migrated NiO nanoparticles form interfacial contact with the Al nanoparticles. Finally, the thermite reaction initiates at the particle-particle interface. Furthermore, the Al nanoparticles migrate to the original NiO layer simultaneously. The nano-thermite reaction occurs between the Al and NiO nanoparticles, which is conducted between the solid compositions. Therefore, the Al/NiO nano-thermite composite follows the condensed-phase reaction mechanism.

The next contribution included in this thesis was to investigate the roles of CNTs in nano-thermite reactions. The mass transfer mechanisms and thermal conductivities affect energy

release and reaction rates. The enhancement of thermal conductivity and mass transfer rates are able to enhance the reactivity of the nano-thermite composite. It is known that CNTs possess extremely high thermal conductivity compared to Al and metal oxidizers. Previous research has shown that a mixture of CNTs and nano-thermite composite has improved reactivity. It is understood that the increase in the thermal conductivity can improve the reactivity of nano-thermite composites, and it is not necessary to conduct further investigation. However, the investigation of the role of CNTs on mass transfer is required to obtain a deeper understanding of the reaction mechanisms. In this work, the multi-layered structure was employed to analyze the interaction between CNTs and Al, and CNTs and NiO. The critical point is to understand whether the CNTs react with Al first to carry the Al elements to the NiO, or the other way around. To achieve this goal, we prepared two comparable samples. In the first sample, the CNTs were mixed with NiO nanoparticles in a single layer. The Al nanoparticles were contained in the other layer. Due to the particle-by-particle contacts between NiO and CNTs, the interaction should occur between the two components before interacting with the Al nanoparticles. The second sample contained the CNTs and Al nanoparticles in a single layer, and the NiO in another layer. As shown in the SEM images, the products of the reacted samples remain in layered structures, which allows the possibility to trace the elements' movement between the layers. Then, EDS was applied to measure the elemental composition in each layer. The second sample, with the mixture of Al nanoparticles and CNTs in a single layer, did not show a difference in the elemental distribution compared with the Al/NiO nano-thermite composite with multi-layered structure.

However, the first sample, in which NiO nanoparticles were mixed with CNTs in a single layer demonstrated that the Ni element does not exist in the Al layers, indicating that the NiO nanoparticles did not migrate to the Al layers. The Al nanoparticles in the original Al layers were transferred to Al_2O_3 as shown by XRD measurement, indicating that the thermite reaction occurred in the layers. The mass spectroscopy data showed that the reaction between NiO and CNTs formed CO or CO_2, and the reaction route for the first sample (Al/NiO+CNT) can be described as follows. The NiO nanoparticles and CNTs reacted to release CO or CO_2 at the initial stage of the thermite reaction. The CO or CO_2 carried the oxygen atoms to the Al layers, followed by the reaction between Al and CO_2. On the other hand, the CNTs did not react with Al in the second sample (Al+CNT/NiO). Therefore, the Al and NiO nanoparticles migrated to the opposite layers simultaneously, similar to the thermite reaction of the Al/NiO nano-thermite composites. The nano-thermite reaction occurred between nanoparticles. Overall, the function of CNTs in the Al/NiO nano-thermite composite is to change the reaction mechanism from solid-solid to condensed-phase mechanism.

The contribution based on the application attempt to weld silicon wafers using nano-thermite composites was achieved. The silicon wafers used in the experiment were 500 μm in thickness with brittle characteristics. Traditional welding technologies, such as friction stir welding, are not suitable to join silicon wafers since they can be damaged during the procedure. Nano-thermite composites with fast reaction rates are able to increase the temperature at the interfacial area to form a joint between the two silicon wafers. Meanwhile, nano-thermites overcome the quenching effect over traditional thermite systems. Based on

the successful joining of the silicon wafers, the properties of nano-thermite composites were investigated regarding the energy release and activation energy. The diverse nano-thermite composites produced different joining qualities on the interface area. Nano-thermite composites with various compositions were prepared to attempt the welding of silicon wafers. Then, the energy release and activation energy of the two samples were investigated. It was shown that the sample with higher energy release and lower apparent activation energy provided enhanced energy on the interfacial area, which then resulted in stronger mechanical strength in the welded zone. With this contribution, the understanding and connections between the theoretical properties and joining quality were obtained, which can be useful in developing potential applications for nano-thermite composites.

7.2 Recommendations for future work

This thesis revealed the reaction mechanisms of nano-thermite composites in the fundamental research section. The different oxidizers showed diverse reaction mechanisms, gas-solid or condensed-phase. According to the general understanding, the increased interfacial contact between the reactants can improve the reactivity of nano-thermite composites. However, the reaction mechanisms can impact the reactivity of nano-thermite composites. In the gas-solid reaction mechanism, the porosity of the microstructures is required to allow the gas decomposed from the oxidizer to migrate to the Al nanoparticles. On the other hand, nano-thermites undergoing the condensed-phase reaction need physical contact between reactants to decrease the diffusion path. In the condensed-phase reaction

mechanism, porosity in the microstructures is not required. The nano-thermite reaction only occurs in the interfacial area of nanoparticles. This knowledge can improve the design of nano-thermite composites. For example, the Al/CuO nano-thermite systems can be formed with porous structures. Increased surface contact between Al and CuO will improve the ignition of the nano-composites in the initial stage. Furthermore, the porosity of these composites can allow the transfer of decomposed oxygen to migrate to reach the Al nanoparticles at the second stage of the nano-thermite reaction. On the other hand, the preparation of nano-thermite composites such as Al/NiO systems, governed by the condensed-phase reaction mechanism, requires enhanced interfacial contact. During the reactions, the molten nickel metal can induce sintering to produce spaces that allow the reactants to migrate and form an interfacial contact. Therefore, the free-standing structures of Al and NiO can improve the reactivity. For example, nanoparticles can be expected to migrate during the thermite reaction, which can move to form an interfacial contact between Al and NiO nanoparticles. Oppositely, the nano-composites with thin-layered structures may exhibit reduced reactivity. Based on this thesis, the first future work is the fabrication of nano-thermite composites with ideal structures according to the reaction mechanisms of the nano-thermite composites to address potential applications. The CuO skeleton with porous structure can be taken into account. Al nanoparticles or sputtering aluminum can be used to form the fuel component. Due to the gas-solid reaction mechanism in the Al/CuO system, these nano-thermite composites can be expected to have high reactivity.

This thesis proposes the investigation of nano-thermite reaction mechanisms under slow

heating rate conditions. However, heating rates play significant roles in nano-thermite reactions. Reaction routes may change under different heating rates. Future work can investigate the nano-thermite reaction mechanisms under high heating rates. Although the nano-thermite reaction in the work can provide a fast local heating rate within the samples, most of the sample remains at the environmental temperature. Nano-thermite composites are self-sustained reactions, where heat produced by the reacted parts initiate the unreacted parts. The local heating rates can satisfy moderate heating rate conditions. However, it is not sufficient to transfer the oxidation of Al nanoparticles from the diffusion-controlled mechanism to the melt-dispersion mechanism. It may occur under extremely high heating rates when using nano-thermite composites with premixed structures. Therefore, it is worthwhile to increase the heating rates in nano-thermite composites. Future work can investigate these high heating rates by introducing different heating methods such as laser radiation on nano-thermite composites with multi-layered structures. The results of such work can provide an understanding of the reaction mechanisms under high heating rates.

Reference

[1] E.L. Dreizin, Metal-based reactive nanomaterials, Prog. Energy Combust. Sci. 35(2) (2009) 141-167.

[2] C. Rossi, K. Zhang, D. Esteve, P. Alphonse, P. Tailhades, C. Vahlas, Nanoenergetic materials for MEMS: A review, J. Microelectromech. Syst. 16(4) (2007) 919-931.

[3] L.L. Wang, Z.A. Munir, Y.M. Maximov, Review Thermite reactions: their utilization in the synthesis and processing of materials, J. Mater. Sci. 28 (1993) 3693-3708.

[4] K. Sullivan, Ignition, Combustion and Tuning of Nanocomposite Thermites, Department of Mechanical Engineering and Chemistry, University of Maryland, 2010, p. 233.

[5] S. Apperson, R.V. Shende, S. Subramanian, D. Tappmeyer, S. Gangopadhyay, Z. Chen, K. Gangopadhyay, P. Redner, S. Nicholich, D. Kapoor, Generation of fast propagating combustion and shock waves with copper oxide/aluminum nanothermite composites, Appl. Phys. Lett. 91(24) (2007) 243109.

[6] G. Jian, N.W. Piekiel, M.R. Zachariah, Time-Resolved Mass Spectrometry of Nano-Al and Nano-Al/CuO Thermite under Rapid Heating: A Mechanistic Study, The Journal of Physical Chemistry C 116(51) (2012) 26881-26887.

[7] Y. Ohkura, S.Y. Liu, P.M. Rao, X. Zheng, Synthesis and ignition of energetic CuO/Al core/shell nanowires, Proc. Combust. Inst. 33(2) (2011) 1909-1915.

[8] V.E. Sanders, B.W. Asay, T.J. Foley, B.C. Tappan, A.N. Pacheco, S.F. Son, Reaction Propagation of Four Nanoscale Energetic Composites (Al/MoO_3, Al/WO_3, Al/CuO, and Bi_2O_3), J. Propul. Power 23(4) (2007) 707-714.

[9] F. Séverac, P. Alphonse, A. Estève, A. Bancaud, C. Rossi, High-Energy Al/CuO Nanocomposites Obtained by DNA-Directed Assembly, Adv. Funct. Mater. 22(2) (2012) 323-329.

[10] R. Shende, S. Subramanian, S. Hasan, S. Apperson, R. Thiruvengadathan, K. Gangopadhyay, S. Gangopadhyay, P. Redner, D. Kapoor, S. Nicolich, W. Balas, Nanoenergetic Composites of CuO Nanorods, Nanowires, and Al-Nanoparticles, Propellants, Explosives, Pyrotechnics 33(2) (2008) 122-130.

[11] K.T. Sullivan, J.D. Kuntz, A.E. Gash, Electrophoretic deposition and mechanistic studies of nano-Al/CuO thermites, J. Appl. Phys. 112(2) (2012) 024316.

[12] S.M. Umbrajkar, M. Schoenitz, E.L. Dreizin, Exothermic reactions in Al–CuO nanocomposites, Thermochim. Acta 451(1-2) (2006) 34-43.

[13] J. Wang, A. Hu, J. Persic, J.Z. Wen, Y. Norman Zhou, Thermal stability and reaction properties of passivated Al/CuO nano-thermite, J. Phys. Chem. Solids 72(6) (2011) 620-625.

[14] M.R. Weismiller, J.Y. Malchi, R.A. Yetter, T.J. Foley, Dependence of flame propagation on pressure and pressurizing gas for an Al/CuO nanoscale thermite, Proc. Combust. Inst. 32(2) (2009) 1895-1903.

[15] K. Zhang, C. Rossi, M. Petrantoni, N. Mauran, A nano initiator realized by integrating Al/CuO-based nanoenergetic materials with a Au/Pt/Cr microheater, Journal of Microelectromechanical System 17(4) (2008) 832-836.

[16] X. Zhou, R. Shen, Y. Ye, P. Zhu, Y. Hu, L. Wu, Influence of Al/CuO reactive multilayer films additives on exploding foil initiator, J. Appl. Phys. 110(9) (2011) 094505.

[17] C. Park, M. Mileham, L.J.v.d. Burgt, E.A. Muller, A.E. Stiegman, The Effects of Stoichiometry and Sample Density on Combustion Dynamics and Initiation Energy of Al/Fe_2O_3 Metastable Interstitial Composites, Journal of Physics and Chemical C 114 (2010) 2814-2820.

[18] J.L. Cheng, H.H. Hng, Y.W. Lee, S.W. Du, N.N. Thadhani, Kinetic study of thermal- and impact-initiated reactions in Al–Fe_2O_3 nanothermite, Combust. Flame 157(12) (2010) 2241-2249.

[19] K.B. Plantier, M.L. Pantoya, A.E. Gash, Combustion wave speeds of nanocomposite Al/Fe_2O_3: the effects of Fe_2O_3 particle synthesis technique, Combust. Flame 140(4) (2005) 299-309.

[20] S.F. Son, B.W. Asay, T.J. Foley, R.A. Yetter, M.H. Wu, G.A. Risha, Combustion of Nanoscale Al/MoO_3 Thermite in Microchannels, J. Propul. Power 23(4) (2007) 715-721.

[21] J. Sun, M.L. Pantoya, S.L. Simon, Dependence of size and size distribution on reactivity of aluminum nanoparticles in reactions with oxygen and MoO_3, Thermochim. Acta 444(2) (2006) 117-127.

[22] K. Zhang, C. Rossi, P. Alphonse, C. Tenailleau, S. Cayez, J.-Y. Chane-Ching, Integrating Al with NiO nano honeycomb to realize an energetic material on silicon substrate, Appl. Phys. A 94(4) (2008) 957-962.

[23] S.H. Fischer, M.C. Grubelich, Theoretical energy release of thermites, intermetallics, and combustible metals, The 24th International Pyrotechnics Seminar, Monterey, 1998.

[24] L. Joseph, D. Davis, S. Kalay, Strengthening the track structure for heavy axle loads:

strengthening track infrastructure provides another method of dealing with ever-increasing car capacities. (TTCI R&D).(Transportation Technology Center Inc.'s research and development), 2002. https://www.highbeam.com/doc/1G1-92081824.html.

[25] D.W. Youngner, S.T. Lu, E. Choueiri, J.B. Neidert, R.E. Black, K.J. Graham, D. Fahey, R. Lucus, X. Zhu, MEMS Mega-pixel Micro-thruster Arrays for Small Satellite Stationkeeping, 14th Annual/USU Conference on Small Satellites.

[26] D.H.L. Jr., S.W. Janson, R.B. Cohen, E.K. Antonsson, Digital MicroPropulsion, Sensors and Actuators A, Physical 80(2) (2000) 143-154.

[27] C. Rossi, D. Briand, M. Dumonteuil, T. Camps, P.Q. Pham, N.F.d. Rooij, Matrix of 10×10 addressed solid propellant microthrusters: Review of the technologies, Sensors and Actuators A: Physical 126(1) (2006) 241-252.

[28] T. Troianello, Precision foil resistors used as electro-pyrotechnic initiators, Electronic Components and Technology Conference, 2001.

[29] H.H. DiBiaso, B.A. English, M.G. Allen, Solid-phase conductive fuels for chemical microactuators, Sensors and Actuators A: Physical 111(2-3) (2004) 260-266.

[30] C. Rossi, D. Esteve, C. Mingues, Pyrotechnic actuator: a new generation of Si integrated actuator, Sens. Actuators 74 (1999) 211-215.

[31] J.-W. Choi, C.H. Ahn, A functional on-chip pressure generator using solid chemical propellant for disposable lab-on-a-chip, (2003).

[32] O. Vasylkiv, Y. Sakka, Nanoexplosion synthesis of multimetal oxide ceramic nanopowders, Nano Lett. 5(12) (2005) 2598-2604.

[33] W. Gutkowski, T.A. Kowalewski, Mechanics of the 21st Century, 2004.

[34] P. Pennarun, C. Rossi, D. Estève, D. Bourrier, Design, fabrication and characterization of a MEMS safe pyrotechnical igniter integrating arming, disarming and sterilization functions, J. Micromech. Microeng. 16(1) (2006) 92-100.

[35] M.A. Trunov, M. Schoenitz, E.L. Dreizin, Effect of polymorphic phase transformations in alumina layer on ignition of aluminium particles, Combust. Theor. Model. 10(4) (2006) 603-623.

[36] L.E. Fried, M.R. Manaa, P.F. Pagoria, R.L. Simpson, Design and synthesis of energetic materials, Annual Review of Materials Research 31 (2001) 291-321.

[37] C. Rossi, D. Estève, Micropyrotechnics, a new technology for making energetic microsystems: review and prospective, Sensors and Actuators A: Physical 120(2) (2005) 297-310.

[38] J.Y. Ahn, S.B. Kim, J.H. Kim, N.S. Jang, D.H. Kim, H.W. Lee, J.M. Kim, S.H. Kim, A micro-chip initiator with controlled combustion reactivity realized by integrating Al/CuO nanothermite composites on a microhotplate platform, Journal of Micromechanics and Microengineering 26(1) (2016) 015002.

[39] G. Taton, D. Lagrange, V. Conedera, L. Renaud, C. Rossi, Micro-chip initiator realized by integrating Al/CuO multilayer nanothermite on polymeric membrane, Journal of Micromechanics and Microengineering 23(10) (2013) 105009.

[40] K.L. Zhang, S.K. Chou, S.S. Ang, X.S. Tang, A MEMS-based solid propellant microthruster with Au/Ti igniter, Sensors and Actuators A: Physical 122(1) (2005) 113-123.

[41] E.W. Price, Effect of multidimensional flamelets in composite propellant combustion, Journal of Propulsion and Powder 11(4) (1995) 717-729.

[42] V.A. Babuk, V.A. Vasilyev, Model of Aluminum Agglomerate Evolution in Combustion Products of Solid Rocket Propellant, J. Propul. Power 18(4) (2002) 814-823.

[43] C.E. Aumann, Oxidation behavior of aluminum nanopowders, Journal of Vacuum Science & Technology B: Microelectronics and Nanometer Structures 13(3) (1995) 1178.

[44] J.Z. Wen, S. Ringuette, G. Bohlouli-Zanjani, A. Hu, N.H. Nguyen, J. Persic, C.F. Petre, Y.N. Zhou, Characterization of thermochemical properties of Al nanoparticle and NiO nanowire composites, Nanoscale Res Lett 8(1) (2013) 184.

[45] K. Sullivan, M. Zachariah, Simultaneous Pressure and Optical Measurements of Nanoaluminum Thermites: Investigating the Reaction Mechanism, J. Propul. Power 26(3) (2010) 467-472.

[46] L. Zhou, N. Piekiel, S. Chowdhury, M.R. Zachariah, Time-Resolved Mass Spectrometry of the Exothermic Reaction between Nanoaluminum and Metal Oxides: The Role of Oxygen Release, J. Phys. Chem. C 114 (2010) 14269-14275.

[47] G.M. Fritz, S.J. Spey, M.D. Grapes, T.P. Weihs, Thresholds for igniting exothermic reactions in Al/Ni multilayers using pulses of electrical, mechanical, and thermal energy, J. Appl. Phys. 113(1) (2013) 014901.

[48] J.A. Floro, Propagation of explosive crystallization in thin Rh–Si multilayer films, Journal of Vacuum Science & Technology A: Vacuum, Surfaces, and Films 4(3) (1986) 631.

[49] M. Petrantoni, C. Rossi, L. Salvagnac, V. Conédéra, A. Estève, C. Tenailleau, P.

Alphonse, Y.J. Chabal, Multilayered Al/CuO thermite formation by reactive magnetron sputtering: Nano versus micro, J. Appl. Phys. 108(8) (2010) 084323.

[50] D.H.L. Jr., S.W. Janson, R.B. Cohen, E.K. Antonsson, Digital micropropulsion, Sens. Actuators 80 (2000) 143-154.

[51] W. Lindsay, D. Teasdale, V. Milanovic, K. Pister, C. Fernandez-Pello, Thrust and Electrical Power from Solid Propellant Microrockets.

[52] S. Tanaka, R. Hosokawa, S.-i. Tokudome, K. Hori, H. Saito, M. Watanabe, M. Esashi, MEMS-Based Solid Propellant Rocket Array Thruster with Electrical Feedthroughs, JSASS 46(151) (2003) 47-51.

[53] C. Rossi, B. Larangot, D. Lagrange, A. Chaalane, Final characterizations of MEMS-based pyrotechnical microthrusters, Sensors and Actuators A: Physical 121(2) (2005) 508-514.

[54] E.L. Dreizin, M. Schoenitz, Correlating ignition mechanisms of aluminum-based reactive materials with thermoanalytical measurements, Prog. Energy Combust. Sci. 50 (2015) 81-105.

[55] B.S. Bockmon, M.L. Pantoya, S.F. Son, B.W. Asay, J.T. Mang, Combustion velocities and propagation mechanisms of metastable interstitial composites, J. Appl. Phys. 98(6) (2005) 064903.

[56] G. Young, K. Sullivan, M. Zachariah, K. Yu, Combustion characteristics of boron nanoparticles, Combust. Flame 156(2) (2009) 322-333.

[57] J. Kwon, J.M. Ducéré, P. Alphonse, M. Bahrami, M. Petrantoni, J.-F. Veyan, C.

Tenailleau, A. Estève, C. Rossi, Y.J. Chabal, Interfacial Chemistry in Al/CuO Reactive Nanomaterial and Its Role in Exothermic Reaction, ACS Appl. Mater. Interfaces 5(3) (2013) 605-613.

[58] B. Mehendale, R. Shende, S. Subramanian, S. Gangopadhyay, P. Redner, D. Kapoor, S. Nicolich, Nanoenergetic Composite of Mesoporous Iron Oxide and Aluminum Nanoparticles, Journal of Energetic Materials 24(4) (2006) 341-360.

[59] J. Wang, S. He, Z. Li, X. Jing, M. Zhang, Z. Jiang, Self-assembled CuO nanoarchitectures and their catalytic activity in the thermal decomposition of ammonium perchlorate, Colloid. Polym. Sci. 287(7) (2009) 853-858.

[60] K.F. Sheldon, Smoke, Dust, and Haze: Fundamentals of Aerosol Dynamics, Oxford Univ. Press, New York, 2000.

[61] K.C. Walter, D.R. Pesiri, D.E. Wilson, Manufacturing and Performance of Nanometric Al/MoO3 Energetic Materials, J. Propul. Power 23(4) (2007) 645-650.

[62] W.L. Perry, B.L. Smith, C.J. Bulian, J.R. Busse, C.S. Macomber, R.C. Dye, S.F. Son, Nano-Scale Tungsten Oxides for Metastable Intermolecular Composites, Propellants, Explosives, Pyrotechnics 29(2) (2004) 99-105.

[63] T.M. Tillotson, A.E. Gash, R.L. Simpson, L.W. Hrubesh, J.H.S. Jr., J.F. Poco, Nanostructured energetic materials using sol-gel methodologies, J. Non-Cryst. Solids 285 (2001) 338-345.

[64] A. Gash, J. Satcher, R. Simpson, B. Clapsaddle, Nanostructured Energetic Materials with Sol-Gel Methods, Materials Research Society Fall 2003 Meeting, Boston, MA, United

States, 2003.

[65] A.E. Gash, T.M. Tillotson, J. Joe H. Satcher, L.W. Hrubesh, R.L. Simpson, New sol-gel synthetic route to transition and main-group metal oxide aerogels using inorganic salt precursors, J. Non-Cryst. Solids 285 (2001) 22-28.

[66] T. Zhang, Z. Wang, G. Li, Y. Luo, Tuning the reactivity of Al/Fe_2O_3 nanoenergetic materials via an approach combining soft template self-assembly with sol–gel process process, J. Solid State Chem. 230 (2015) 1-7.

[67] J.L. Cheng, H.H. Hng, H.Y. Ng, P.C. Soon, Y.W. Lee, Synthesis and characterization of self-assembled nanoenergetic Al–Fe_2O_3 thermite system, J. Phys. Chem. Solids 71(2) (2010) 90-94.

[68] S.M. Umbrajkar, S. Seshadri, M. Schoenitz, V.K. Hoffmann, E.L. Dreizin, Aluminum-Rich Al-MoO_3 Nanocomposite Powders Prepared by Arrested Reactive Milling, J. Propul. Power 24(2) (2008) 192-189.

[69] S. Umbrajkar, M.A. Trunov, M. Schoenitz, E.L. Dreizin, R. Broad, Arrested Reactive Milling Synthesis and Characterization of Sodium-Nitrate Based Reactive Composites, Propellants, Explosives, Pyrotechnics 32(1) (2007) 32-41.

[70] S.M. Umbrajkar, M. Schoenitz, E.L. Dreizin, Control of Structural Refinement and Composition in Al-MoO_3 Nanocomposites Prepared by Arrested Reactive Milling, Propellants, Explosives, Pyrotechnics 31(5) (2006) 382-389.

[71] M. Schoenitz, T.S. Ward, E.L. Dreizin, Fully dense nano-composite energetic powders prepared by arrested reactive milling, Proc. Combust. Inst. 30(2) (2005) 2071-2078.

[72] D. Stamatis, Z. Jiang, V.K. Hoffmann, M. Schoenitz, E.L. Dreizin, Fully Dense, Aluminum-Rich Al-CuO Nanocomposite Powders for Energetic Formulations, Combust. Sci. Technol. 181(1) (2008) 97-116.

[73] M. Schoenitz, S.M. Umbrajkar, E.L. Dreizin, Kinetic Analysis of Thermite Reactions in Al-MoO_3 Nanocomposites, J. Propul. Power 23(4) (2007) 683-687.

[74] A. Ermoline, D. Stamatis, E.L. Dreizin, Low-temperature exothermic reactions in fully dense Al–CuO nanocomposite powders, Thermochim. Acta 527 (2012) 52-58.

[75] S.M. Umbrajkar, C.-M. Chen, M. Schoenitz, E.L. Dreizin, On problems of isoconversion data processing for reactions in Al-rich Al–MoO_3 thermites, Thermochim. Acta 477(1-2) (2008) 1-6.

[76] D. Stamatis, E.L. Dreizin, K. Higa, Thermal Initiation of Al-MoO_3 Nanocomposite Materials Prepared by Different Methods, J. Propul. Power 27(5) (2011) 1079-1087.

[77] D.K. Diop, L. Simonot, N. Destouches, G. Abadias, F. Pailloux, P. Guérin, D. Babonneau, Magnetron Sputtering Deposition of Ag/TiO_2 Nanocomposite Thin Films for Repeatable and Multicolor Photochromic Applications on Flexible Substrates, Advanced Materials Interfaces 2(14) (2015) 1500134 (1)-1500134 (9).

[78] M.L. Pantoya, E.M. Hunt, Nanochargers: Energetic materials for energy storage, Appl. Phys. Lett. 95(25) (2009) 253101.

[79] J. Wang, E. Besnoin, A. Duckham, S.J. Spey, M.E. Reiss, O.M. Knio, M. Powers, M. Whitener, T.P. Weihs, Room-temperature soldering with nanostructured foils, Appl. Phys. Lett. 83(19) (2003) 3987.

[80] E. Ma, C.V. Thompson, L.A. Clevenger, K.N. Tu, Self-propagating explosive reactions in Al/Ni multilayer thin films, Appl. Phys. Lett. 57(12) (1990) 1262.

[81] J.D. Ferguson, K.J. Buechler, A.W. Weimer, S.M. George, SnO_2 atomic layer deposition on ZrO_2 and Al nanoparticles: Pathway to enhanced thermite materials, Powder Technol. 156(2-3) (2005) 154-163.

[82] A. Prakash, A.V. McCormick, M.R. Zachariah, Synthesis and Reactivity of a Super-Reactive Metastable Intermolecular Composite Formulation of Al/$KMnO_4$, Advabced Materials 17(7) (2005) 900-903.

[83] A.E. Gash, T.M. Tillotson, J. Joe H. Satcher, J.F. Poco, L.W. Hrubesh, R.L. Simpson, Use of Epoxides in the Sol-Gel Synthesis of Porous Iron(III) oxide Monoliths from Fe(III) Salts, Chem. Mater. 13 (2001) 999-1007.

[84] T. Bazyn, N. Glumac*, H. Krier, T.S. Ward, M. Schoenitz, E.L. Dreizin, Reflected Shock Ignition and Combustion of Aluminum and Nanocomposite Thermite Powders, Combust. Sci. Technol. 179(3) (2007) 457-476.

[85] J.R. Luman, B. Wehrman, K.K. Kuo, R.A. Yetter, N.M. Masoud, T.G. Manning, L.E. Harris, H.A. Bruck, Development and characterization of high performance solid propellants containing nano-sized energetic ingredients, Proc. Combust. Inst. 31(2) (2007) 2089-2096.

[86] K.J. Blobaum, M.E. Reiss, J.M. Plitzko, T.P. Weihs, Deposition and characterization of a self-propagating CuO_x/Al thermite reaction in a multilayer foil geometry, J. Appl. Phys. 94(5) (2003) 2915-2922.

[87] A.J. Gavens, D. Van Heerden, A.B. Mann, M.E. Reiss, T.P. Weihs, Effect of intermixing

on self-propagating exothermic reactions in Al/Ni nanolaminate foils, J. Appl. Phys. 87(3) (2000) 1255.

[88] K.J. Blobaum, A.J. Wagner, J.M. Plitzko, D. Van Heerden, D.H. Fairbrother, T.P. Weihs, Investigating the reaction path and growth kinetics in CuO[sub x]/Al multilayer foils, J. Appl. Phys. 94(5) (2003) 2923.

[89] K.T. Sullivan, M.A. Worsley, J.D. Kuntz, A.E. Gash, Electrophoretic deposition of binary energetic composites, Combust. Flame 159(6) (2012) 2210-2218.

[90] K.T. Sullivan, C. Zhu, D.J. Tanaka, J.D. Kuntz, E.B. Duoss, A.E. Gash, Electrophoretic Deposition of Thermites onto Micro-Engineered Electrodes Prepared by Direct-Ink Writing, The Journal of Physical Chemistry B 117(6) (2013) 1686-1693.

[91] D. Zhang, X. Li, B. Qin, C. Lai, X. Guo, Electrophoretic deposition and characterization of nano-Al/Fe_2O_3 thermites, Mater. Lett. 120 (2014) 224-227.

[92] H. Seim, M. Nieminen, L. Niinisto, H. Fjellvag, L.-S. Johansson, Growth of $LaCoO_3$ thin films from b-diketonate precursors, Appl. Surf. Sci. 112 (1997) 243-250.

[93] P. Tagtstrom, P. Martensson, U. Jansson, J.O. Carlsson, Atomic Layer Epitaxy of Tungsten Oxide Films Using Oxyfluorides as Metal Precursors, J. Electrochem. Soc. 146(8) (1999) 3139-3143.

[94] T.S. Yang, W. Cho, M. Kim, K.-S. An, T.-M. Chung, C.G. Kim, Y. Kim, Atomic layer deposition of nickel oxide films using Ni (dmamp) 2 and water, Journal of Vacuum Science & Technology A: Vacuum, Surfaces, and Films 23(4) (2005) 1238.

[95] L. Besra, M. Liu, A review on fundamentals and applications of electrophoretic

deposition (EPD), Prog. Mater Sci. 52(1) (2007) 1-61.

[96] K. Moore, M.L. Pantoya, S.F. Son, Combustion Behaviors Resulting from Bimodal Aluminum Size Distributions in Thermites, J. Propul. Power 23(1) (2007) 181-185.

[97] E.L. Dreizin, Metal-based reactive nanomaterials, Progress in Energy and Combustion Science 35 (2009) 141-167.

[98] J.A. Puszynski, Processing and characterization of aluminum-based nanothermites, J. Therm. Anal. Calorim. 96(3) (2009) 677-685.

[99] L.P.H. Jeurgens, W.G. Sloof, F.D. Tichelaar, E.J. Mittemeijer, Structure and morphology of aluminium-oxide films formed by thermal oxidation of aluminium, Thin Solid Films 418 (2002) 89-101.

[100] J.C. Sanchez-Lopez, A.R. Gonzalez-Elipe, A. Fernandez, Passivation of nanocrystalline Al prepared by the gas phase condensation method: An x-ray photoelectron spectroscopy study, J. Mater. Res. 13(3) (1998) 703-710.

[101] L.P.H. Jeurgens, W.G. Sloof, F.D. Tichelaar, E.J. Mittemeijer, Thermodynamic stability of amorphous oxide films on metals: Application to aluminum oxide films on aluminum substrates, Phys. Rev. B 62(7) (2000) 4707-4719.

[102] A. Rai, K. Park, L. Zhou, M.R. Zachariah, Understanding the mechanism of aluminium nanoparticle oxidation, Combust. Theor. Model. 10(5) (2006) 843-859.

[103] M.A. Trunov, M. Schoenitz, X. Zhu, E.L. Dreizin, Effect of polymorphic phase transformations in Al_2O_3 film on oxidation kinetics of aluminum powders, Combust. Flame 140(4) (2005) 310-318.

[104] S. Chowdhury, K. Sullivan, N. Piekiel, L. Zhou, M.R. Zachariah, Diffusive vs Explosive Reaction at the Nanoscale, J. Phys. Chem. C 114 (2010) 9191-9195.

[105] B.J. Henz, T. Hawa, M.R. Zachariah, On the role of built-in electric fields on the ignition of oxide coated nanoaluminum: Ion mobility versus Fickian diffusion, J. Appl. Phys. 107(2) (2010) 024901.

[106] V. Levitas, Burn time of aluminum nanoparticles: Strong effect of the heating rate and melt-dispersion mechanism, Combust. Flame 156(2) (2009) 543-546.

[107] V.I. Levitas, M.L. Pantoya, B. Dikici, Melt dispersion versus diffusive oxidation mechanism for aluminum nanoparticles: Critical experiments and controlling parameters, Appl. Phys. Lett. 92(1) (2008) 011921.

[108] E.V. Chernenko, L.F. Afanas'eva, V.A. Lebedeva, V.I. Rozenband, Inflammability of mixtures of metal oxides with aluminum, Combustion, Explosion and Shock Waves 24(6) (1989) 639-646.

[109] S.R. Ahmad, D.A. Russell, Studies into Laser Ignition of Unconfined Propellants, Propellants, Explosives, Pyrotechnics 26 (2001) 235-245.

[110] P. Dimitriou, V. Hlavacek, S.M. Valone, R.G. Behrens, G.P. Hansen, J.L. Margrave, Laser-Induced Ignition in Solid-state Combustion, AlChE J. 35(7) (1989) 1085-1096.

[111] K.K. Kuo, J.U. Kim, B.L. Fetherolf, T. Torikai, Preignition Dynamics of RDX-Based Energetic Materials Under CO_2 Laser Heating, Combust. Flame 95 (1993) 351-361.

[112] A.N. Ali, S.F. Son, B.W. Asay, M.E. Decroix, M.Q. Brewster, High-irradiance laser ignition of explosives, Combust. Sci. Technol. 175(8) (2003) 1551-1571.

[113] M.L. Mileham, M.P. Kramer, A.E. Stiegman, Laser Initiation Processes in Thermite Energetic Materials Using Laser Desorption Ionization Time-of-Flight Mass Spectrometry, J. Phys. Chem. C 111 (2007) 16883-16888.

[114] S. Wang, Y. Yang, H. Yu, D.D. Dlott, Dynamical Effects of the Oxide Layer in Aluminum Nanoenergetic Materials, Propellants, Explosives, Pyrotechnics 30(2) (2005) 148-155.

[115] Y. Yang, Z. Sun, S. Wang, D.D. Dlott, Fast Spectroscopy of Laser-Initiated Nanoenergetic Materials, J. Phys. Chem. B 107 (2003) 4485-4493.

[116] M.A. Zamkov, R.W. Conner, D.D. Dlott, Ultrafast Chemistry of Nanoenergetic Materials Studied by Time-Resolved Infrared Spectroscopy: Aluminum Nanoparticles in Teflon, J. Phys. Chem. C 111 (2007) 10278-10284.

[117] J.J. Granier, M.L. Pantoya, Laser ignition of nanocomposite thermites, Combust. Flame 138(4) (2004) 373-383.

[118] N. Glumac, H. Krier, T.I.M. Bazyn, R. Eyer, Temperature Measurements of Aluminum Particles Burning in Carbon Dioxide, Combust. Sci. Technol. 177(3) (2005) 485-511.

[119] J. Servaites, H. Krier, J.C. Melcher, Ignition and Combustion of Aluminum Particles in Shocked $H_2O/O_2/Ar$ and $CO_2/O_2/Ar$ Mixtures, Combust. Flame 125 (2001) 1040-1054.

[120] D.G. Tasker, B.W. Asay, J.C. King, V.E. Sanders, S.F. Son, Dynamic measurements of electrical conductivity in metastable intermolecular composites, J. Appl. Phys. 99(2) (2006) 023705.

[121] D. Prentice, M.L. Pantoya, B.J. Clapsaddle, Effect of Nanocomposite Synthesis on the

Combustion Performance of a Ternary Thermite, J. Phys. Chem. B 109 (2005) 20180-20185.

[122] Y.-S. Kwon, A.A. Gromov, A.P. Ilyin, E.M. Popenko, G.-H. Rim, The mechanism of combustion of superfine aluminum powders, Combust. Flame 133(4) (2003) 385-391.

[123] D.S. Moore, S.F. Son, B.W. Asay, Time-Resolved Spectral Emission of Deflagrating Nano-Al and Nano-MoO_3 Metastable Interstitial Composites, Propellants, Explosives, Pyrotechnics 29(2) (2004) 106-111.

[124] J.Y. Malchi, R.A. Yetter, T.J. Foley, S.F. Son, The Effect of Added Al_2O_3 on the Propagation Behavior of an Al/CuO Nanoscale Thermite, Combust. Sci. Technol. 180(7) (2008) 1278-1294.

[125] S.F. Son, M. Quinn Brewster, Radiation-Augmented Combustion of Homogeneous Solids, Combust. Sci. Technol. 107(1-3) (1995) 127-154.

[126] M. Bahrami, G. Taton, V. Conédéra, L. Salvagnac, C. Tenailleau, P. Alphonse, C. Rossi, Magnetron Sputtered Al-CuO Nanolaminates: Effect of Stoichiometry and Layers Thickness on Energy Release and Burning Rate, Propellants, Explosives, Pyrotechnics 39(3) (2014) 365-373.

[127] H.J. Borchardt, F. Daniels, The Application of Differentical Thermal Analysis to the Study of Reaction Kinetics, JACS 79 (1956) 41-46.

[128] H.E. Kissinger, Reaction Kinetics in Differential Thermal Analysis, Anal. Chem. 29(11) (1957) 1702-1706.

[129] L. Galfetti, L.T.D. Luca, F. Severini, L. Meda, G. Marra, M. Marchetti, M. Regi, S. Bellucci, Nanoparticles for solid rocket propulsion, J. Phys.: Condens. Matter 18(33) (2006)

S1991-S2005.

[130] M.W. Beckstead, K. Puduppakkam, P. Thakre, V. Yang, Modeling of combustion and ignition of solid-propellant ingredients, Prog. Energy Combust. Sci. 33(6) (2007) 497-551.

[131] A. Dokhan, E.W. Price, J.M. Seitzman, R.K. Sigman, The effects of bimodal aluminum with ultrafine aluminum on the burning rates of solid propellants, Proc. Combust. Inst., 2002, pp. 2939-2945.

[132] L. T., D. Luca, Burning of Aluminized Solid Rocket Propellants: from Micrometric to Nanometric Fuel Size, International Autumn Seminar on Propellants, Explosives and Pyrotechnics, China, 2007.

[133] K.T. Higa, Energetic Nanocomposite Lead-Free Electric Primers, J. Propul. Power 23(4) (2007) 722-727.

[134] J.C. Hinshaw, F. West, R.J. Blau, Richmond, Thermite compositions for use as gas generants comprising basic metal carbonates and/or basic metal nitrates, Thiokol Corporation, Ogden, Utah, 1995.

[135] C. Hong, S. Murugesan, S. Kim, G. Beaucage, J. Choi, C.H. Ahn, A functional on-chip pressure generator using solid chemical propellant for disposable lab-on-a-chip Sixteenth Annual International Conference, Kyoto, 2003, pp. 16-19.

[136] A.A. Norton, M.A. Minor, Pneumatic Microactuator Powered by the Deflagration of Sodium Azide, J. Microelectromech. Syst. 15(2) (2006) 344-354.

[137] O. Vasylkiv, Y. Sakka, V.V. Skorokhod, Nano-Blast Synthesis of Nano-size CeO_2-Gd_2O_3 Powders, J. Am. Ceram. Soc. 89(6) (2006) 1822-1826.

[138] Y. Lin, A.A. Nepapushev, P.J. McGinn, A.S. Rogachev, A.S. Mukasyan, Combustion joinining of carbon/carbon composites by a reactive mixture of titanium and mechanically activated nickel/aluminum powders, Ceram. Int. 39(7) (2013) 7499-7505.

[139] J.D.E. White, A.H. Simpson, A.S. Shteinberg, A.S. Mukasyan, Combustion joining of refractory materials: Carbon–carbon composites, J. Mater. Res. 23(01) (2011) 160-169.

[140] G. Feng, Z. Li, R. Liu, S. Feng, Effects of Joining Conditions on Microstructure and Mechanical Properties of Cf/Al Composites and TiAl Alloy Combustion Synthesis Joints, Acta Metall. Sin. (Engl. Lett.) 28(4) (2015) 405-413.

[141] J. Deng, G. Li, L. Shen, Y. Luo, Application of Al/B/Fe_2O_3 Nano Thermite in Composite Solid Propellant, Bulletin of Chemical Reaction Engineering & Catalysis 11(1) (2016) 109.

[142] J. Hoffman, Explosives found in world trade center dust, 2009.

[143] L. Durães, B.F.O. Costa, R. Santos, A. Correia, J. Campos, A. Portugal, Fe_2O_3/aluminum thermite reaction intermediate and final products characterization, Materials Science and Engineering: A 465(1-2) (2007) 199-210.

[144] D.G. Piercey, T.M. Klapotke, Nanoscale aluminum - metal oxide (thermite) reactions for application in energetic materials, Central European Journal of Energetic Materials 7(2) (2010) 115-129.

[145] D. Dzelnitzki, Mundersbach, Plasma welding of aluminum materials, EWM Hightec Welding GmbH (2000).

[146] H.C. Hamaker, Formation of a deposit by electrophoresis, Transactions of the Faraday

Society 35 (1939) 279-287.

[147] D.A. Kaplowitz, G. Jian, K. Gaskell, A. Ponce, P. Shang, M.R. Zachariah, Aerosol Synthesis and Reactivity of Thin Oxide Shell Aluminum Nanoparticles via Fluorocarboxylic Acid Functional Coating, Particle & Particle Systems Characterization 30 (2013) 881-887.

[148] J. Kang, S. Atashin, S.H. Jayaram, J.Z. Wen, Frequency and temperature dependent electrochemical characteristics of carbon-based electrodes made of commercialized activated carbon, graphene and single-walled carbon nanotube, Carbon 111 (2017) 338-349.

[149] H. Sui, S. Atashin, J.Z. Wen, Thermo-chemical and energetic properties of layered nano-thermite composites, Thermochim. Acta 642 (2016) 17-24.

[150] M.V. Coulet, B. Rufino, P.H. Esposito, T. Neisius, O. Isnard, R. Denoyel, Oxidation Mechanism of Aluminum Nanopowders, J. Phys. Chem. C 119(44) (2015) 25063-25070.

[151] E.V. Chernenko, L.F. Afanas'eva, V.A. Lebedeva, V.I. Rozenband, Inflammability of mixtures of metal oxides with aluminum, Combustion Explosive Shock Waves 24 (1989) 639-646.

[152] K.T. Sullivan, N.W. Piekiel, C. Wu, S. Chowdhury, S.T. Kelly, T.C. Hufnagel, K. Fezzaa, M.R. Zachariah, Reactive sintering: An important component in the combustion of nanocomposite thermites, Combust. Flame 159(1) (2012) 2-15.

[153] S. Wang, C. An, J. Wang, B. Ye, Reduce the Sensitivity of CL-20 by Improving Thermal Conductivity Through Carbon Nanomaterials, Nanoscale Res Lett 13:85(1) (2018) 1-8.

[154] S. Aksel, D. Eder, Catalytic effect of metal oxides on the oxidation resistance in carbon

nanotube–inorganic hybrids, J. Mater. Chem. 20(41) (2010) 9149-9154.

[155] J.M. Parnis, S.A. Mitchell, P.A. Hackett, Complexation and Abstraction Channels in the Al+CO_2 reaction, Chem. Phys. Lett. 151(6) (1988) 485-488.

[156] K. Honma, D. Hirata, Reaction dynamics of Al + CO_2 -> AlO + CO studied by a crossed-beam velocity map imaging technique, J. Chem. Phys. 147(1) (2017) 013903.

[157] M. Sharma, V. Sharma, Effect of carbon nanotube addition on the thermite reaction in the Al CuO energetic nanocomposite, Philos. Mag. (2017) 1-18.

[158] H. Sui, L. LeSergent, J.Z. Wen, Diversity in addressing reaction mechanisms of nano-thermite composites with layer by layer structure at interface, Adv. Eng. Mater. 1700822 (2017) 1-11.

[159] S. Rossi, E.L. Dreizin, C.K. Law, Combustion of Aluminum Particles in Carbon Dioxide, Combust. Sci. Technol. 164(1) (2001) 209-237.

[160] J. Čížek, I. Procházka, M. Cieslar, R. Kužel, J. Kuriplach, F. Chmelík, I. Stulíková, F. Bečvář, O. Melikhova, R.K. Islamgaliev, Thermal stability of ultrafine grained copper, Phys. Rev. B 65(9) (2002) 094106.

[161] Z. Li, G. Feng, K. Xu, X. Zhang, Microstructure and formation mechanism of SHS joining between Cf/Al composites and TiAl intermetallic with Al-Ni-CuO interlayer, Rare Met. 34(1) (2015) 17-21.

[162] J. Cao, J.C. Feng, Z.R. Li, Joining of TiAl intermetallic by self-propagating high-temperature synthesis, J. Mater. Sci. 41(15) (2006) 4720-4724.

[163] E.B. Motlagh, J.V. Khaki, M.h. Sabzevar, Welding of aluminum alloys through

thermite like reaction in Al-CuO-Ni system, Mater. Chem. Phys. 133 (2012) 757-763.

[164] S. Li, Y. Zhou, H. Duan, Joining of SiC ceramic to Ni-based superalloy with functionally gradient material fillers and a tungsten intermediate layer, J. Mater. Sci. 38 (2003) 4065-4070.

[165] A.J.C.L.d. Carvalho, Ni/Ti reactive multilayers for joining, Department of Mechanical Engineering, University of Coimbra, 2014, p. 194.

[166] J. Wang, E. Besnoin, A. Duckham, S.J. Spey, M.E. Reiss, O.M. Knio, T.P. Weihs, Joining of stainless-steel specimens with nanostructured Al/Ni foils, J. Appl. Phys. 95(1) (2004) 248-256.

[167] A. Duckham, S.J. Spey, J. Wang, M.E. Reiss, T.P. Weihs, E. Besnoin, O.M. Knio, Reactive nanostructured foil used as a heat source for joining titanium, J. Appl. Phys. 96(4) (2004) 2336-2342.

[168] Z. Shen, J. Chen, Y. Ding, J. Hou, B. Shalchi Amirkhiz, K. Chan, A.P. Gerlich, Role of interfacial reaction on the mechanical performance of Al/steel dissimilar refill friction stir spot welds, Sci. Technol. Weld. Joining 23(6) (2018) 462-477.

[169] Z. Shen, Y. Chen, J.S.C. Hou, X. Yang, A.P. Gerlich, Influence of processing parameters on microstructure and mechanical performance of refill friction stir spot welded 7075-T6 aluminium alloy, Sci. Technol. Weld. Joining 20(1) (2015) 48-57.

[170] Z. Shen, Y. Ding, O. Gopkalo, B. Diak, A.P. Gerlich, Effects of tool design on the microstructure and mechanical properties of refill friction stir spot welding of dissimilar Al alloys, J. Mater. Process. Technol. 252 (2018) 751-759.

[171] Y. Chen, J. Chen, B. Shalchi Amirkhiz, M.J. Worswick, A.P. Gerlich, Microstructures and properties of Mg alloy/DP600 steel dissimilar refill friction stir spot welds, Sci. Technol. Weld. Joining 20(6) (2015) 494-501.

[172] G. Bohlouli-Zanjani, J.Z. Wen, A. Hu, J. Persic, S. Ringuette, Y.N. Zhou, Thermo-chemical characterization of a Al nanoparticle and NiO nanowire composite modified by Cu powder, Thermochim. Acta 572 (2013) 51-58.

[173] G.C. Egan, T. LaGrange, M.R. Zachariah, Time-Resolved Nanosecond Imaging of Nanoscale Condensed Phase Reaction, J. Phys. Chem. C 119 (2015) 2792-2797.

[174] R. Fan, H. Lv, K. Sun, W. Wang, X. Yi, Kinetics of thermite reaction in Al-Fe_2O_3 system, Thermochim. Acta 440 (2006) 129-131.

[175] Z. Gu, Q. Cui, J. Chen, J. Buckley, T. Ando, D. Erdeniz, P. Wong, A. Hadjiafxenti, P. Epaminonda, I.E. Gunduz, C. Rebholz, C.C. Doumanidis, Fabrication, characterization and applications of novel nanoheater structures, Surf. Coat. Technol. 215 (2013) 493-502.

[176] A.A. Giardini, A study of the directional hardness in silicon, Am. Mineral. 43 (1958) 957-969.

[177] F. Saceleanu, S. Atashin, J.Z. Wen, Investigation of the effects of phase transformations in micro and nano aluminum powders on kinetics of oxidation using thermogravimetric analysis, Phys. Chem. Chem. Phys. 19(29) (2017) 18996-19009.

[178] H. Sui, B. Li, J.Z. Wen, Interaction between Single-Walled Carbon Nanotubes and Reactive Nanoparticle Constituents in Multilayered Al/NiO Nanocomposite, ACS Applied Energy Materials 1 (2018) 5245-5256.

[179] V.I. Levitas, B.W. Asay, S.F. Son, M. Pantoya, Melt dispersion mechanism for fast reaction of nanothermites, Appl. Phys. Lett. 89(7) (2006) 071909.

[180] V.I. Levitas, B.W. Asay, S.F. Son, M. Pantoya, Mechanochemical mechanism for fast reaction of metastable intermolecular composites based on dispersion of liquid metal, J. Appl. Phys. 101(8) (2007) 083524.

[181] V.I. Levitas, M.L. Pantoya, K.W. Watson, Melt-dispersion mechanism for fast reaction of aluminum particles: Extension for micron scale particles and fluorination, Appl. Phys. Lett. 92(20) (2008) 201917.

[182] W. Zhang, B. Yin, R. Shen, J. Ye, J.A. Thomas, Y. Chao, Significantly enhanced energy output from 3D ordered macroporous structured Fe_2O_3/Al nanothermite film, ACS Appl Mater Interfaces 5(2) (2013) 239-42.

[183] G. Zheng, W. Zhang, R. Shen, J. Ye, Z. Qin, Y. Chao, Three-dimensionally Ordered Macroporous Structure Enabled Nanothermite Membrane of Mn_2O_3/Al, Sci Rep 6 (2016) 22588.

[184] H.-C. Shin, M. Liu, Copper Foam Structures with Highly Porous Nanostructured Walls, Chem. Mater. 16 (2004) 5460-5464.

Appendices: Formation of porous CuO on conductive electrode via electroplating

In Chapter 8, the future work suggests that the nano-thermite composites, which possess a gas-solid reaction mechanism, can be formed with porous structures that improve the reactivity of nano-thermites. In this appendix, the initial experiment is then conducted to provide a potential method to achieve the purpose. Nano-thermites contain Al and oxidizers compositions. The aluminum component is sensitive to the surrounding environment, which can be oxidized by the oxygen when it exposes in the air atmosphere. Although passivation layers can be formed to prevent further oxidation of aluminum, the ratio of Al_2O_3 is significantly increased in the nanoscales. However, the oxidizers are stable in the air environment, which can be formed as the frame work to support the formation of nano-thermite composites. There are several achievements forming oxidizers skeleton on glass plates, which are followed by the deposition of aluminum nano-layers via the vapor deposition technology [182, 183]. The methods applied in these works have the drawbacks that the complex apparatus is required. Meanwhile, the procedures are also complicated, which is hard to control the products. Therefore, the new way forming CuO skeletons on conductive electrodes is then proposed for providing the future direction.

As showing in the previous work, the Cu deposition with porous structures can be formed on conductive electrodes through electroplating [184]. It can be expected that the Cu deposition can be oxidized on the surface of the conductive electrode to form CuO with a porous structure. Based on this thinking, the experiments are conducted to form the Cu

deposition on the stainless steel electrode. We deposited the Cu on the electrode according to the literature at the initial stage that the mixture of $CuSO_4$ and H_2SO_4 is prepared [184]. The concentrations $CuSO_4$ of H_2SO_4 and are 0.4 mol/L and 1.5 mol/L, respectively. The prepared solution is shown in Figure A.1. Then, the solution is added to the beaker, where the stainless steel electrodes are inserted to immerse into the solution perpendicularly. The Cu is then deposited on the cathode electrode with the electric field of 10V/cm for 2 min. The Cu deposition on the electrode is shown in Figure A.2. The uneven surface can be seen in Figure A.2. The SEM images in the future are required to confirm the morphology of the Cu deposition on the electrode.

Figure A.1 Solution of mixture of $CuSO_4$ (0.4 mol/L) and H_2SO_4 (1.5 mol/L)

Figure A.2 Cu deposition on the surface of stainless steel electrode

The CuO skeleton on the electrode is the purpose, which can be coated with Al by sputtering device. The Cu can be oxidized by heating up in the oven under air atmosphere. Therefore, it is worthwhile to measure the oxidation temperature of Cu with TGA/DSC measurement. The deposited Cu is then put into TGA/DSC crucible, which is heated up to 1200 °C with the heating rate of 20 °C/min under air atmosphere. The TGA/DSC result is shown in Figure A.3.

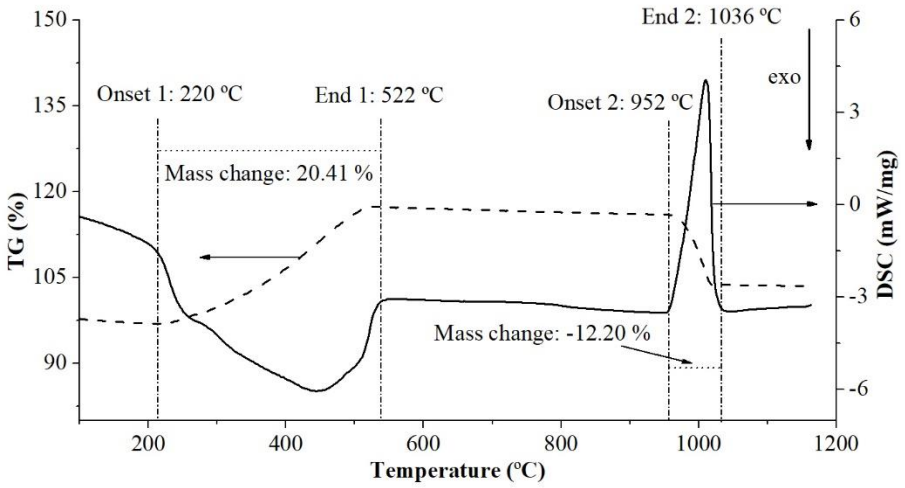

Figure A.3 TGA/DSC data of deposition Cu heated up to 1200 °C with heating rate of 20 °C/min under air atmosphere

The total mass of Cu does not change until 220 °C, where the oxidation initiates to cause a mass increase in the TGA curve. Meanwhile, the DSC curve shows the peak with downward direction, indicating the exothermic reaction between Cu and oxygen. The oxidation procedure is then completed at around 522 °C. The mass decrease initiates at 952 °C with an endothermic peak, which corresponds to the decomposition of CuO. The total mass increase between the temperatures of 220 °C and 522 °C is 20.41 %, which is larger than the total mass decrease of -12.20 % between 952 °C and 1036 °C. It can be assumed that the Cu is oxidized to CuO at the first stage. Then, the CuO is decomposed to Cu_2O at the higher temperature between 952 °C and 1036 °C. The confirmation is required for the assumption in the future work. However, the purpose of conducting the TGA/DSC measurement is to confirm the oxidation temperature of Cu to CuO without the decomposition of CuO. Therefore, the oxidation temperature of deposited Cu can be set at 600 °C.

For the future work, the porous morphology of oxidized Cu on the surface of electrodes is supposed to be observed with SEM devices. The ratio of $CuSO_4$ and H_2SO_4 can be changed to tune the porous sizes after oxidation of Cu on the electrode.